Dissertation

Submitted to the

Combined Faculties for the Natural Sciences and for Mathematics

of the Ruperto-Carola University of Heidelberg, Germany

for the degree of

Doctor of Natural Sciences

presented by

M.Phil. Yeung-Yeung Leung

born in: Hong Kong, China

Oral examination: 18 April 2016

Title

Functional conservation of the AKT kinase action on the synaptic vesicle release machinery between *Drosophila* and rat

Referees:

Prof. Dr. Christoph M. Schuster

Prof. Dr. Hilmar Bading

TABLE OF CONTENTS

List of Figures

List of Tables

List of Abbreviations

α-SNAP	α-soluble NSF Attachment Protein
A	Abdominal
ACh	Acetylcholine
ACSF	Artificial Cerebrospinal Fluid
AKT	Protein kinase B
APV	2-Amino-5-phosphonopentanoic acid
AraC	β-D-arabinofuranoside
ASD	Autism Spectrum Disorder
ATP	Adenosine triphosphate
BAPTA-AM	1,2-Bis(2-aminophenoxy)ethane-N,N,N',N'-tetraacetic acid tetrakis (acetoxymethyl ester)
bic	Bicuculline
brp	bruchpilot
Ca^{2+}	double-ionized calcium
CaM	Calmodulin
CaMKII	Calcium/calmodulin-dependent protein kinase
cac	Cacophony
CalX	Na/Ca exchanger
cpGFP	circularly permuted Green Fluorescent Protein
Cpx	Complexin
DIV	Day In Vitro
DM	Dissociation Medium
DMEM	Dulbecco's modified Eagle's medium#
DMSO	Dimethyl sulfoxide
DNQX	6,7-Dinitroquinoxaline-2,3-dione
eEJP	evoked Excitatory Junctional Potential
ER	Endoplasmic reticulum
fps	frames per second
FRET	Fluorescence Resonance Energy Transfer
GABA	γ-aminobutyric acid

GFP	Green fluorescent protein
GM	Growth Medium
HEPES	4-(2-hydroxyethyl)-1-piperazineethanesulfonic acid
HL3	Hemolymph-like 3 solution
HRP	Horse-Radish Peroxidase
HVA	High Voltage Activated
IMDM	Iscove's Modified Dulbecco Medium
IP3	Inositol triphosphate
KD	„knockdown" experiment type
LVA	Low Voltage Activated
M13	M13 peptide
mEJP	miniature Excitatory Junctional Potential
mEPSP	miniature Excitatory Postsynaptic Potential
mGluR	Metabotropic glutamate receptor
mIPSP	miniature Inhibitory Postsynaptic Potential
mTOR	mammalian Target of Rapamycin
mTORC2	mammalian Target of Rapamycin Complex 2
myr-AKT	myristoylated AKT
NCX	Na^{+}-Ca^{2+} exchanger
NMDA	N-methyl-D-aspartic acid
NMJ	Neuromuscular Junction
NSF	N-ethylmaleimide-Sensitive Factor
oligo	oligonucleotide
PALM	Photoactivated light microscopy
PBS	Phosphate buffered saline
PDK1	Protein Kinase-1
PH	Pleckstrin Homology
PI3K	Phosphatidylinositol 3-kinase
PIP2	Phosphatidylinositol 4,5-bisphosphate
PIP3	Phosphatidylinositol (3,4,5)-triphosphate
PMCA	plasma membrane calcium ATPase

PPD	Paired-Pulse Depression
PPF	Paired-Pulse Facilitation
PPR	Paired-Pulse Ratio
PTEN	Phosphatase and tensin homolog
rAAV	recombinant Adeno-Associated Virus
Rf	dynamic range
RIM	Rab3-Interacting Molecule
RIM-BP	RIM- Binding Protein
RNAi	RNA interference
roi	region of interest
rpS7	ribosomal protein S7
Ser	Serine
sav	surface area to volume ratio
SERCA	Sarco-ER calcium ATPase
shRNA	small hairpin RNA
SM	*S*ec1/*M*unc18-like proteins
SNAP	Soluble N-ethylmaleimide-sensitive factor Attachment Protein
SNAP-25	Synaptosomal-Associated Protein 25
SNARE	Soluble N-ethylmaleimide-sensitive factor Attachment Protein Receptor Proteins
STED	Stimulated emission depletion microscopy
SIM	Structured illumination microscopy
Syt	Synaptotagmin
Thr	Threonine
T	Thoracic
t-SNARE	plasma membrane SNARE proteins
TM	Transfection Medium
TnC	Troponin C
TSC2	Tuberous Sclerosis Complex 2
TTX	Tetrodotoxin
UAS	Upstream Activation Sequence

v-SNARE	vesicular SNARE protein
VAAC	Voltage Activated Calcium Channel
VAMP	Vesicle-Associated Membrane Protein
wt	wild type

1. SUMMARY

Spontaneous vesicle release has long been dismissed as a stochastic byproduct of vesicle release machinery to achieve high fidelity evoked release. Nevertheless, studies of the decade have identified its important role in the development and function of synapses. Interestingly, spontaneous neurotransmitter release appears to be regulated differently at individual vesicle release sites, but how this dynamic regulation is achieved is largely unclear. Our earlier study at the *Drosophila* neuromuscular junction (NMJ) has revealed a novel synaptic function of the ubiquitous kinase AKT in regulating spontaneous vesicle release. Since AKT has been repeatedly reported as a risk gene for several neurological disorders, the potential conservation of this pathway in the mammalian central nervous system might implicate an intriguing new mechanism for human diseases.

This study revealed that the AKT regulation of spontaneous vesicle release is conserved in the hippocampal cultured neuron. Suppressed AKT activity induced a greater degree of enhancement in excitatory over inhibitory spontaneous neurotransmitter release, and elicited oscillatory bursting activity in hippocampal neurons. Both of which closely link to the etiology of Schizophrenia and Autism Spectrum Disorders. Since acute AKT inhibition suppressed high frequency triggered evoked vesicle release at both hippocampal synapses and *Drosophila* NMJ, this data suggested that AKT might function in dynamically regulating the clamping status of vesicle release machinery, which may offer a well-fitting mechanism for how release sites exhibit a spectrum of preference for evoke/spontaneous vesicle release. Intriguingly, recombinant adeno-associated virus (rAAV)-shRNA mediated knockdown of the ubiquitously expressed AKT isoform, AKT1, reduced the rate of spontaneous vesicle release, whereas silencing the predominantly brain expressed AKT3 resulted in elevation. Since compensatory expressions of the two isoforms were observed, understanding how the interplay between the AKT isoforms leads to the differential outcome may provide provocative clues in disease etiology.

The second part of this thesis presents the experimental data that contributed in a collaborative project to construct a highly realistic three-dimensional mathematical model of calcium dynamics in *Drosophila* NMJ boutons. Our experimental data show a linear relationship between bouton surface to volume ratio and stimulation induced peak calcium rise. Compared to bigger size type 1b bouton, the smaller size type 1s bouton elicited more robust upsurge in peak calcium at lower stimulation frequency and exhibited faster rise kinetics at all stimulation frequency within the physiology range. Nevertheless, the variation of calcium dynamics of the two bouton types seems not fully explainable by size, isolation of the critical parameters would require detailed computational analysis.

2. ZUSAMMENFASSUNG

Die spontane Freisetzung von Neurotransmittern wurde lange Zeit als ein zufälliges Nebenprodukt beim Aufbau einer zuverlässigen evozierten Vesikel-Freisetzung angesehen. Dennoch haben neuere Untersuchungen wichtige Rollen in der Entwicklung und Funktion von Synapsen identifiziert. Interessanterweise scheint die spontane Freisetzung von Neurotransmittern an einzelnen aktiven Zonen unterschiedlich reguliert zu sein, wobei es aber weitgehend unklar ist, wie eine solche dynamische Regulation erreicht werden könnte. Unsere bisherigen Untersuchungen an neuromuskulären Endplatten von *Drosophila* (NMJ) haben eine neue synaptische Funktion der ubiquitären Kinase AKT in der Regulation der spontanen Vesikelfreisetzung identifiziert. Da AKT als Risikogen für verschiedene neurologische Erkrankungen beschrieben wurde, könnte eine mögliche evolutionäre Konservierung dieser neuen synaptischen AKT Rolle einen grundlegenden Mechanismus zur Erklärung menschlicher Erkrankungen darstellen.

Im Rahmen dieser Arbeit konnte gezeigt werden dass die Regulation der spontanen Vesikelfreisetzung durch AKT auch in hippocampalen Neuronenkulturen von Ratten konserviert ist. Supprimierte AKT Aktivität induzierte in diesen Neuronen eine stärkere spontane Freisetzung von erregenden als von hemmenden Neurotransmittern und bewirkte zusätzlich eine oszillierende „bursting“ Aktivität innerhalb des Netzwerks. Beide Effekte könnten entscheidende Rollen in der Ätiologie von Schizophrenie und Erkrankungen des Autismus Spektrums spielen. Die weitere Beobachtung, dass die Blockade von AKT in hippocampalen Neuronen und *Drosophila* NMJs längerfristig auch die Effizienz von hochfrequent evozierten Vesikelfreisetzungen beeinträchtigte, könnte bedeuten dass AKT den Klemmzustand von Vesikelfreisetzungsmaschinerien generell und dynamisch reguliert um so ein breites Spektrum von funktionell unterschiedlichen Aktiven Zonen einzustellen. Interessanterweise zeigten AKT-Isoform-spezifische shRNA vermittelte „knockdown“ (KD) Experimente mit eigens hergestellten rekombinanten Adeno-Assoziierten Viren, dass AKT1-KD und AKT3-KD entgegengesetzte Effekte auf die Rate der spontanen Vesikelfreisetzung in hippocampalen Neuronen verursachen. Dies könnte darauf hinweisen, dass das funktionell kompensatorische Zusammenspiel beider AKT-Isoformen bzw. dessen Dysregulation verantwortlich sein könnte für Ätiologie unterschiedlicher Krankheitsbilder.

Im zweiten Teil der Arbeit wurden quantitative physiologische Daten zur präsynaptischen Kalziumdynamik an *Drosophila* NMJs mit besonderem Fokus auf die Unterschiede zwischen zwei Boutontypen erhoben, um damit die Erweiterung eines bereits etablierten drei-dimensionalen computationalen Modells von glutamatergen Boutons zu ermöglichen.

3. INTRODUCTION

3.1. Three kinetically distinct modes of neurotransmitter release

Synaptic vesicles are exocytose at two major forms: evoked and spontaneous release. Evoked release (which can be subdivided into synchronous and asynchronous release) is strictly dependent of calcium and is coupled to the time of stimulation, whereas spontaneous release is independent of the presynaptic action potentials and occurs stochastically.

3.1.1. Synchronous vesicle release

Synchronous (also called "phasic") vesicle release is regarded as the most important form of neurotransmission, which serves to transmit tightly timed coupled information in the nervous system. When an action potential invades a presynaptic terminal, voltage-gated calcium channels are opened for a brief influx of calcium. The vesicle release could be induced as rapidly as 50μs after a calcium transient develops (Sabatini and Regehr, 1996). To accomplish synchronous release, a fast calcium sensor is required to act on the brief calcium waves instantly (Llinas et al., 1992, 1995). Moreover, the synaptic vesicle has to dock at the active zone and position itself properly near the calcium channels, so that they can response to the localized nano/microdomain calcium signal instantly (Adler et al., 1991).

Fast synchronous vesicle release is steeply dependent on calcium (Dodge and Rahamimoff, 1967; Augustine and Charlton, 1986; Borst and Sakmann, 1996; Reid et al., 1998; Hagler and Goda, 2001; Rozov et al., 2001; Blatow et al., 2003). The relationship of vesicle release frequency in response to intracellular calcium concentration ($[Ca^{2+}]i$) can be approximated by a power law with exponents between 3 - 6 (Lou et al., 2005; Sun et al., 2007). Vesicle release is mostly synchronous at elevated $[Ca^{2+}]i$ (0.3 - 3μM), where the calcium cooperativity in triggering vesicle fusion is high (~4). On the other hand, vesicles tend to release spontaneously at basal $[Ca^{2+}]i$ (~ 20 - 30 nM), where the calcium cooperativity is low (<1) (Lou et al., 2005; Ramirez and Kavalali, 2011).

3.1.2. Asynchronous vesicle release

Asynchronous vesicle release is loosely time locked (at a timescale of millisecond) to an action potential that spans for more then one second (Barrett and Stevens, 1972; Geppert et al., 1994; Goda and Stevens, 1994; Atluri and Regehr, 1998). It employs the same pool of readily releasable vesicle as that of synchronous vesicle release (Lu and Trussell, 2000; Otsu and Murphy, 2004) and is triggered by slow but high-affinity calcium sensors, which operate in between action potentials or sometimes out-compete synchronous release (Barrett and Stevens, 1972; Goda and Stevens, 1994; Cummings et al., 1996; Atluri and Regehr, 1998; Lu and Trussell, 2000; Hagler and Goda, 2001; Atwood and Karunanithi, 2002; Otsu and Murphy, 2004). This type of vesicle release occurs during high-frequency stimulation. When the readily releasable pool vesicles are depleted, the accumulating residual calcium triggers the release of newly refilled vesicles and switches the mode of release from synchronous to asynchronous (Atluri and Regehr, 1998; Jensen et al., 2000; Kirischuk and Grantyn, 2003). The decay of asynchronous release with time reflects a diffusion collapse of nanodomain followed by microdomain, the binding of calcium to slow buffers (Muller et al., 2007), as well as calcium extrusion and reuptake (Kim et al., 2005).

In contrary to the prominent function of synchronous release, the biological significance of asynchronous release is rather obscure. This form of release occurs at behaviorally relevant stimulation patterns (Hefft and Jonas, 2005). It may serves to sustain synaptic transmission during high-frequency firing (Lu and Trussell, 2000) and provides modulating effects in the nervous system by smoothing the inhibitory “tone” (Lu and Trussell, 2000) and generating long-lasting inhibition (Hefft and Jonas, 2005).

3.1.3. Spontaneous vesicle release

In the absence of stimulation, vesicles are released in stochastic but finite manner at low probability. Those spontaneous events exist in electrophysiological recordings as miniature postsynaptic currents (Fatt p, 1950; Fatt and Katz, 1952), which are commonly referred as “minis”.

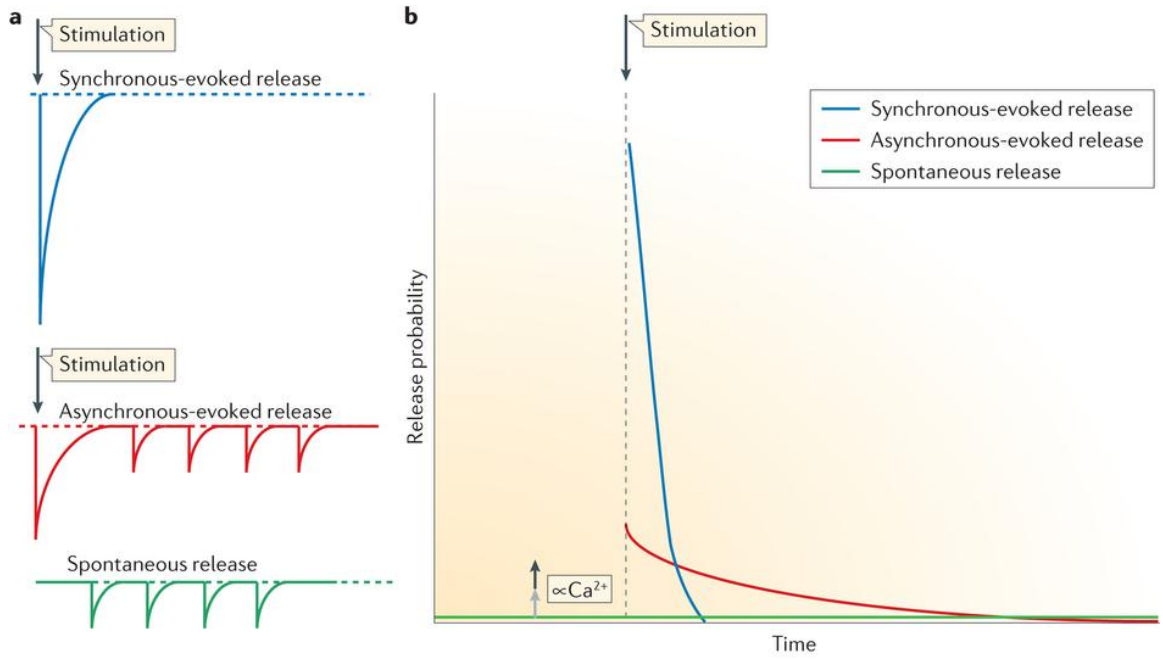

Figure 3.1: Three kinetically distinct modes of neurotransmitter release

Three forms of neurotransmitter release that differ in calcium dependence and time coupled to stimulation. **A** Graphical reconstitution of typical electrophysiological recordings that illustrates the postsynaptic current responses towards synchronous-evoked, asynchronous-evoked, and spontaneous release. **B** Schematic representation of relative decay time courses of neurotransmitter release probability after presynaptic stimulation. For synchronous-evoked release (blue), presynaptic action potentials induce calcium influx trigger vesicle fusion within 1 ms. For asynchronous-evoked release (red), the decay of release probability lasts for 1 sec or more, vesicle release is only loosely coupled to the arrival of the presynaptic action potential. For spontaneous release (green), vesicle fusion is independent of the presynaptic action potential's time course and occurs stochastically. The rate of such release is nevertheless regulated in proportion to intracellular calcium levels. (Adapted from Kavalali, 2014)

The exact mechanism of spontaneous release remains a conundrum, it is believed to be a product of low-probability random conformational alternations of the vesicle fusion machinery (Kaeser and Regehr, 2013). Since vesicle release can be triggered by only one or two voltage activated calcium channels (VACCs; Augustine et al., 1991; Stanley, 1993; Shahrezaei et al., 2006; Bucurenciu et al., 2008), stochastic activation of VACCs could also contribute to the mechanism of spontaneous release in glutamatergic and GABAergic synapses (Goswami et al., 2012; Williams et al., 2012; Ermolyuk et al., 2013). Furthermore, subthreshold presynaptic calcium sparks could increase the

occurrence of conformational changes in the release machinery, leading to increased spontaneous release (Llano et al., 2000; Angleson and Betz, 2001; Emptage et al., 2001; Sharma and Vijayaraghavan, 2003). Though at much lower extend compared to evoked release, spontaneous release still exhibits a gentle linear dependence on calcium (Lou et al., 2005; Sun et al., 2007; Groffen et al., 2010). Nevertheless, a sizable portion of spontaneous release was reported to be calcium independent (Deitcher et al., 1998; Chung and Kavalali, 2006; Glitsch, 2008), mechanisms of which are largely unknown.

3.2. Biological importance of spontaneous release

Spontaneous vesicle releases have long been dismissed as a stochastic byproduct of vesicle fusion machinery to achieve high fidelity evoked release (Otsu and Murphy, 2003; Zucker, 2005; Sutton and Schuman, 2009; Ramirez and Kavalali, 2011). However, recent studies of the decade have revealed functional importance of this neglected form of release.

3.2.1. Acute modulation

A typical central neuron harbors thousands of synapses. In each synaptic bouton, the rate of spontaneous release is around 0.01 Hz (Geppert et al., 1994; Murthy and Stevens, 1999; Sara et al., 2005). For synapses with higher rate of spontaneous events (e.g. 50 fold higher rate in acetycholine transmission), dendritic summation of spontaneous quanta (Sharma and Vijayaraghavan, 2003) may modulate the electrical activity of the neuron and exert a global influence on neuronal excitability. In more extreme cases, even a single quantum can trigger an action potential firing in compact neurons that have high membrane resistance (Carter and Regehr, 2002), or alter spike timing and postsynaptic excitability (Otmakhov et al., 1993; Sharma and Vijayaraghavan, 2003).

3.2.2. Homeostatic plasticity

Spontaneous events are also capable to modulate the magnitude and duration of various homeostatic plasticity (Sutton et al., 2004; Sutton et al., 2006; Sutton et al., 2007;

Aoto et al., 2008; Kavalali et al., 2011). Postsynaptic receptors including the metabotropic glutamate receptors (mGluR1 and mGluR5 in particular), AMPA receptors (that lack GluA2 subunits) and NMDA receptors with an incomplete Mg^{2+} block (especially those carrying subunit with lower Mg^{2+} affinity: NR2C or NR2D) are capable to transmit spontaneous signals at resting membrane potentials (Jahr and Stevens, 1990; Sutton et al., 2006; Sutton et al., 2007; Espinosa and Kavalali, 2009; Autry et al., 2011; Nosyreva et al., 2013; Gideons et al., 2014). Those spontaneous calcium signals can induce downstream signaling such as activity of postsynaptic CamKII and eukaryotic elongation factor 2 kinase (Otsu and Murphy, 2003; Sutton et al., 2007). A reduction of spontaneous signals would down scale the postsynaptic calcium signaling and the corresponding downstream signals, which results in homeostatic regulations to augment synaptic efficacy (Sutton and Schuman, 2006; Kavalali et al., 2011).

3.2.3. Structural modulation

Spontaneous events are a prevailing feature of nascent synaptic contacts (Mozhayeva et al., 2002; Andreae et al., 2012), the propensity of which increase during the course of synaptic development (Hsia et al., 1998; Mozhayeva et al., 2002). It was reported that they are involved in the suppression of dendritic local protein translation, stabilization of synapses, maintaining dendritic spines and regulating local synaptic terminal growth (McKinney et al., 1999; Otsu and Murphy, 2003; Sutton et al., 2006; Sutton and Schuman, 2006; Choi et al., 2014).

3.3. The synaptic vesicle release machinery

Synaptic vesicle exocytosis is the most tightly regulated membrane fusion reaction because rapid vesicle release in response to an action potential is essential for synaptic transmission. This is achieved by an orchestra of highly coordinated proteins, which mediate the initial recognition, tethering of donor and acceptor membranes, sensing of the calcium signal and providing forces to pull two separate lipid membranes into a continuous bilayer. Those proteins are collectively referred to the vesicle release machinery (Jahn et al., 2003; Malsam et al., 2008).

3.3.1. SNARE complex and SM proteins

The core vesicle fusion machinery is composed of the SNARE/SM (SNARE: soluble N-ethylmaleimide-sensitive factor (NSF) attachment protein (SNAP) receptor proteins; SM: *S*ec1/*M*unc18-like proteins) protein complex. Vesicle fusion occurs when the vesicular SNARE protein (v-SNARE): synaptobrevin/vesicle-associated membrane protein (VAMP), and the plasma membrane SNARE proteins (t-SNARE): syntaxin-1 and synaptosomal-associated protein 25 (SNAP-25) form a "*trans*"-complex (Sollner et al., 1993b). This four-α helical SNARE bundle progressively zipper (Hanson et al., 1997), which provide a force to overcome repulsion of the two hydrophilic surfaces and drives the lipid bilayers into fusion (Rizo and Rosenmund, 2008). After landing on the plasma membrane, the fusion pore expands, which transform the "*trans*"-SNARE complexes into "*cis*"-SNARE complexes. The "*cis*"-SNARE complexes are then dissociated through an energy dependent process by the ATPase NSF, which binds itself to the SNARE complexes via the adaptor protein: α-soluble NSF attachment protein (α-SNAP). The SNAREs are then dissociated, sorted, and endocytosed (Murthy and De Camilli, 2003; Galli and Haucke, 2004; Jahn and Scheller, 2006; Sudhof and Rothman, 2009).

SM proteins, the essential coagonists of SNARE proteins, are required for all SNARE-dependent fusion reactions. For example, Munc18-1 functions by binding to the closed conformation of syntaxin-1. While remaining attached, it interacts with the assembling SNARE complex and mediates the fusion process (Hata et al., 1993; Dulubova et al., 1999; Misura et al., 2000; Dulubova et al., 2007; Khvotchev et al., 2007; Gerber et al., 2008; Deak et al., 2009; Zhou et al., 2012).

3.3.2. The calcium sensor Synaptotagmin

The vesicle transmembrane proteins, Synaptotagmins (Syt), are made up of a short N-terminal intravesicular sequence, a single transmembrane region, a linker sequence, and two cytoplasmic calcium binding PKC-homologous repeats (C2 domains) at the C-terminal (Perin et al., 1990; Perin et al., 1991b; Brose et al., 1995). In *Drosophila melanogaster*, only 7 Syts genes were found (Lloyd et al., 2000), while in mammalian systems, 16 genes encoding Syts (plus a Syt-related gene encoding the B/K

protein that lacks the transmembrane region) were identified. They can be classified into the calcium dependent group (N-terminal disulfide-bonded cysteine residues absence: Syt1, 2, 7, 9 or presence: Syt3, 5, 6, 10) and calcium independent group (Syt4, 8, 11, 12, 13, 14, 15, 16) (Sudhof, 2012).

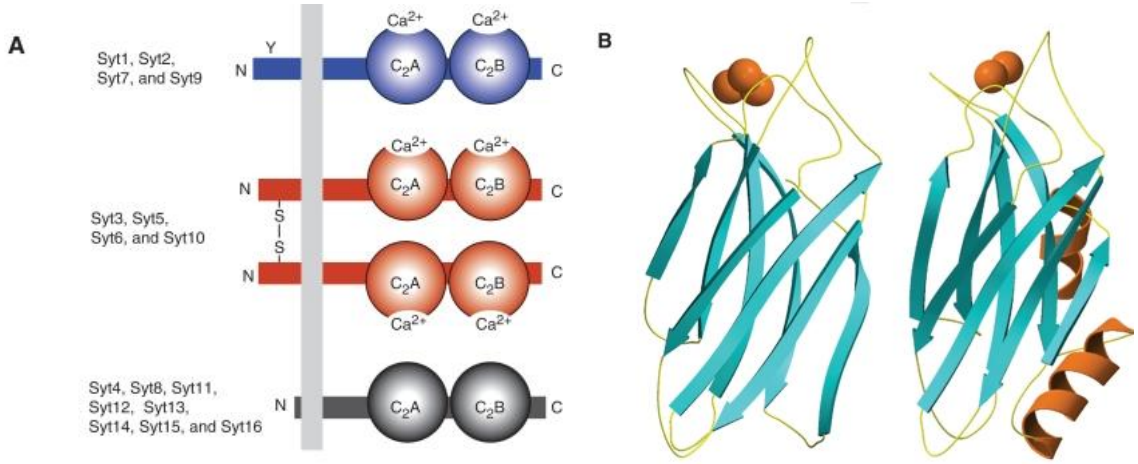

Figure 3.2: Canonical domain structures and grouping of 16 mammalian Synaptotagmins

A Synaptotagmins (Syts) consist of N-terminal a short vesicular sequence, followed by a transmembrane region, a linker sequence and two C2-domains. There are 8 calcium binding Syt which subdivided according to the absence (Syt1, 2, 7, and 9; blue) or presence (Syt3, 5, 6, and 10; red) of N-terminal sdisulfide-bonded cysteine residues, and 8 non calcium binding Syt (Syt4, 8, 11, 12, 13, 14, 15, 16; black). Note that Syt1 and Syt2 contain an N-glycosylated sequence, while Syt7 is extensively alternatively spliced in the linker sequence (Han et al., 2004). **B** Atomic structures of Syt1 C2A and C2B domains. Calcium ions (red spheres) bind to the flexible loops of an eight-stranded β-sandwich (Sutton et al., 1995; Ubach et al., 1998; Fernandez-Chacon et al., 2001). The Syt1 C2A domain contains three calcium binding sites, the central two shares between all calcium binding C2 domains, whereas the one on the left is absent in the C2B domain. (Adapted from Sudhof, 2012)

Syt1, the most extensively studied member of Syts, is a key calcium sensor that regulates both spontaneous and fast synchronous release. Syt1 deletions results in elevated spontaneous vesicle releases which remains calcium dependent but with reduced calcium cooperativity and triggered at lower calcium concentrations (Littleton et al., 1994; Maximov and Sudhof, 2005; Pang et al., 2006). Calcium binds to both C2 domains (C2A and C2B domains) of Syt1 via the negatively charged aspartate residues (Perin et al., 1990; Perin et al., 1991a; Sutton et al., 1995; Ubach et al., 1998; Desai et al., 2000).

Availability of calcium enhances the C2 domains binding to phospholipids (Davletov and Sudhof, 1993; Fernandez-Chacon et al., 2001), syntaxin-1 (Li et al., 1995) and assembled SNARE complexes (Bennett et al., 1992; Chapman et al., 1995).

Intriguingly, the Syt1 C2A and C2B domains exert discordant effects towards different forms of release. It was reported that calcium binding to the C2B but not C2A domain is required for synchronous release (Littleton et al., 1994; Littleton et al., 2001; Mackler et al., 2002; Stevens and Sullivan, 2003; Nicholson-Tomishima and Ryan, 2004; Nishiki and Augustine, 2004a, b; Shin et al., 2009; Yoshihara et al., 2010). Blocking the calcium binding to the C2A domain, however, decreases the magnitude and calcium cooperativity of release (Shin et al., 2009). Interestingly, the C2A domain seems to play a role in spontaneous release. Mutation that neutralizes the aspartate residues in C2A but not C2B domain fully rescue the increased spontaneous fusion in Syt1 null mutants. Nevertheless, neutralizing the aspartate residues in both domains do not reduce, but even further enhance the rate of spontaneous release in Syt1 null mutants (Lee et al., 2013b). Taken together, the two C2 domains seem to function cooperatively to elicit conformational changes in Syt1 that results in variable fusion properties (Meinrenken et al., 2003; Fuson et al., 2007).

3.3.3. The fusion clamp of vesicle release machinery

It was found that more than 95% of spontaneous fusion in murine central neurons was contributed by calcium binding to Syt1 (Xu et al., 2009), paradoxically however, deletion of Syt1 results in elevated spontaneous release. This is because Syt1 do not just function as a calcium dependent activator, but simultaneously a clamp of spontaneous exocytosis. This clamping function is executed in cohort with the small cytoplasmic protein complexin.

There are four members of complexins in mammals and only one single member in *Drosophila* (Brose, 2008). This 140-amino-acids highly charged protein possesses a central α helix, which binds in an antiparallel fashion to the center of the helical SNARE bundle at a groove formed by syntaxin 1 and synaptobrevin (McMahon et al., 1995; Reim

et al., 2001; Tokumaru et al., 2001; Bracher et al., 2002; Chen et al., 2002). Complexin deficient mammalian neurons exhibit a suppressed fast synchronous release and an enhanced spontaneous release (Reim et al., 2001), a phenotype that resembles a subtle version of Syt1 deletion. Complexin assists vesicle priming by binding to the partially assembled SNARE complexes (Hobson et al., 2011). More importantly, it functions as a fusion clamp by competing with synaptotagmin for SNARE complex binding. In response to action potential induced calcium influx, calcium activated synaptotagmin displaces the clamping of complexin which permits vesicle fusion (Giraudo et al., 2006; Tang et al., 2006; Yang et al., 2010; Jorquera et al., 2012; Kaeser-Woo et al., 2012). After the displacement, complexin further assists the fusion process by becoming an activator of the SNARE/SM protein complex (Tang et al., 2006; Xue et al., 2007; Maximov et al., 2009; Martin et al., 2011; Sudhof, 2013; Xu et al., 2013).

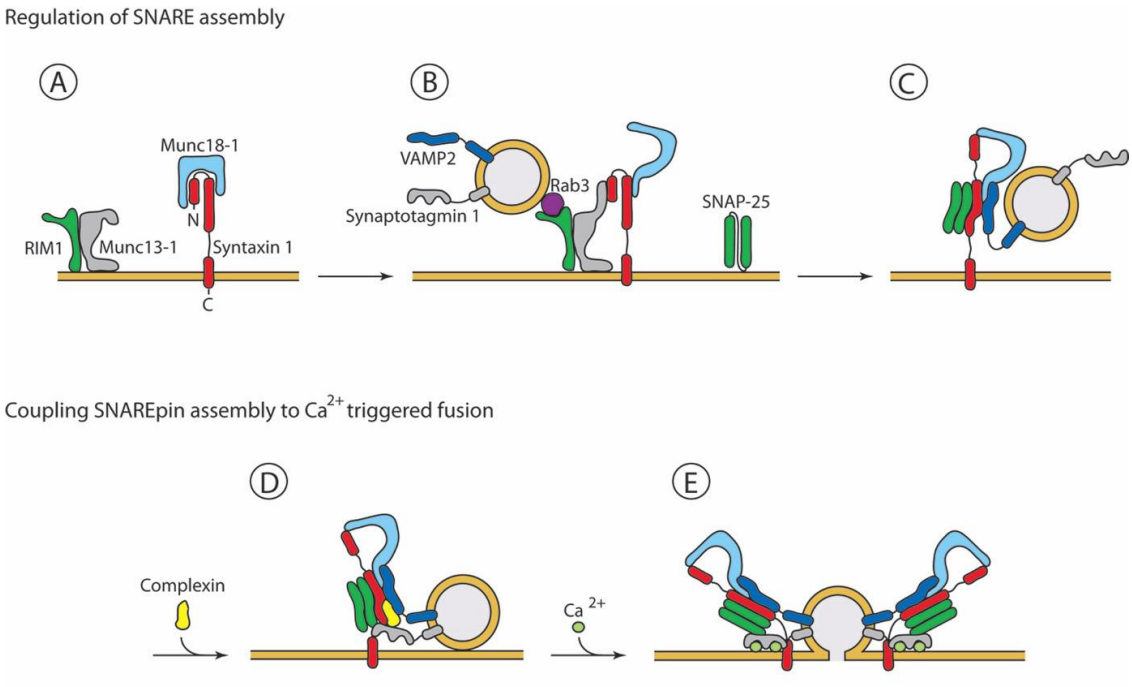

Figure 3.3: Schematic mechanism of SNAREs assembly and calcium triggered fusion

A Munc18-1 binds to the "closed" conformation of syntaxin-1. **B** Docking of vesicle catalyzes syntaxin-1 conversion into an "open" conformation. **C** SNAP-25 binds syntaxin-1 to form the t-SNARE complex which binds VAMP2 on synaptic vesicles, forming the trans-SNARE complex. **D** Complexin binds to the trans-SNARE and prevents the completion of trans-SNARE complex zippering, thereby clamping vesicle release. **E** calcium binded Synaptotagmin 1 displaces the complexin clamp and triggers fast vesicle fusion. (Adapted from Malsam et al., 2008)

3.3.4. Molecular tethering of the vesicle release machinery

To facilitate rapid vesicle release in response to an action potential, calcium channels are tethered to the docked and primed vesicles at the spatially organized active zone. The active zone membrane is associated with an electron-dense cytomatrix, which is comprised of large multidomain protein scaffords that provide interaction surfaces to spatiotemporally organize proteins and enzymatic reactions (Gundelfinger et al., 2003; Wang et al., 2009). The central components that function in recruiting calcium channels and mediating the docking and priming of vesicles are the three multidomain proteins called RIM (for Rab3-interacting molecule; Wang et al., 1997), RIM-BP (RIM- Binding Protein; Wang et al., 2000), and Munc13. RIM plays a central role in mediating the colocalization of all critical proteins to the active zone. RIM and RIM-BP bind with each other as well as calcium channels to form a tight cluster (Kaeser et al., 2011). RIM also binds to the vesicular Rab3 and Rab27 GTP-binding proteins, which facilitate vesicles docking (Gracheva et al., 2008; Han et al., 2011; Kaeser et al., 2011; Fernandez-Busnadiego et al., 2013). Furthermore, it binds and activates Munc13 (Brose et al., 1995; Betz et al., 2001; Deng et al., 2011), which catalyzes the syntaxin-1 conformational changes from closed to open (Richmond et al., 2001; Ma et al., 2012).

In addition, clustering of calcium-channel is promoted by the *Drosophila* protein bruchpilot (brp; Kittel et al., 2006) and its mammalian homolog Rab6 interacting protein (ELKS/CAST1; Kiyonaka et al., 2012), SNARE proteins (Sheng et al., 1994; Mochida et al., 1996), the active zone protein bassoon (Frank et al., 2010), and presynaptic neurexins (Missler et al., 2003).

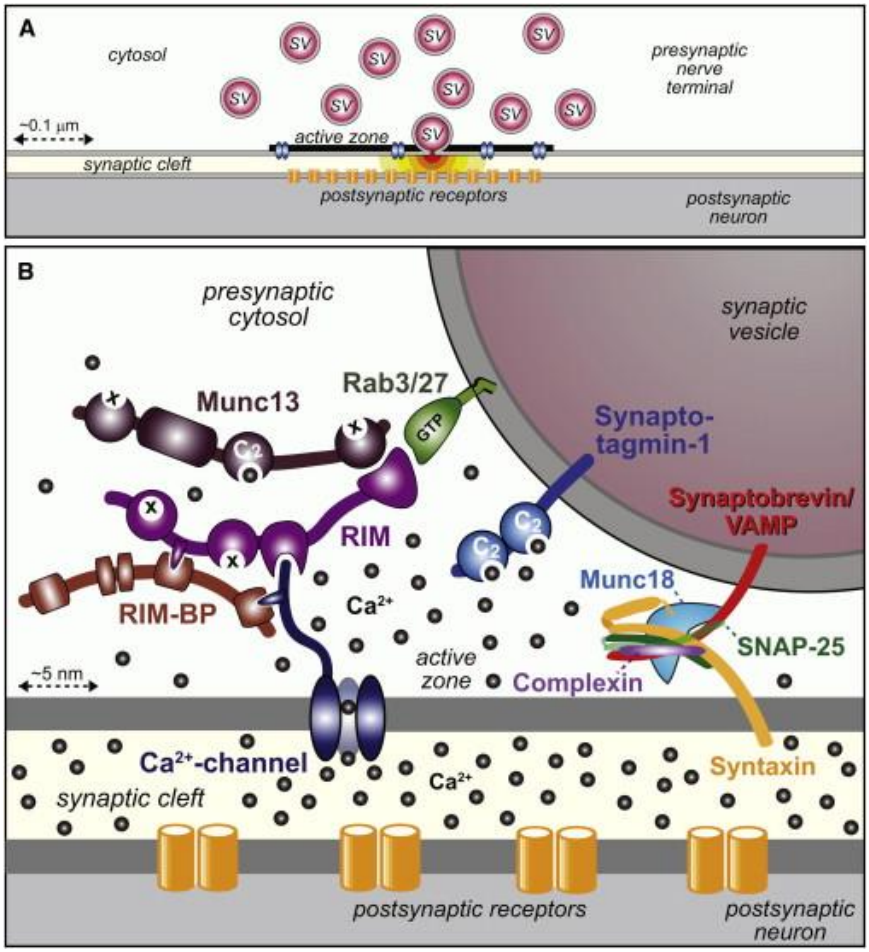

Figure 3.4: Organization of the vesicle release machinery

A Schematic illustration of a synaptic active zone containing calcium channels (blue), synaptic vesicles (red), and postsynaptic receptors cluster (orange). **B** Simplified model of the organization of release machinery. The core machinery, the SNARE/SM protein complex, composed of the v-SNARE proteins: synaptobrevin/VAMP, t-SNARE proteins: syntaxin-1, and SNAP-25 and the SM protein: Munc18-1. The active zone protein complex: RIM, Munc13, and RIM-BP organized in close proximity to the calcium channel. RIM binding to 1) vesicular rab proteins (Rab3 and Rab27 isoforms) which mediates vesicle docking; 2) Munc13 which activates vesicle priming; 3) the calcium channel, both directly and via RIM-BP, and recruits the calcium channels within 100 nm of the docked vesicles. (Adapted from Sudhof, 2013)

3.4. The serine/threonine kinase AKT

The 60-kDa serine/threonine kinase AKT (or protein kinase B, PKB; Bellacosa et al., 1991) is a central signaling node downstream of both extracellular (e.g. insulin, growth factors and cytokines) and intracellular (e.g. Ras) ligands (Dudek et al., 1997;

Downward, 1998; Yano et al., 1998; Bhave et al., 1999). It is involved in multiple cellular processes including cell proliferation, cell survival, cell size control, cell migration, transcription, translation, and metabolism (Marte and Downward, 1997; Coffer et al., 1998; Hanada et al., 2004). Owing to its central involvement in those divergent signaling processes, it is one of the most critical and versatile protein kinases in human physiology and diseases (Bellacosa et al., 2005; Engelman et al., 2006).

The AKT protein family in the mammalian system consist of three isoforms (AKT1/PKBα, AKT2/PKBβ, and AKT3/PKBγ), which share extensive homology with protein kinases A, G, and C at their kinase domains. The amino acid sequences of the AKT isoforms are highly conserved from murine to humans (Yang et al., 2004). All isoforms contain an N-terminal pleckstrin homology (PH) domain, an interdomain linker, a kinase domain, and a C-terminal hydrophobic regulatory motif (Alessi and Cohen, 1998; Coffer et al., 1998; Downward, 1998; Datta et al., 1999).

3.4.1. AKT Pathway

AKT is inactive when it is interacting with the 3-phosphoinositide dependent protein kinase-1 (PDK1) through both their PH and kinase domains. This ‘‘PH-in’’ conformer prevents PDK1 to phosphorylate the activation loop of AKT (Calleja et al., 2007). AKT is activated by translocation to the plasma membrane mediated by the PH domain interaction with phosphatidylinositol (3,4,5)-triphosphate (PIP3), a product of phosphatidylinositol 4,5-bisphosphate (PIP2) phosphorylation by phosphatidylinositol 3-kinase (PI3K) (Alessi and Cohen, 1998). This translocation allows the formation of a ‘‘PH-out’’ conformer which enables the phosphorylation of Thr308 at the activation loop of AKT by PDK1 (Calleja et al., 2007), and the autophosphorylation of Ser473 by Akt itself (Toker and Newton, 2000) or by mammalian target of rapamycin (mTOR) complex 2 (mTORC2; Alessi et al., 1996a; Sarbassov et al., 2005; Jacinto et al., 2006; **Figure 3.5**). Phosphorylation at Thr308 bestows the AKT kinase activity, while at Ser473 engages AKT signaling to a specific set of substrates (Guertin et al., 2006; Jacinto et al., 2006). Collective phosphorylation of both the Thr308 and Ser473 residues result in more than a 1000-fold increase in AKT activity (Alessi and Cohen, 1998).

The negative regulator of this pathway is the lipid phosphatase PTEN, which dephosphorylates PIP3 to PIP2, thereby withdrawing the membrane localization signal for AKT membrane associated activities (Maehama and Dixon, 1998; Stambolic et al., 1998; Hyun et al., 2000).

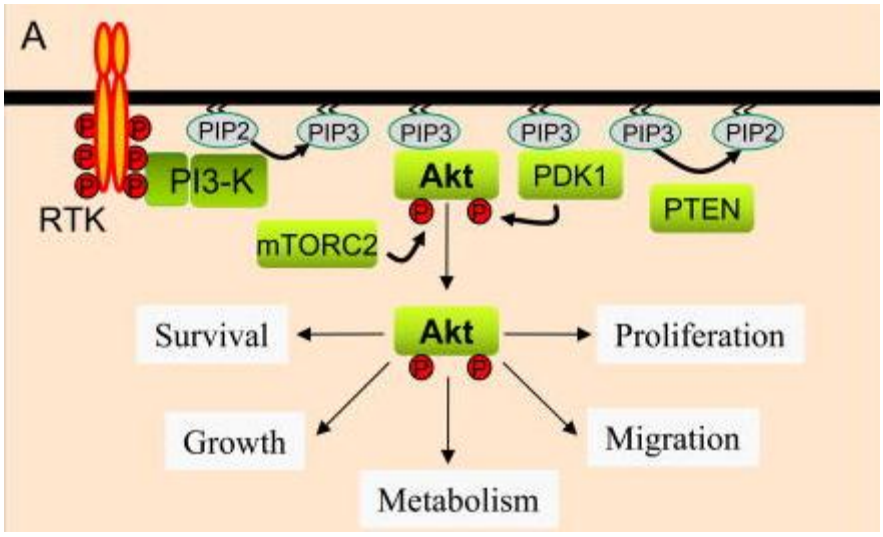

Figure 3.5: The AKT pathway and function

A Schematic illustration of the AKT signaling pathway. Activated PI3-kinase converts PIP2 into PIP3, which recruits PH domains containing proteins to the plasma membrane, including AKT and PDK1. AKT is then phosphorylated by PDK1 at the kinase domain and by mTORC2 at the hydrophobic motif. Dependent on cellular context, activated AKT phosphorylates a wide array of downstream targets which regulate a broad spectrum of cellular functions. (Adapted from Gonzalez and McGraw, 2009b)

3.4.2. AKT substrates

AKT phosphorylates a plethora of substrate proteins at the serine(S)/threonine(T) residue of a consensus sequence, R-X-R-X-X-S/T-B (Alessi et al., 1996b; Datta et al., 1999), where R is the abbreviation of Arginine, X is a site for any amino acid and B represent bulky hydrophobic residues. But yet, ~25% out of the 100+ reported non-redundant AKT substrates do not contain the consensus site (Manning and Cantley, 2007).

The huge body of identified AKT substrates include: GSK-3α and β(Cross et al., 1995; Diehl et al., 1998), mechanistic target of rapamycin (mTOR; Nave et al., 1999), Tuberous Sclerosis Complex 2 (TSC2) (Inoki et al., 2002), BCL-2 family member Bad (Datta et al., 1997), forkhead transcription factors (Brunet et al., 1999), c-Raf (Zimmermann and Moelling, 1999), and caspase-9 (Cardone et al., 1998). Many of them play important roles in cell survival, growth and metabolism.

3.4.3. AKT functional role in nervous system

AKT is highly expressed in the central nervous system, it is involved in a wide range of neuronal functions including neuronal cell survival (Dudek et al., 1997; Datta et al., 1999), dendrite and spine morphogenesis (Dudek et al., 1997; Jaworski et al., 2005; Grider et al., 2009; Lee et al., 2011a; Majumdar et al., 2011), axonal growth (Atwal et al., 2000; Markus et al., 2002), late forms of synaptic plasticity (Huang et al., 2013), postsynaptic neurotransmitter receptor localization (Serantes et al., 2006; Lee et al., 2013a), bulk endocytosis of synaptic vesicles (Smillie and Cousin, 2012) and general excitability (Howlett et al., 2008; Lin et al., 2011).

The importance of AKT in the nervous function is further demonstrated by its association with human physiological diseases including Schizophrenia (Emamian et al., 2004; Thiselton et al., 2008; Freyberg et al., 2010; Mathur et al., 2010; Emamian, 2012; Ripke et al., 2014), Autism spectrum disorder (Ebert and Greenberg, 2013) and Bipolar disease (Toyota et al., 2003; Karege et al., 2010).

3.5. Mammalian AKT isoforms

3.5.1. Sequence identity and diversity

The overall amino acid sequence of the three AKT isoforms (AKT1/PKBα, AKT2/PKBβ, and AKT3/PKBγ) share high similarity (~80%), whereas the similarity of pleckstrin homology domain is >75%, linker region >17%, kinase domain >87%, and the C-terminal hydrophobic motif >66% (Kumar and Madison, 2005). The two key activation phosphorylation sites are highly conserved (AKT1: Thr308/Ser473; AKT2:

Thr309/Ser473; AKT3: Thr305/Ser472) (Alessi et al., 1996b). Nevertheless, sequence alignment of human AKT isoforms has identified regions (with refers to amino acids numbering in AKT1: 43–50, 111–145, and 453–465) with substantial sequence diversity (Santi and Lee, 2009).

3.5.2. Tissue and cellular expression

Their functional specificity can be inferred from the isoforms' distinct tissue distribution. AKT1 is widely expressed across tissues including the brain, heart, lung, skeletal muscle, thymus, and skin; AKT2 is predominantly expressed in insulin-responsive tissues, such as adipose tissue, heart, liver, kidney, and skeletal muscle; whereas AKT3 is mostly expressed in the brain, with lower expression in skeletal muscle, pancreas, heart, and kidney (Konishi et al., 1994; Altomare et al., 1995; Chong et al., 2005; Yang et al., 2005). The functional differences can be further demonstrated in the diverse isoforms subcellular compartmentalization. AKT1 localizes mainly in the cytoplasm and a substantial portion at the plasma membrane. AKT2 localizes mainly at the mitochondria (which is at its phosphorylated and active form; Bijur and Jope, 2003) and a minor population at the Golgi apparatus. AKT3, on the other hand, localizes in the nuclear membrane, and is the only AKT isoform presented in the nucleus (Gonzalez and McGraw, 2009a; Santi and Lee, 2009). Furthermore, deregulation of specific isoform was reported in cancers, where hyperactivity of AKT1 in thyroid and non-small cell lung cancers (Lee et al., 2011b; Saji et al., 2011); AKT2 in glioma (Zhang et al., 2009); and AKT3 in melanoma (Stahl et al., 2004) were observed.

3.5.3. *In vivo* function

The specialized physiological function of the isoforms is more prominent in the phenotypic data of knockout mice. AKT1−/− mice are having reduced viability, the survivors exhibit 15–20% shrinkage in body size (Chen et al., 2001). They also have a smaller brain, liver and heart. Diminished cell numbers were found in the brain and liver (Easton et al., 2005), indicating the involvement of AKT1 in regulating proliferation. A reduction in cell size was observed in the heart (Easton et al., 2005), reflecting the functioning of AKT1 in cell growth in a rather tissue specific manner. The differential

effect of AKT1 knockout in different tissue suggested the dependence of AKT1 signaling on cellular context. The AKT2−/− mice developed a Type-2 diabetes mellitus phenotype, which highlighted its importance in glucose metabolism (Cho et al., 2001). AKT3−/− mice did not show growth retardation but exhibited a 25% reduction in brain size contributed by both reduction in cell number and cell size (Easton et al., 2005), which revealed its specific function in brain development. Interestingly, more severe phenotypes were observed in AKT isoforms double knockout mice. AKT1/2−/− mice survived only shortly after birth and manifested severe dwarfism, skeletal muscle atrophy, impaired skin, adipogenesis, and osseous development (Peng et al., 2003), which reflects a functional redundancy between AKT1 and 2. AKT1/3−/− mice embryo died between E11-E12, indicating the functional overlap of AKT1 and 3 in the developmental stage (Yang et al., 2005). AKT2/3−/− mice are viable but exhibited smaller body size (Dummler et al., 2006), which demonstrated a dominant role of AKT1 in development and body function.

3.5.4. Affinity and catalytic efficiency

The three isoforms show interesting differences in their biochemical properties. AKT2 exhibited the lowest affinity for ATP and around 5-fold higher K_m value (substrate concentration to attain half maximum of the reaction rate) than that of AKT1 and 3 (Zhang et al., 2006). This property may allow AKT2 to serve as an ATP sensor in regulating glucose metabolism.

The catalytic efficiency of AKT isoforms also varies. Protein expression analysis revealed that AKT3 dominated 50% of total AKT activity in the mouse brain (Easton et al., 2005; Zhang et al., 2006). Consistently, AKT3 was shown phosphorylating ~15-fold more effectively than AKT1, while AKT1 being ~10-fold more effective than AKT2 (Cristiano et al., 2006). Interestingly, the difference in catalytic efficiency varies with substrate identity. In experiments using purified isoforms and model peptide substrates, AKT3 is ~47-fold more active than AKT1 in phosphorylating the synthetic peptide RPRAATF, but is only 5-fold more active in phosphorylating ribosomal protein S7 (rpS7; Lee et al., 2011c). Nevertheless, the hierarchy ranking (i.e. AKT3>AKT1>AKT2)

of catalytic efficiency across isoforms did not change, small amounts of AKT3 seem to be sufficient to attain its cellular function (Lee et al., 2011c).

3.6. *Drosophila* AKT modulates spontaneous vesicle release

The *Drosophila* genome contains only one copy of AKT (Franke et al., 1994; Staveley et al., 1998) that is expressed ubiquitously during development (Howlett et al., 2008; Lin et al., 2011), and localized at the presynaptic terminals of larval neuromuscular junctions (NMJ; Martin-Pena et al., 2006; Howlett et al., 2008; Lin et al., 2011). The *Drosophila* AKT protein's critical phosphorylation sites are Ser505 and Thr342, which are homologous to the mammalian activation sites Ser473 and Thr308, respectively (Linassier et al., 1997; Staveley et al., 1998; Scanga et al., 2000; Jin et al., 2001).

An earlier study in our laboratory has identified a novel role of AKT in regulating spontaneous vesicle release at the glutamatergic synapses of *Drosophila* NMJ (Ge*, Leung* et al., *under revision*). Suppressing AKT activity by acute pharmacological (30 mins MK-2206) treatments (**Figure 3.6 A-B**) or genetic AKT-RNAi mediate knockdown (**Figure 3.6 C**) strongly enhanced the rate of spontaneous transmitter release, the mechanism of which being independent of extracellular calcium (**Figure 3.6 B**, black bars). Conversely, over-expression of a membrane-linked constitutive active form of AKT (myristoylated AKT; myr-AKT; Verdu et al., 1999) suppressed spontaneous release (**Figure 3.6 C**). This bidirectional effect of hyper/hypo-AKT activity suggested that the prevailing rate of spontaneous transmitter release is subjected to tight homeostatic regulation by presynaptic AKT. Our data further demonstrated that the AKT-mediated regulation of spontaneous release requires a PIP3 dependent membrane anchorage of AKT (Marte and Downward, 1997). Sequestration of PIP3 by inhibiting PI3K (LY-294002) resulted in the enhancement of spontaneous vesicle release to an extent similar to inhibiting AKT directly (**Figure 3.6 D**), while blocking the degradation of PIP_3 by the lipid-phosphatase PTEN (VO-OHpic or PTEN-RNAi) significantly reduced spontaneous vesicle release (**Figure 3.6 E**).

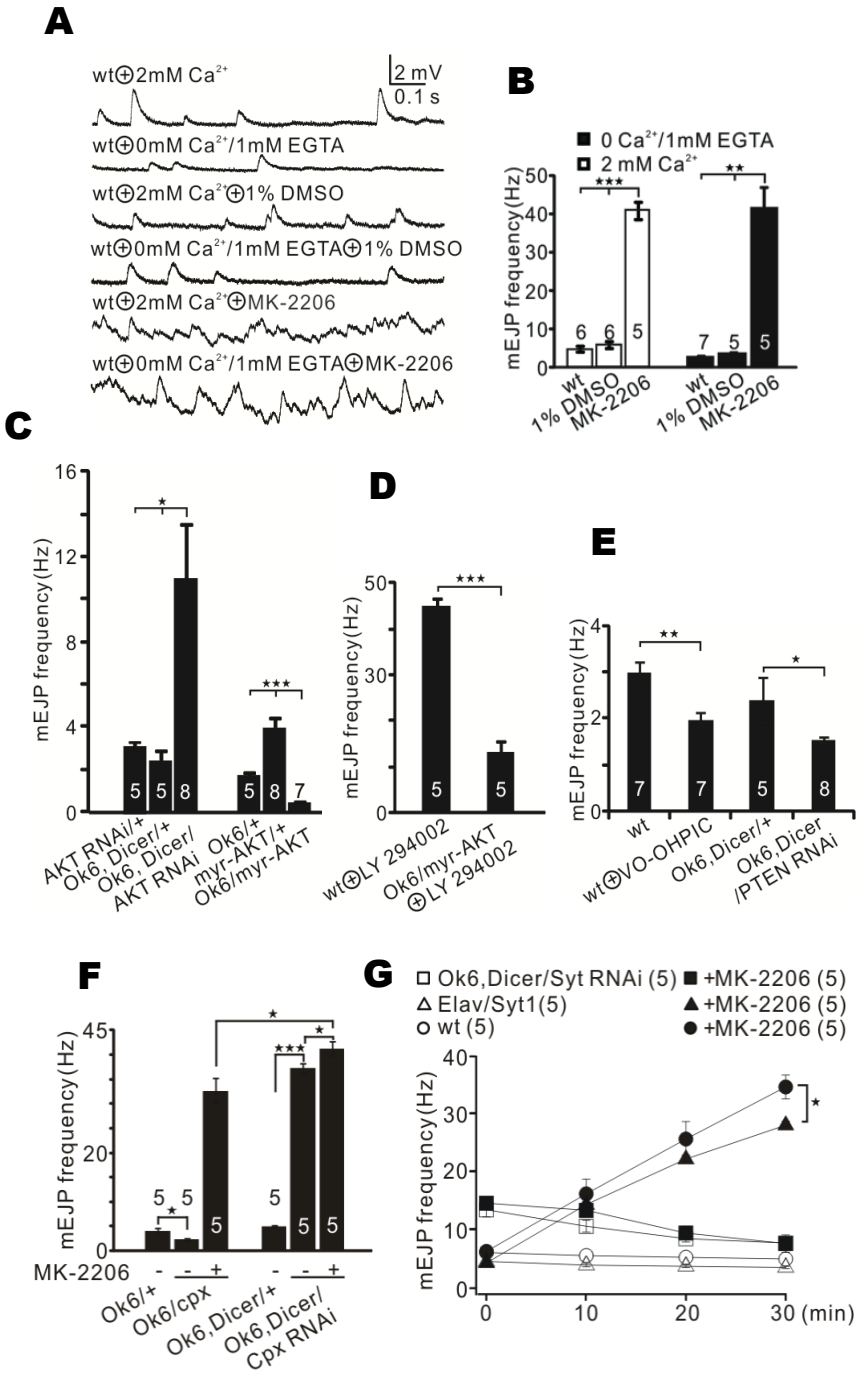

Figure 3.6: The AKT pathway regulates spontaneous vesicle release at *Drosophila* larvae NMJ

A Representative traces of miniature excitatory junctional potentials (mEJPs) recorded under the indicated conditions from *Drosophila* larvae NMJ. **B** AKT inhibition (MK-2206) strongly increased the frequency of mEJPs relative to controls in the presence or absence of extracellular calcium. **C** AKT-knockdown in motor neurons increased the frequency of mEJPs, over-expression of constitutive active myristoylated AKT (myr-AKT) suppressed it. **D** The PI3K inhibitor LY-294002

enhanced the frequency of mEJPs. This effect was reduced by overexpressing the myr-AKT transgene, which confirmed that the effect of PI3K inhibition acts via AKT. **E** PTEN inhibition (VO-OHPIC) or PTEN knockdown reduced the frequency of mEJP. **F** Overexpression of Complexin (Cpx) in motor neurons reduced the rate of mEJP and weakened the effect of inhibiting AKT (MK-2206). Cpx-knockdown strongly enhanced the rate of mEJP, which increased further by AKT inhibition. **G** The mEJP frequency changes in the course of 30 mins MK-2206 (filled data points) or DMSO (unfilled data points) treatments in the indicated genotypes. Synaptotagmin1(Syt1)-knockdown (squares) abolished the sensitivity of mEJP frequency towards MK-2206 treatment. Data represent means ± S.E.M *p<0.05; **p<0.01; ***p<0.001 (Adapted from Ge*, Leung* et al., *under revision*).

Interestingly, successive experiments suggested that the mechanism of the AKT-mediated regulation of spontaneous release relies on the fusion clamp of the vesicle release machinery. First, over-expression of Complexin (Cpx) which resulted in a strengthened fusion clamp significantly weakened the effect of inhibiting AKT, while Cpx-knockdown exacerbated the enhancement of spontaneous release by AKT inhibition (**Figure 3.6 F**). Second, knockdown of Synaptotagmin 1 (Syt 1) abolished the sensitivity of spontaneous release frequency towards AKT-blockade (filled squares in **Figure 3.6 G**). Taken together, our finding from the *Drosophila* NMJ suggested that AKT acts along the PI3K-PTEN-AKT signaling pathway onto the calcium sensor Syt 1, which results in functional shift of the vesicular fusion-clamp machinery leading to an altered rate of spontaneous vesicle release.

3.7. Aim of study I

Our earlier finding from the *Drosophila* NMJ suggested that AKT regulates spontaneous vesicle release by acting along the PI3K-PTEN-AKT signaling pathway onto the calcium sensor Syt 1 (Ge*, Leung* et al., *under revision*). Since the preference for spontaneous versus evoked vesicle release seems to be regulated differentially at individual synapse, this finding offers a well fitting mechanism for which a dynamic regulation is achieved. Interestingly, the AKT signaling pathway and the vesicle release machineries are evolutionarily highly conserved. In addition, AKT has been repeatedly reported as risk gene for neurological diseases such as Schizophrenia (Zheng et al., 2012) and Autism Spectrum Disorders (ASD; Ebert and Greenberg, 2013). Our identification of

a novel synaptic role of AKT at *Drosophila* NMJs and its potential conservation in the mammalian system might implicate an intriguing new mechanism that could be responsible for human disease conditions. To gather more insights into the functional role of AKT on the vesicle release machinery in the *Drosophila* NMJ and mammalian central synapse, this study aims to:

1. **Examine whether spontaneous vesicle release is regulated by AKT in rat hippocampal cultured neurons, at both excitatory and inhibitory synapses.** The effects of acute pharmacological inhibition of AKT, the AKT positive (PI3K) and negative (PTEN) modulators, as well as the sensitivity of AKT inhibition towards extracellular calcium were examined.

2. **Investigate whether AKT regulate the vesicle release machinery in a way that affects evoked vesicle release, at both *Drosophila* NMJs and hippocampal cultured neurons.** This is to provide insight onto whether the same group of molecular players involving spontaneous and/or evoked vesicle release is under the control of AKT, and implicate the potential dynamic switching of the vesicle release machinery clamping function by AKT activity.

3. **Access the effect of acute blockage of AKT on neuronal spiking activity.** The spike frequency, burst activity and overall neuronal excitability were accessed under pharmacological blockage of the AKT/PI3K pathway. Identifying the neuronal spike properties under acute AKT inhibition would envision our interpretation of the AKT etiological mechanism in neurological disease conditions such as Schizophrenia and ASD, where AKT hypo-activity was reported.

4. **Test the effect of knocking-down Synatotagmin 1 and specific AKT isoforms on AKT modulated spontaneous vesicle release at hippocampal synapses.** To this end, recombinant adeno-associated virus (rAAV) carrying specific shRNAs were produced to mediate the corresponding gene silencing. The knock-down targets were: Synatotagmin 1, the calcium sensor that is required to translate AKT activity onto the vesicle release machinery at *Drosophila* NMJ; AKT1, the ubiquitously expressed AKT isoform; and AKT3, the AKT isoform that predominantly expressed in the

brain. The goal is to understand the degree of conservation of the AKT pathway, to examine the potential downstream target of AKT in hippocampal neurons, and to explore the AKT isoforms specificity. Furthermore, the working rAAVs would provide a robust tool for *in vivo* experiments in the future study.

3.8. Calcium dynamics

Calcium is a ubiquitous messenger involved in a wide array of signaling pathways. To selectively orchestrate those downstream signals, spatial temporal control of the calcium signal is of great importance for cellular function.

The spatiotemporal calcium dynamics is mainly controlled by the kinetics of the calcium 'sources' (e.g. influx through the plasma membrane and the release from intracellular stores), the spatial diffusion of calcium, the binding to calcium buffer systems (mobile and immobile calcium-binding systems) and the working of the calcium 'sinks' (e.g. extrusion out of the plasma membrane or uptake to the intracellular calcium stores). They are regulated differentially to tailor for the divergent cellular signals. For example, to achieve fast exocyctosis, the voltage-gated calcium channel and release sites are tightly clustered (via direct physical association or tethering by scaffolding proteins) and bathed in strong buffers, which confines the signal towards the calcium sensors and excludes it from slow long-range pathways. In contrast, hormone and peptide secretion employs a looser coupling between calcium source and target, which renders them more vulnerable to the calcium uptake, pumps and exchangers function (Oheim et al., 2006; Fakler and Adelman, 2008).

3.8.1. Calcium nano/microdomain

To classify the spatial-temporally different calcium mediated processes, (Neher, 1998; Augustine et al., 2003) proposed the terminology: nanodomain and microdomain. Nanodomain refers to the immediate vicinity of calcium channels (within ~20 to 50 nm of the calcium source). The signaling processes within this region are influenced by BAPTA (a fast calcium chelator with binding rate constants 150 times quicker than

EGTA (Naraghi and Neher, 1997). Microdomain refers to the subcellular regions of elevated calcium (between 50 nm and 1 μm from the calcium source). Processes that are equally sensitive to BAPTA and EGTA are located in this region (Naraghi and Neher, 1997).

In both calcium domains, the magnitude and speed of the calcium signal relate inversely, although at different scales, to the distance between the calcium source and sensor. In nanodomains, the peak calcium reaches around 100 μM, the calcium rise and decay takes microseconds. In microdomains on the other hand, the peak calcium ~1-5 μM is substantially smaller, and the calcium rise and decay occurs at millisecond timescale (Naraghi and Neher, 1997; Fakler and Adelman, 2008).

Moreover, nano or microdomain can be manipulated dynamically to achieve plasticity. Tight calcium channel and sensor coupling within the nanodomain (10 to 20 nm) tends to dominate at mature brain (Fedchyshyn and Wang, 2005; Bucurenciu et al., 2008; Christie et al., 2010; Scimemi and Diamond, 2012; Schmidt et al., 2013; Brachtendorf et al., 2015), while loose coupling within the microdomain (~100 nm) were preferentially expressed in early developmental stages (Borst and Sakmann, 1996; Meinrenken et al., 2002) or in plastic synapses of matured neurons (Nadkarni et al., 2012). Loose coupling permits presynaptic short term facilitation through saturation of endogenous calcium buffers (Rozov et al., 2001), while the transformation into tight coupling by alternation in the coupling distance and local calcium buffers concentration may contribute a presynaptic mechanism for long term potentiation (Kamiya et al., 2002; Vyleta and Jonas, 2014).

3.8.2. The calcium channels

The voltage-activated calcium channels (VACC) are the main calcium entry path for triggering synaptic transmission in neurons (Tsien et al., 1988; Dunlap et al., 1995; Catterall et al., 2005). They consist of typically 4-5 subunits: the main α1, α2 and δ subunit, and auxiliary β and γ subunits (Takahashi et al., 1987; Catterall, 2011). In vertebrates, 10 VACC α-subunits were classified into three families according to sequence similarities: Cav1, Cav2 and Cav3 (Dolphin, 2009). They are further grouped

into L, P/Q, N, R or T -type (Tsien et al., 1988; Wheeler et al., 1994; Jun et al., 1999; Catterall, 2011) according to electrophysiological and pharmacological characteristic. The T (transient)-type channels activate and inactivate quickly which conducts small currents, they belong to the low voltage activated (LVA) channels, which are activated at around -70 mV (Carbone and Lux, 1984; Nowycky et al., 1985). The L, P/Q, N and R-types belong to the high voltage activate (HVA) channels which require -30 mV for activation. The L-type channels were identified by their large and long lasting current conductance (Carbone and Lux, 1984; Nowycky et al., 1985). The N(neuronal), P-, Q-, and R-type calcium channels are most prominent in neurons, they exhibit intermediate conductance characteristic between L and T-type channels (Nowycky et al., 1985), and were distinguished according to their sensitivity towards peptide toxins (summarized in **Table 3.1**; Llinas and Yarom, 1981; Nowycky et al., 1985; Llinas et al., 1989; Mintz et al., 1992; Randall and Tsien, 1995; Tottene et al., 1996; Newcomb et al., 1998). Sychronous and spontaneous vesicle releases are triggered mainly by calcium influx through P/Q or N-type channels (Momiyama and Takahashi, 1994; Jun et al., 1999; Wheeler et al., 2008). Interestingly, recent study has shown that P/Q-, N- and R-type channels accounts for half of all spontaneous glutamate release at rat cultured hippocampal synapses, in which the R-type channels exhibit a prominent inclination towards spontaneous over-evoked release (Ermolyuk et al., 2013).

Table 3.1: Classification of vertebrate VACC (Adapted from Welling, 2009)

family	current	former name	new name	distribution	blockers
HVA channels	L-type	α_{1S}	$Ca_V1.1$	skeletal	DHPs (e.g. Nifedipine), PAAs (e.g. Verapamil), BTZs (e.g. Diltiazem)
		α_{1C}	$Ca_V1.2$	heart smooth muscle[1]	
		α_{1D}	$Ca_V1.3$	neuroendocrine[2]	
		α_{1F}	$Ca_V1.4$	retina	
	P/Q-type	α_{1A}	$Ca_V2.1$	neuronal	ω-Agatoxin IVA
	N-type	α_{1B}	$Ca_V2.2$	neuronal	ω-Conotoxin GVIA
	R-type	a_{1E}	$Ca_V2.3$	neuronal	SNX 482
LVA channels	T-type	α_{1G}	$Ca_V3.1$	neuronal, cardiac	Mibefradil[3], Kurtoxin[3], Ni^{2+}
		α_{1H}	$Ca_V3.2$	neuronal, cardiac	Mibefradil[3], Kurtoxin[3], Ni^{2+}
		α_{1I}	$Ca_V3.3$	neuronal	Mibefradil[3], Kurtoxin[3], Ni^{2+}

[1] also expressed in endocrine and neuronal cells, [2] also described in cardiac pacemaker cells and cochlear hair cells, [3] not highly specific

The *Drosophila* genome contains three gene products encoding the VACC α1 subunits, each correspond to the putative homolog of the vertebrate family (*Dmca1D*: Ca_v1; *Dmca1A*: Ca_v2; *DmαG*: Ca_v3; Zheng et al., 1995; Littleton and Ganetzky, 2000; King, 2007). They are all activated at around −40 mV (Leung and Byerly, 1991; Gielow et al., 1995).

Dmca1A, also known as *cacophony* (*cac*), is homologous to the vertebrate N, P, and Q-type channels. It is expressed at the central synapses (Gu et al., 2009) and the NMJ. In the NMJ, it plays an important role in synaptic release vesicle (Kawasaki et al., 2000; Kawasaki et al., 2002; Kawasaki et al., 2004) and developmental regulation (Xing et al., 2005). The *Drosophila* N-type calcium channels do not contain a synprint domain, the bind site for syntaxin in mammalian N-type channels) (Littleton and Ganetzky, 2000), mechanism on how it is tethered to the vesicle release machinery is remained to be elucidated.

Dmca1D is homologous to the vertebrate L-type channels (Zheng et al., 1995). It is responsible for the somatodendritic HVA current at *Drosophila* motor neurons (Worrell and Levine, 2008) and the major dihydropyridine-sensitive current in *Drosophila* larval muscle fibers (Ren et al., 1998).

Dmα1G is homologous to the vertebrate LVA T-type channel. It is expressed in muscle (Gielow et al., 1995) and potentially in embryonic motor neurons (Baines and Bate, 1998). The function of this gene remains unclear. Nevertheless, its sequence homology with the vertebrate T-type channel (Littleton and Ganetzky, 2000) and the existence of steady-state inactivation current at −30 mV in larval body wall muscle (Gielow et al., 1995; Ren et al., 1998) infers its potential function in conducting the *Drosophila* LVA current.

3.8.3. Calcium buffers and sink

Besides the influx control from channels, the sequestration of free calcium by buffering and extrusion from the cytoplasm plays an important role in the overall dynamics. Typically, more than 95% of the calcium influx through a single action potential is rapidly sequestrated by endogenous fast calcium buffers (Neher, 1995). Those

buffers include the parvalbumin, calbindin and calretinin, and also the calcium sensors troponin C (TnC) and calmodulin (CaM) (Gariepy and Hodges, 1983) which confers the downstream signaling function.

Cytoplasmic calcium is also actively removed by pumps and exchangers, either into internal store (endoplasmic reticulum (ER) and mitochrondria) or outside the plasma membrane. In *Drosophila* larval motor terminals, calcium extrusion is predominantly executed by the plasma membrane calcium ATPase (PMCA), which was also strongly expressed at *Drosophila* larval NMJ (Chouhan et al., 2010). Moreover, calcium uptake through the SERCA (sarco-ER calcium ATPase) into the ER is also substantially involved in calcium clearance at these motor terminals (Sanyal et al., 2005; Lnenicka et al., 2006). However, blocking the *Drosophila* Na/Ca exchanger (CalX) and calcium uptake by mitochondria did not appear to play an important role in removing free cytosolic calcium during single or 5 seconds of 10 Hz action potential stimulation (Chouhan et al., 2010).

3.8.4. Bouton types at the Drosophila neuromuscular junction

The *Drosophila* NMJ is a robust system for the study of synapse physiology. Relative to the mammalian system, it is genetically easy to manipulate and molecularly simple. Above all, the functional roles of many molecules that have been identified in the *Drosophila* NMJ are conserved in vertebrates (Vactor et al., 1993).

The motor neuron axons terminals that are innervating the NMJ consist of swollen structures: the synaptic boutons, which are grouped into three types. The predominantly large boutons were referred as type I, while the small boutons were referred as type II (Johansen et al., 1989). According to size differences, type I boutons were subdivided into type 1b (“big”, diameter about 3-6 μm) and type 1s (“small”, diameter about 2-4 μm) (Atwood et al., 1993b; Budnik, 1996). An additional bouton type that is exclusive for harboring insulin in their terminal, found only on a few muscles, was referred to as type III (Johansen et al., 1989; Gorczyca et al., 1993; Jia et al., 1993; Nishikawa and Kidokoro, 1995; Guan et al., 1996; DiAntonio et al., 1999; **Figure 3.7**).

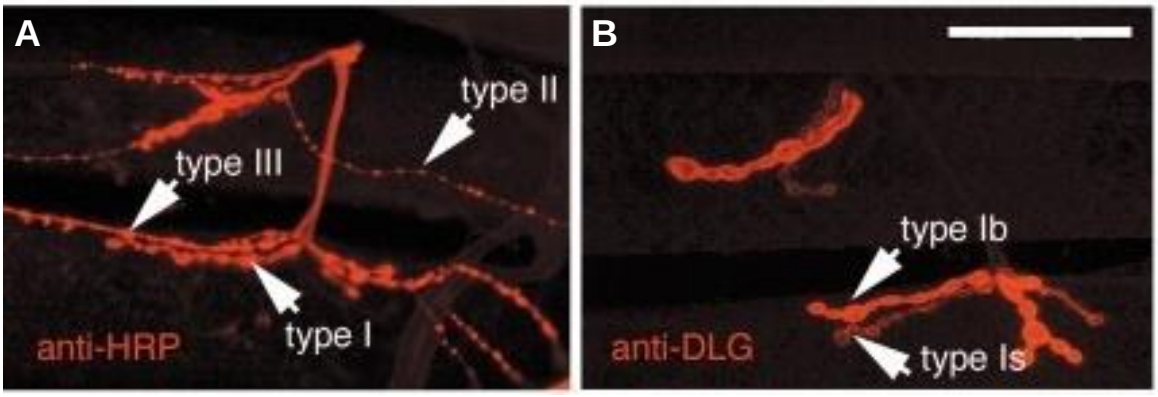

Figure 3.7: Type of motor neuron at *Drosophila* NMJs

Immunohistochemistry image of *Drosophila* NMJs muscles 12 and 13 stained with (**A**) anti-HRP for the presynaptic arbor and (**B**) anti-DLG for postsynaptic muscle region, which illustrated the bouton Type 1b, 1s, II and III processes. Scale bar: 50 µm. (Modified from Packard et al., 2002)

3.8.5. Type 1b and 1s boutons at *Drosophila* neuromuscular junction

In the *Drosophila* larvae, each motor neuron is committed to develop one type of bouton only, the determination of bouton type is thought to be an outcome of both environmental and cell-autonomous factors (Hoang and Chiba, 2001). At muscle 6/7, a conventional site for electrophysiology recording, the innervations were mostly type 1b and 1s. In general, 1b motor neurons are muscle specific, which innervate one or few muscles, while the 1s are less muscle specific where each neuron innervates a large number of muscles (Johansen et al., 1989; Gorczyca et al., 1993; Jia et al., 1993; Nishikawa and Kidokoro, 1995; Guan et al., 1996; DiAntonio et al., 1999).

With regard to physiology, type 1s motor neurons exhibit a less depolarized resting potential and less hyperpolarized voltage threshold, longer spike delay in response to current injection (Choi et al., 2004; Schaefer et al., 2010), and larger evoked excitatory junctional potentials (eEJPs) amplitudes (Lnenicka and Keshishian, 2000). It has been proposed that the type Ib and Is synapses resemble the tonic and phasic nerve endings respectively (Atwood et al., 1993a; Kurdyak et al., 1994; Nishikawa and Kidokoro, 1995; Stewart et al., 1996). The insensitivity to short and non-summating input of type 1s motorneurons confers the function of a low-pass filter (Byrne et al., 1979), which might serve in orchestrating a large number of functionally related muscles. On the other hand,

the higher tendency to spike and shorter spike delay of type 1b motorneurons allows them to execute specific muscle contraction pattern, which serves for fine tuning the locomotion (Choi et al., 2004).

3.8.6. Three-dimensional modeling of the *Drosophila* NMJ bouton

Our laboratory has established a joint collaborative project with the theoretical group of Prof. Gillian Queisser (Goethe-Universität Frankfurt), in which a detailed three-dimensional mathematical model of presynaptic vesicle dynamics of the synaptic bouton of *Drosophila* NMJ was developed (M. M. Knodel, 2014). This model reconstituted highly detailed three-dimensional density profiles of presynaptic vesicles by numerical simulations, which provide a robust tool for reproducing the local dynamics of vesicles as a function of bouton size, vesicle release probability and stimulation pattern.

There we demonstrated that vesicle diffusion is the key factor that limited neurotransmission at extended high frequency stimulation, which aligned well with experimental observations. We further tested those mathematic parameters on the functional profiles of the two bouton types. The type 1b bouton has a lower release probability (5%) (M. M. Knodel, 2014), owing to its bigger size, it accommodates more release sites (800 synapses at muscle 6/7; Atwood et al., 1993b) and harbors larger functional reservoir of vesicles. The combined bouton properties allows it to serve optimally for sustained bouts of synaptic activity (natural firing frequency ramp from 20-40-20Hz;M. M. Knodel, 2014). In contrast, the release probability of type 1s is substantially higher (40%; M. M. Knodel, 2014), it accommodates fewer release sites (250 synapses at muscle 6/7; Atwood et al., 1993b) and a smaller pool of mature vesicles, which renders the vesicles to become rapidly diffusion-limited and thus only able to sustain short trains of stimulation (natural firing frequency below 20Hz; Lnenicka and Keshishian, 2000; M. M. Knodel, 2014). This study demonstrated the importance of the physical properties of bouton in synaptic transmission, the size of the bouton is likely regulated to best fit their prevailing firing pattern.

3.9. Aim of study II

The previous collaborative project described above provided a framework for the theoretical reconstruction of the *Drosophila* NMJ bouton in a highly precise and realistic manner, which can be implemented for testing the physical dynamics of other biological players in relation to their functional outcome. One of the most critical biological player that govern a wide array of cellular signaling pathway is calcium. Importantly, calcium is also a key signal for the triggering of presynaptic vesicle release, its spacial regulation is one of the most critical component to be incorporated into the model of presynaptic vesicle dynamics. Therefore, we established a collaborative effort with Martin Stepniewski (AG Prof. Gillian. Queisser, Goethe-Universität Frankfurt) who is simulating a three-dimensional model of calcium dynamics at the synaptic bouton of *Drosophila* NMJ. And this second part of project is to provide experimental data to validate and adjust the mathematical parameters for the construction of a realistic theoretical model, here we aims to:

1. **Access the calcium dynamics within the active zones**. Electrophysiological measurement of paired-pulse ratio would provide data for the simulation of calcium buffering properties and speed of residual calcium clearance in the active zones.

2. **Measure the individual bouton peak calcium rise induced by single stimulation**. This crude data of single stimulation induced peak calcium rise in the entire bouton were estimated by quantitative calcium life imaging, which allows us to test the relationship between peak calcium rise and bouton size.

3. **Compare the calcium dynamics of the two differently sized bouton types that function in disparate ranges of firing frequency**. The calcium dynamics including peak calcium rise, rise tau and decay tau elicited by different physiological stimulation frequency were accessed by calcium life imaging, the performance of the two distinct bouton types were compared. Since the two bouton types function optimally at different firing frequencies, we opt to test if this optimization is achieved by the control of calcium dynamics and if this control is at any degree regulated by the size of the bouton.

4. MATERIALS AND METHODS

4.1. Culture and preparations

4.1.1. Primary hippocampal neuronal culture

Primary hippocampal neurons from new-born Sprague Dawley® rats (*Rattus norvegicus*) were prepared as described previously (Bading and Greenberg, 1991). Hippocampi from the new-born pups were dissected in 1:9 volume ratio of Ky/Mg solution (Ky/Mg, **Table 4.1**) and dissociation medium (DM, **Table 4.2**). The tissue was dissociated in enzyme solution (**Table 4.3**) for 20 min at 37°C, the process was repeated once with replenishment of fresh enzyme solution. Enzyme activity was then halted by trypsin inhibitor solution (**Table 4.4**) at 37°C for 5 min, this process was repeated 3 times with fresh inhibition solution exchange. The hippocampi were then washed 3 times with neurobasal-A/growth medium (GM, **Table 4.5**) and then dissociated into single cell suspension by gentle pipeting. The suspension was then diluted in Opti-MEM (Invitrogen, supplemented with 20 mM Glucose) to achieve a concentration of about 0.5 hippocampi/2 ml. Cells were plated on poly-D-lysine/laminin (2µg poly-D-lysine/cm^2 + 1µg laminin/cm^2, BD Biosciences) coated 35mm plastic dishes containing four 12mm diameter glass coverslips (2 ml/dish) or 4-well plates with or without coverslip (500 µl/well) to achieve a density of 400-600 cells/ mm^2. 2.5 hours after plating, the medium was replaced with fresh GM (2 ml/dish). On day *in vitro* (DIV) 3, the culture was treated with cytosine β-D-arabinofuranoside (AraC, Sigma-Aldrich) at a working concentration of 2.8 µM to inhibit non-neuronal cells proliferation. On DIV 8, GM was changed to transfection medium (TM, **Table 4.7**). Thereafter, the cultures were maintained by half medium changed every other day and stored in a humidified incubator at 37 °C with 5 % CO_2.

Table 4.1: Ky/Mg solution (Ky/Mg)	
Kynurenic acid	158.56 mg
Phenol Red	0.4 ml
NaOH (1 M)	5x 200 µl
Hepes (1 M)	0.4 ml
$MgCl_2$ (2 M)	4.0 ml
H_2O	to 80.0 ml

Sterile filtered through 0.22 µm Millipore filter and stored in 5 ml aliquots at -80°C

Table 4.2: Dissociation medium (DM)	
Na_2SO_4 (1 M)	20.45 ml
K_2SO_4 (0.25 M)	30.0 ml
$MgCl_2$ (1.9 M)	0.77 ml
$CaCl_2$ (1 M)	0.063 ml
Hepes (1 M)	0.25 ml
Phenol Red	0.5 ml
Glucose (2.5 M)	2.0 ml
H_2O	to 250.0 ml

Sterile filtered through 0.22 µm Millipore filter

Table 4.3: Enzyme Solution	
DM	45.0 ml
Ky/Mg	5.0 ml
L-cysteine	22.5 mg
(Adjust pH with 0.2 M NaOH until Phenol Red turns slightly to purple)	
Papain latex	500 units

After papain latex was completely dissolved (takes 15 min), sterile filtered through 0.22 µm Millipore filter, aliquoted and stored at -20°C

Table 4.4: Inhibitor solution	
Ky/Mg	9.6 ml
DM	86.4 ml
Trypsin inhibitor	1.0 g
(Adjust pH with 0.2 M NaOH)	
Papain latex	500 units

After trypsin inhibitor was completely dissolved (takes 10 min), sterile filtered through 0.22 µm Millipore filter, aliquoted and stored at -20°C

Table 4.5: NB-A / Growth medium (GM)	
Neurobasal A-medium	96.5 ml
B27	2.0 ml
1 % Ratserum	1.0 ml
L-glutamine (200 mM)	0.25 ml
Pen/Strep	0.5 ml

Sterile filtered through 0.22 µm Millipore filter

Table 4.6: Salt Glucose Glycin solution (SGG)	
NaCl (5 M)	11.4 ml
NaHCO3(7.5 % solution)	14.6 ml
MgCl2 (1.9 M)	0.264 ml
CaCl2 (1 M)	1.0 ml
KCl (3 M)	0.882 ml
Hepes (1 M)	5.0 ml
Glucose (2.5 M)	6.0 ml
Glycin (1 M)	0.5 ml
Na-pyruvate (0.1 M)	2.5 ml
Phenol Red	1.0 ml
H2O	to 500.0 ml

Sterile filtered through 0.22 µm Millipore filter

Table 4.7: Transfection medium (TM)	
SGG	88.0 ml
MEM (without glutamine)	10.0 ml
Insulin-Transferrin-Selenium	1.5 ml
Pen/Strep	0.5 ml

Sterile filtered through 0.22 µm Millipore filter

4.1.2. Preparation of *Drosophila* larval neuromuscular junction

Drosophila larvae of the desired genotypes were reared under standardized culture conditions (constant 25°C, 75% humidity, and standard cornmeal fly food, **Table 4.8**) and used as mid-third instar larvae shortly before the onset of the wandering stage. Size-matched mid third instar larvae (4 days after egg laying) were dissected in Hemolymph-like 3 solution (Stewart et al., 1994; HL3, **Table 4.9**). Larvae were pinned to the bottom of a Sylgard®-covered (Sylgard® 184, Dow Corning Corporation, MI, USA) recording chamber and opened up along the dorsal midline. All internal organs including the trachea, gut, and fat body were removed to expose the larval body wall muscles. All segmental nerves were severed and the ventral brain was detached. Freshly prepared larval filets were then drawn to image or electrophysiology recording.

Table 4.8: Cornmeal fly food ingredients

Ingredients	Weight	Percentage%
Corn meal	800 g	6,4%
Malt extract	800 g	6,4%
Dry yeast	180 g	1.44%
Soy bean meal	100 g	0.8%
Molasses	220 g	1.76%
Agar	80 g	0.64%
Propionic acid	62.5 ml	0.5%
Water	10-12 liter	

Table 4.9: Hemolymph-like 3 solution (HL3)

NaCl	70 mM
KCl	5 mM
$NaHCO_3$	10 mM
HEPES	5 mM
Trehalose	5 mM
Sucrose	115 mM
$CaCl_2$	0.5/7.5/1.0/1.5 mM
$MgCl_2$	2/20 mM

pH adjusted to 7.2

4.2. Generation and use of short hairpin RNA gene silencing rAAV

4.2.1. Cloning of the shRNA plasmids targeting Syt1, AKT1 and AKT3 of rats

DNA oligonucleotides (oligos) containing the short hairpin RNA (shRNA) sequences for gene silencing and linkers for cloning were synthesized (**Table 4.10,** Eurofins Genomics).

Table 4.10: Sequence information of DNA oligonucleotides

	Target sequence (5'-3')	Forward oligos (5'-3')	Reverse oligos (5'-3')
shAKT1	ACAACTCAGGTGCTGAGGA (Katome et al., 2003)	GATCCCCACAACTCAGGTGCTGAGGATTCAAGAGATCCTCAGCACCTGAGTTGTTTTTTGGAAA	AGCTTTTCCAAAAAACAACTCAGGTGCTGAGGATCTCTTGAATCCTCAGCACCTGAGTTGTGGG
shAKT3	ATAATATTGGAGAGGAAGA (Katome et al., 2003)	GATCCCCATAATATTGGAGAGGAAGATTCAAGAGATCTTCCTCTCCAATATTATTTTTTGGAAA	AGCTTTTCCAAAAAATAATATTGGAGAGGAAGATCTCTTGAATCTTCCTCTCCAATATTATGGG
shSyt1	GAGCAAATCCAGAAAGTGCAA (Xu et al., 2007; Yang et al., 2010; Bacaj et al., 2013)	GATCCCCGAGCAAATCCAGAAAGTGCAATTCAAGAGATTGCACTTTCTGGATTTGCTCTTTTTGGAAA	AGCTTTTCCAAAAAGAGCAAATCCAGAAAGTGCAATCTCTTGAATTGCACTTTCTGGATTTGCTC GGG

1pmol of each forward and reverse DNA oligos were mixed with 5µl of 10x T4 DNA Ligase Reaction Buffer (New England Biolabs) and annealed in a thermocycler in a reaction volume of 50 µl. At an insert to vector ratio of around 3-fold molar excess, 0.06pmol of the annealed oligos were added and ligated to the rAAV-mCherry vector at the BamHI and the HindIII restriction sites using 1 µl of T4 ligase (New England Biolabs) and 10 µl of 2x Quick ligase Buffer (New England Biolabs) in a reaction volume of 20 µl. Ligations were incubated for 20 mins at room temperature. The ligated products and a control plasmid shSCR_mCherry (with an insert carrying the same hairpin backbone but non-targeting shRNA sequence 5′-GTGCCAAGACGGGTAGTCA-3′, kindly provided by Dr. Yan-Wei Tan, Neurobiology, Im Neuenheimer Feld 364, University of Heidelberg, 69120 Heidelberg, Germany) were transformed into competent cells according to the following protocol.

4.2.2. Transformation of bacteria with the ligation products

After thawing on ice for 30 min, 50 µl aliquots of competent cells (DH5α Escherichia coli bacteria) were gently mixed with the circular DNA plasmid or the 20 µl ligation product. The mixture was incubated on ice for 30 min and heat shocked for 45 sec at 42°C in a heating block and rapidly returned on ice for 3 min. 200 µl of standard LB-medium was then added to the cells and incubated at 37 °C with shaking for 1 hour. 50 µl of the cells were then spread on LB plate containing 100µg/ml Ampicillin and incubated 16 hours at 37 °C. Colonies were picked and grown in 5ml of Ampicillin containing LB at 37 °C shaking overnight. Plasmid DNA was then prepared with QIAprep Spin Miniprep Kit (QIAGEN) according to the manufacturer's instructions. Successful clones were identified by sequencing (Eurofins Genomics) using the reverse primer 5'-CTTCCCGTCAAGGTAGGACT-3' that anneals at ~200bp after the cloning sites. Clones carrying the correctly inserted and intact sequence were cultured in 200ml Ampicillin containing LB at 37 °C shaking overnight. Amplified plasmid was then prepared by PureLink HiPure Plasmid Maxiprep Kit (Invitrogen) following the manufacturer's instructions.

4.2.3. Production of recombinant Adeno-associated virus

The vectors used for constructing and packaging recombinant Adeno-Associated Virus (rAAV) have been described previously (Klugmann et al., 2005). The rAAV-mCherry vector contains a U6 promoter controlling shRNA expression and a CamKII promoter driving mCherry expression. The recombinant and replication-deficient chimeric serotypes rAAV1/2 were produced by co-transfection of human kidney cell line 293 (HEK293, ATCC, Manassas, Virginia) by standard calcium phosphate precipitation.

One week prior to transfection, HEK 293 cell was seeded onto T75 flasks, cultured in Dulbecco's modified Eagle's medium (DMEM, Life Technologies/Invitrogen, Carlsbad, CA, **Table 4.11**) at 37 °C in a humidified incubator supplied with 5 % CO_2. When the cells reached 70 - 80% confluency about 2 days later, the cells were split and re-seeded onto three T175 flasks. When the cells reached 70 - 80% confluency about 2 days later, cells were split into twenty 15 cm cell culture dishes (Nunc, 168381) and

cultured until 70-80% confluency. 2-3 hours before transfection, the medium was exchanged with 25 ml of fresh Iscove's modified Dulbecco medium (IMDM; Life Technologies/Invitrogen, Carlsbad, CA) containing 5% heat-inactivated fetal calf serum (Life Technologies/Invitrogen, Carlsbad, CA) without antibiotics.

For production of each virus, a mixture of the AAV packaging helper plasmids (150μg of mini-adenovirus helper plasmid pFΔ6, 37.5 μg of AAV2 helper plasmid pRV1, 37.5 μg of AAV1 helper 4 plasmid pH21 and 75 μg of rAAV-mCherry plasmid carrying the shRNA of interest) and 1300 μl of 2.5 M $CaCl_2$ were filled up to 13ml with sterile milliQ H_2O and added to 13ml of 2 x HeBS buffer (HEPES, 50mM, NaCl 280 mM, Na_2HPO_4 1.5 mM, pH 7.05, sterilized by filter) and vortexed. After standing for 2 min, 5ml of the transfection mix was added drop-wise onto each of the five 15 cm plates in a circular motion. After 16 hours, the medium was replaced with DMEM and culture for another 44-49 hours. Cells were then harvested with a tissue-scratcher, centrifuged for 5 min at 800 × g, and resuspended in 100 mM NaCl in 10mM Tris-HCl (pH 8.5). The cells were then lysed in 0.5 % sodium deoxycholate monohydrate (Sigma-Aldrich, Munich, Germany) and incubated with 50 U/ml Benzonase® Nuclease (Sigma-Aldrich, Munich, Germany) at 37°C for 1 hour. The lysate was centrifuged at 4°C at 3000 × g for 15 min to remove cell debris and the supernatant containing virus particles was frozen at -20°C. HiTrap™ Heparin HP Columns (GE-Healthcare, Uppsala, Sweden) were pre-equilibrated with 10 ml of 150 mM NaCl/20mM Tris (pH8.0). The thawed virus particles were loaded onto a column with a flow rate of 1 ml/min. The column was washed with 20 ml of 100 mM NaCl/20mM Tris (pH 8.0), followed by 1 ml 200 mM NaCl/20mM Tris (pH 8.0) and 1 ml 300 mM NaCl/20mM Tris (pH 8.0). Purified virus particles were then eluted by increasing concentrations of NaCl/Tris (pH 8.0) buffers: 1.5 ml 400 mM NaCl/20mM Tris (pH 8.0), 3 ml 450 mM NaCl/20mM Tris (pH 8.0), 1 ml 500 mM NaCl/20mM Tris (pH 8.0). Eluted virus was concentrated in an Amicon® Ultra-4 centrifugation filter Units (Millipore, Schwalbach, Germany) at 2000 g for 2 min and washed twice with 3.5 ml PBS. The concentrated virus was then sterilized by filtration through a 0.2 μm/13 mm diameter syringe filter.

Table 4.11: Dulbecco's modified Eagle's medium(DMEM)	
DMEM (High glucose)	500 ml
Heat inactivated calf serum (56°C for 30 min)	50 ml
1x MEM Non-essential amino acids	5 ml
Sodium pyruvate	5 ml
Pen/Strep	2.5 ml

Sterile filtered through 0.22 µm Millipore filter

4.2.4. Virus infection

The virus solution was tested in cultured hippocampal neurons on DIV 4 to assess the infection efficiency and toxicity in neurons. The infection efficiency was calculated on day 8 post infection by counting the number of virus positive cells (mCherry expression) and dividing them by the total cell number. In our hands 0.5-1.0µl /well of our working virus solution was sufficient to achieve infection rates of about 70-80 %. This sums up to approximately 2-5 × 10^9 particles/ml.

4.3. Western blot and immunodetection of antigens

Hippocampal neuron whole cells were extracted in 1x sample buffer (Add 1% 1M DTT in w/v before use) and boiled for 5 min at 95°C before loading on polyacrylamide gels. Samples were loaded together with the Colour Plus Protein Ladder (New England BioLabs® Inc.) and resolved in 10% SDS-polyacrylamide gels (separating gel: **Table 4.12**, Stacking gel: **Table 4.13).** Electrophoresis was performed at 100V and 140V during passage through the separating gel and resolving gel, respectively, and subsequently transferred to a nitrocellulose membrane (Waterman) at 30V for 16 hours under 4°C. Membrane was blocked in 5% milk in PBST (8mM Na_2HPO_4, 150mM NaCl, 2mM KH_2PO_4, 3mM KCl, 0.05% Tween® 20, pH 7.4) at room temperature for 1 hour, and then incubated with primary antibodies (**Table 4.14**) at 4°C overnight. After washing 4 x 15min with PBST, the membrane was incubated with horse-radish peroxidase (HRP) conjugated secondary antibodies for 1 hour at room temperature. After washing with PBST 4 x 15 min, the antigen-antibody complexes were detected by enhanced chemiluminescence (equal volume of "Super Signal West Pico Stable Peroxide Solution" and "Super Signal West Pico Stable Luminol/Enhancer Solution", Thermo Fisher

Scientific). The membrane was then exposed to X-ray film (Amersham Hyperfilm ECL), and developed with a Kodak developing machine. The nitrocellulose membrane was stripped (2M Glycine, adjust to pH2.2 by HCl) for 25 min, washed 3x 15min in PBST, reblocked with 10% milk in PBST for 35mins, and re-probed again if needed.

Table 4.12: Separating gel	
H_2O	3786 µl
30% Acrylamide	2134 µl
4x Lower Buffer (1.5M Tris-HCl, 0.4% SDS, pH 8.8)	2000 µl
10% APS	80 µl
TEMED	4µl

Table 4.13: Stacking gel	
H_2O	2294 µl
30% Acrylamide	666 µl
4x Upper Buffer (0.5M Tris-HCl, 0.4% SDS, pH 6.8)	1000 µl
10% APS	40 µl
TEMED	4 µl

Table 4.14: Antibody

Antibody	**Source**	**Dilution**
Monoclonal rabbit anti-AKT1	Cell signaling #2938	1:1000
Monoclonal mouse anti-AKT3	Cell signaling #8018	1:1000
Monoclonal mouse anti-Tubulin	Sigma #T6199	1:1000
Monoclonal mouse anti-Syt 1	M48 (Matthew et al., 1981), a kind gift from Prof. Thomas Söllner, Biochemistry Center (BZH), University of Heidelberg	1:1000

4.4. Electrophysiology

4.4.1. Whole cell patch clamp recording at dissociated hippocampal neurons

Whole-cell patch-clamp current clamp recordings were performed at cultured hippocampal neurons on coverslips at DIV11–14, a time by which they have developed a rich network of excitatory and inhibitory synaptic interconnections (Hardingham et al., 2001). Coverslips were secured in a recording chamber and mounted on a fixed-stage upright microscope (Examiner Z1, Carl Zeiss). Recordings were made with Axoclamp 900A amplifier (Axon CNS, Molecular Devices), digitized through a Digidata 1440A (Axon CNS, Molecular Devices), and acquired using pClamp 10.2 software (Molecular Devices). Patch electrodes (Borosilicate glass with filament, GB150F-10, 0.86x1.5x100mm, Science products) were made with a glass microelectrode puller (Model P-97, Sutter Instruments). Cultures were constantly perfused (1.5 ml/min by peristaltic pumps, Ismatec) with artificial cerebrospinal fluid (ACSF, saturated with carbogen:95% O_2 and 5% CO_2, **Table 4.15**) and maintained at 30-33°C (Single Channel Automatic Heater Controller TC-324B, Warner Instruments). Patch electrodes were filled with intracellular solution (**Table 4.16**) which gave 6-8 MΩ electrode resistances in ACSF.

Recordings of miniature excitatory postsynaptic potentials (mEPSPs) and miniature inhibitory postsynaptic potentials (mIPSPs) were made in the presence of 1 μM Tetrodotoxin (TTX, Tocris). For mIPSP recordings, glutamatergic inputs were blocked with 50 μM 2-Amino-5-phosphonopentanoic acid (APV, competitive NMDA receptor antagonist, Abcam) and 20 μM 6,7-Dinitroquinoxaline-2,3-dione (DNQX, competitive kainate, quisqualate 'non-NMDA' glutamate receptor antagonist, Tocris). Patch electrodes were filled with a modified intracellular solution (**Table 4.17**). To enhance the electrochemical force for driving Cl^- ions into the cell to favor the visualization of mIPSPs, the Cl^- ion concentration in the internal solution was reduced to 0.5mM resulting in a more negative equilibrium potential for Cl^- ions (-150mV by Nernst Equation; Nernst, 1888).

Drug treatment effects were typically established at perfusion time (1.5 ml/min): DMSO (30 min, Merck), MK-2206 (5 min, SelleckChem), LY-294002 (15 min, LC-Laboratories), VO-OHPIC (30 min, BioVision), Bicuculline (8 min, ENZO Life Science). Recordings under extracellular calcium free conditions were performed in calcium free ACSF (**Table 4.18**). All analyzed recordings were drawn from cells with resting potential more negative than -50 mV. Frequency counts of mEPSPs, mIPSPs, spikes and bursts were averaged from 60 seconds recordings. Bursts of action potentials were defined as a series of at least three action potentials with ≤ 50 ms inter-spike interval. Depolarization duration was measured as the average time period in which the cell membrane was depolarized beyond -45 mV per event taken from 5 isolated single spikes or 3-5 bursts per cell. Data was analyzed using Clampfit 10 (Axon Instruments), Igor Pro (Wavemetrics) and Minianalysis 6.0 (Synaptosoft).

Table 4.15: Artificial cerebrospinal fluid (ACSF)

NaCl	125 mM
KCl	3.5 mM
NaH_2PO_4	1.2 mM
$CaCl_2$	2.4 mM
$MgCl_2$	1.3 mM
Glucose	10 mM
$NaHCO_3$	26 mM

pH=7.35-7.4 in saturation with carbogen:95% O_2 and 5% CO_2, 295mOsmol

Table 4.16: Internal solution

K^+Gluconate	138 mM
HEPES	10 mM
NaCl	9 mM
EGTA	5 mM
$CaCl_2$	0.25 mM
Mg-ATP	4 mM
Na3-GTP	0.3 mM
K2-Phosphocreatine	10 mM

pH adjusted to 7.3 by KOH, 290mOsmol

Table 4.17: Internal solution for mIPSP recording	
K+Gluconate	147 mM
HEPES	10 mM
EGTA	5 mM
$CaCl_2$	0.25 mM
Mg-ATP	4 mM
Na3-GTP	0.3 mM
K2-Phosphocreatine	10 mM

pH adjusted to 7.3 by KOH, 290mOsmol

Table 4.18: Calcium free ACSF	
NaCl	127.9 mM
EGTA	1 mM
KCl	3.5 mM
NaH_2PO_4	1.2 mM
$MgCl_2$	1.3 mM
Glucose	10 mM
$NaHCO_3$	26 mM

pH=7.35-7.4 in saturation with carbogen:95% O_2 and 5% CO_2, 295mOsmol

4.4.2. Sharp electrode recordings at *Drosophila* larval neuromuscular junctions

The *Drosophila* larval neuromuscular junction (NMJ) glutamatergic synapse is a well established system for physiological and structural analyses of synaptic function (Jan and Jan, 1976a). A *Drosophila* larval body wall consist of 3 thoracic (T) and 8 abdominal (A) segments (**Figure 4.1 A**), each hemisegment harbors 30 muscles which compose of multinucleated cells from the fusion of a dozen myoblasts (Crossley, 1978; Hoang and Chiba, 2001). In each half of the symmetrical body, muscles are innervated by a total of 32 motorneurons axons from four different nerve branches in a pattern that has high fidelity (Jan and Jan, 1976b; Johansen et al., 1989; Keshishian et al., 1996; . Experiments were performed on third instar larvae of *Drosophila melanogaster* wild type (wt): OregonR. As described previously (Sigrist et al., 2003; Steinert et al., 2006), muscle cells (muscle 6, abdominal segment A2-3) were impaled with a 15 - 20 MΩ sharp microelectrode (Borosilicate glass with filament, GB150F-10, 0.86x1.5x100mm, Science products) filled with 3 M KCl (**Figure 4.1 B**), where intracellular whole cell current clamps were established. Bridge-mode recordings were acquired and amplified with a

Axoclamp 900A amplifier (Axon CNS, Molecular Devices), digitized through a Digidata 1440A (Axon CNS, Molecular Devices), and recorded using pClamp 10.2 software (Molecular Devices). For nerve stimulation, cut end of the intersegmental nerve was drawn into a suction electrode (Borosilicate glass with filament, GB100F-10, 0.58x1.00x100mm, Science products) where suprathreshold voltage pulses were delivered (Stimulus Isolator A365, World Precision Instruments). All analyzed recordings were drawn from cells with resting potential more negative than -60 mV. Amplitudes of eEJPs and mEJPs were averaged from 60 eEJPs and 100 mEJPs per cell. The amplitude of eEJPs within trains of stimulation (**Figure 5.5**) is given as the difference between the crest (eEJP peak) and trough (lowest potential before eEJP peak) in the train eEJPs waveform.

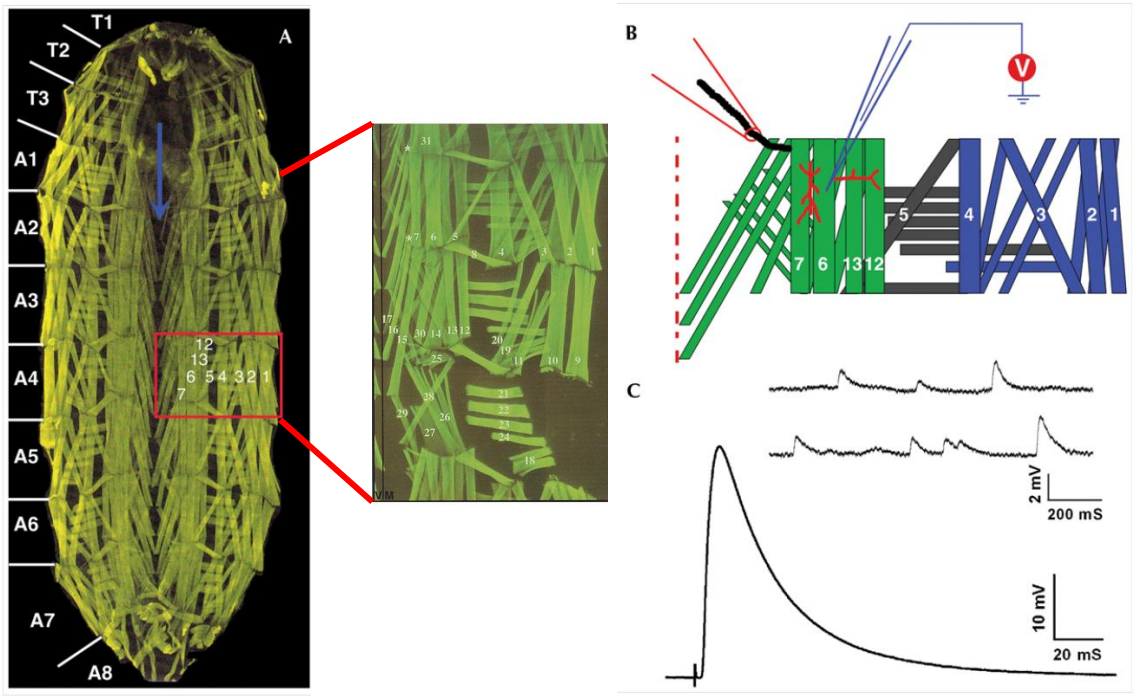

Figure 4.1: *Drosophila* larval body wall muscle and intracellular recording of NMJ potentials

A Body wall muscle of a third instar larvae fillet preparation stained with FITC-phalloidin. The thoracic (T) and abdominal (A) segments follow a repeated pattern of musculature arrangements. The ventral midline is indicated by the blue arrow. Muscle number (1-31) were illustrated at the expanded panel (right). **B** Hemisegment of the body-wall ventral (green), lateral (black), and dorsal (blue) muscles (Hoang and Chiba, 2001). Numbers (white) denote the major surface muscles. A segmental nerve is picked up by a suction electrode where the motor axon within the nerve is stimulated. A sharp microelectrode is used to record the miniature excitatory junctional potential (mEJPs) and evoked excitatory junctional potential (eEJP) from ventral longitudinal muscle 6 at segments A4 (in our experiments segments A2 or 3). **C** Sample recording of mEJPs (upper two traces) and eEJP (lower trace). (Modified from Broadie et al., 1994; Bellen HJ, 2000; Zhang and Stewart, 2010; Kazuyoshi Itoh, 2013)

4.4.2.1. Baseline adjustment for overlapping eEJPs

For the analysis of paired-pulse ratio (PPR) experiments, a pair of tight temporally spaced stimulations was delivered to the motor nerve of the *Drosophila* larva, and the corresponding overlapping eEJPs were recorded at NMJs. Since the eEJP of the second pulse overlaps onto the first pulse, the decay phase of the first eEJP (P1) was extrapolated, where the membrane potential of which the second eEJP (P2) add onto was estimated (**Figure 4.2 A**). For inter-pulse intervals of 25ms, the decay phase of P1 follows roughly a linear scale, a linear function was therefore fitted to the P1 decay phase to extrapolate the base of P2 (red dot in **Figure 4.2 B**, upper left trace). In paired-pulse experiments with inter-pulse intervals of 50-100ms, the decay phase of P1 was fitted to a first order exponential function (**Figure 4.2 A & B**). At the time point when P2 reached its peak amplitude (black dots), an adjusted baseline of P2 (red dots) was estimated. P1 decay phase extrapolation and P2 base estimation were performed with custom-written program script in Matlab R2012a (MathWorks).

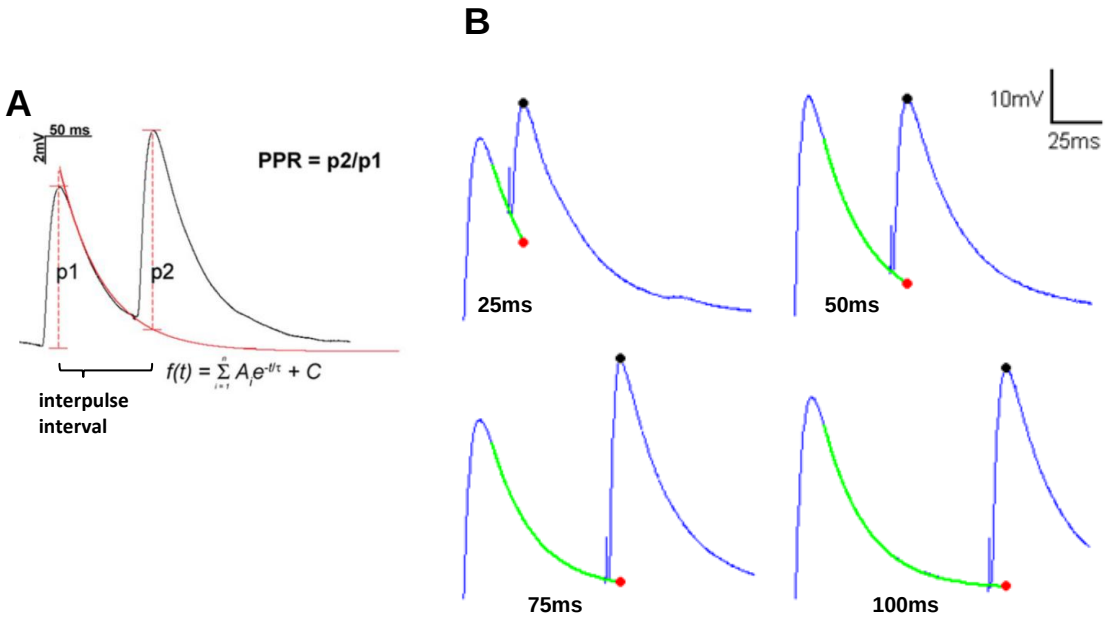

Figure 4.2: Baseline adjustment for overlapping eEJPs

A Illustration of the decay phase of the first eEJP (P1) estimated by fitting to a first order exponential function, which give rise to an adjusted baseline of the second eEJP(P2). (Adapted from Kim et al., 2009) **B** Example traces (blue) of the paired pulse eEJP response towards interpulse interval of 25ms (upper left trace), 50ms (upper right trace), 75ms (lower left trace) and 100ms (lower left trace), recorded at 1.5mM $[Ca^{2+}]$. The decay phase of the first pulse was fitted by a linear function (for interpulse interval of 25ms), or single first order exponential function (for interpulse interval of 50-100ms). The fitted curve (green) overlays perfectly on the recorded trace, incorporating the time when P2 reach its peak amplitude (black dot) yield the adjusted baseline for P2 (red dot).

4.4.2.2. Correction for Nonlinear Summation

When a large number of vesicles is released by a presynaptic stimulation, the amplitude of post-synaptic response (e.g. eEJP) is not strictly proportional to the number of quanta (number of released vesicle). Instead, the contribution of each quantum to the total eEJP amplitude becomes smaller the larger the eEJP gets. To increase the precision of measuring evoked vesicle release, non-linear summation of quanta can be corrected for by the "Martin correction factor" (McLachlan and Martin, 1981):

$$v' = v/(1 - f[v/E])$$

Equation 4.1: "Martin correction factor"
where the following variables were used:

- *v'* is the expected amplitude when quanta are summed linearly
- *v* is the experimental amplitude
- *E* is the driving force (i.e. resting potential- reversal potential). Since the reversal potential for the *Drosophila* NMJ is estimated to be 0 mV (Jan and Jan, 1976b), *E* = resting potential in this case.
- *f* is the membrane capacitance factor ($\Delta t/\tau$). The extensive arbor of *Drosophila* NMJ covers a significant portion of the postsynaptic muscle surface, which approximate to an RC circuit: *f* = 0.55.

4.5. Imaging

4.5.1. Phluorin imaging at dissociated hippocampal neurons

Direct measurement of presynaptic vesicle release was accomplished by expressing pH sensitive GFP (pHluorin)-vesicle protein fusion (Miesenbock et al., 1998) in hippocampal neurons. The lumen of synaptic vesicles is acidic (pH5.5) due to the activity of a vesicular H^+-ATPase (Nelson, 1992). This luminal pH is substantially lower than the pH of the extracellular environment (pH7.4). Since the pK value of pHluorins is about 7.1 (Sankaranarayanan et al., 2000), fluorescence of pHluorin is quenched within the acidic vesicle lumen, but it is well detectable upon vesicle fusion with the plasma membrane (**Figure 4.3 A**). Hippocampal neurons were infected by a recombinant adeno-associated virus (rAAV; 0.5 µl of virus stock per well) carrying an expression cassette for SypHluorin2x: two phluorins incorporated into the second intravesicular loop of synaptophysin (Zhu et al., 2009;**Figure 4.3 B**), which is a generous gift from Prof. Thomas Kuner (Institute for Anatomy and Cell Biology, University of Heidelberg, Germany). Imaging was performed after at least 10 days of infection (DIV 17-21) for optimal SypHluorin (2x) expression.

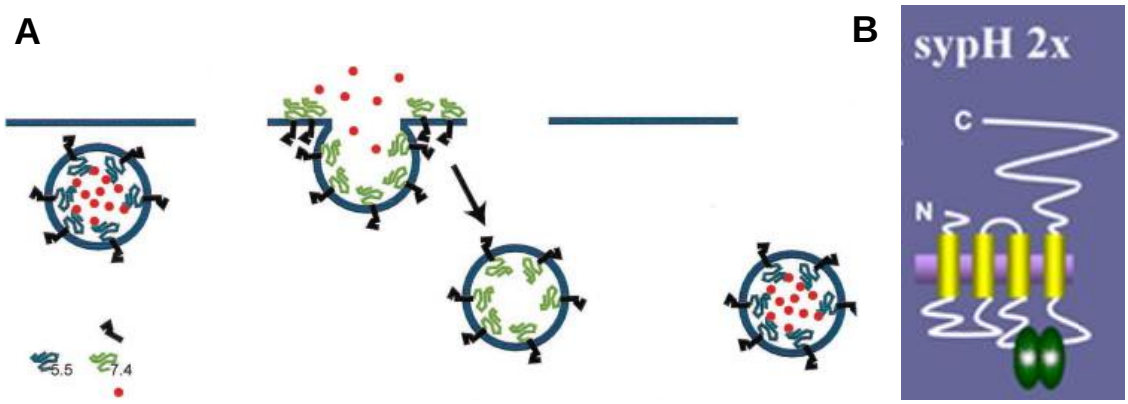

Figure 4.3: Mechanism of the pHluorin probe for imaging vesicle exocytosis

A Exocytosis relieves the proton-dependent quenching of ecliptic-pHluorin fluorescence. The pHluorin molecule is expressed in the acidic vesicle lumen (pH of 5.5), where the pHluorin fluorescence is completely quenched. Upon firing of action potentials, the vesicles were released to plasma membrane, which exposed the pHluorin to the extracellular environment at pH 7.4. The proton-dependent quenching was collapsed which results in an increase in fluorescence. (Adapted from Sankaranarayanan et al., 2000) **B** Schematic representation of SypHluorins 2x: two phluorins (green oval) incorporated into the second intravesicular loop of synaptophysin. (Adapted from Zhu et al., 2009)

Images were recorded from cultured hippocampal neurons on coverslips constantly perfused (1.5 ml/min, 30-33°C) with ACSF in the presence of 50μM APV and 20 μM DNQX to block recurrent activity. Field stimulation is achieved by a parallel pair (10mm spacing) of silver bath electrodes that deliver pulses (1ms of 10 mA current) of alternating polarity across the chamber. Ammonium chloride (NH4Cl) containing ACSF was prepared by substituting 50 mM NaCl in normal saline with NH4Cl (**Table 4.19**). Alkalinizing of vesicles within the button is achieved by diffusion of ammonia (NH_3, in equilibrium with ammonium ions NH_4^+) across cell membranes (Roos and Boron, 1981), which provides a maximum fluorescence value. ACSF of pH of 5.5 was prepared by reducing $NaHCO_3$ concentration (**Table 4.20**), the low pH quench surface expressed SypHluorin2x, which generate a minimum background value of that bouton.

Fluorophores were exited at 465 nm with LED illumination (Colibri 2, Carl Zeiss, Germany). Images were acquired at 3x3 binning by a CCD camera (AxioCam HSm, Carl Zeiss, Germany) mounted on a fixed-stage upright microscope (Examiner Z1, Carl Zeiss) through a 63x, 0.9 NA water-immersion objective (Examiner Z1, Zeiss) and the filter set

(61 HE, DFT 495 + 605, BP 474/28, BP 585/35, DBP 527/54 + 645/60, Carl Zeiss, Germany). Imaging data was collected with AxioVision Software (AxioVision 4.8.2, Carl Zeiss, Germany). For imaging of fluorescence response to 20Hz stimulation, images were acquired at 5 frames per second (fps) with 192 ms exposure. For imaging of maximum and minimal fluorescence (where culture were superfused with ACSF containing NH_4Cl or ACSF at pH5.5 respectively), images were acquired at 0.2fps with 192 ms exposure.

In each captured image, 900-1300 of synaptic puncta were first identified by step-wised image thresholding to isolate individual puncta, followed by manual selection (visual inspection of the morphological signature of synapse) for any missed or fused puncta. The average fluorescence values within the pixels in the region of interest (roi) were then extracted with the use of ImageJ software (NIH). The decay slope of the fluorescence trace before stimulus onset were linearly fitted, the value of which was then divided from the raw fluorescence traces to correct for photobleaching, with the use of a custom-written program script in Matlab R2012a (MathWorks). The fluorescence values (F) were then subtracted and divided by the baseline fluorescence before stimulation (F0) to yield the factional fluorescent changes (δF), i.e. $\delta F=(F-F0)/F0$. All the 900-1300 synaptic regions that accommodated in the image field were averaged as one data point. For the image recorded under NH_4Cl or low pH treatment, during which the cultures were subjected to around 5-7 mins of superfusion, drifting of image were adjusted by image alignment with the use of *Align_slices in stack* plugin (Tseng, 2015), which employs a cross-correlation algorithm to find the maximum overlap between the drifted image and template.

Table 4.19: ACSF containing NH_4Cl

NaCl	75 mM
KCl	3.5 mM
NaH_2PO_4	1.2 mM
$CaCl_2$	2.4 mM
$MgCl_2$	1.3 mM
NH_4Cl	50 mM
Glucose	10 mM
$NaHCO_3$	26 mM

In saturation with carbogen:95% O_2 and 5% CO_2, 295mOsmol

Table 4.20: ACSF at pH=5.5	
NaCl	125 mM
KCl	3.5 mM
NaH_2PO_4	1.2 mM
$CaCl_2$	2.4 mM
$MgCl_2$	1.3 mM
Glucose	60 mM
$NaHCO_3$	0.52 mM

pH=5.5 in saturation with carbogen:95% O_2 and 5% CO_2, 295mOsmol

4.5.2. Calcium life imaging at *Drosophila* larval neuromuscular junction

Virgins of the elav^{C155} pan-neuronal Gal4-driver line were crossed to males flies carrying UAS-GCaMP6m on the third chromosome (Chen et al., 2013), the progeny express GCaMP6m in all neurons under the GAL4-UAS system (Brand and Perrimon, 1993). GCaMP (Nakai et al., 2001) is made of a circularly permuted green fluorescent protein (cpGFP; Baird et al., 1999; Nakai et al., 2001), with the calcium binding calmodulin (CaM), and CaM interacting M13 peptide (M13) located at close proximity to the chromophore. Fluorescence is permitted upon calcium binding and the formation of the CaM-M13 complex inside the cpGFP β barrel (Akerboom et al., 2009).

NMJ bouton calcium fluorescence was recorded at muscle 6/7 in abdominal segment A2-3 bathed with HL3 solution (**Table 4.9**, with 1.5mM $CaCl_2$ and 2 mM $MgCl_2$). 7mM of glutamate were present in the HL3 to desensitize postsynaptic glutamate receptors and prevent muscle contraction without influencing presynaptic Calcium dynamics (Macleod et al., 2004). Fmax, the maximal fluorescence when GCaMP6m is saturated with Calcium, was measured at 2 seconds of 300Hz of nerve stimulation. Fmin, the minimal fluorescence when Calcium is taken out from the GCaMP6m, was obtained after 40mins incubation of 1mM EGTA, 200µM BAPTA-AM and 20mM $MgCl_2$ in Calcium free HL3. Images were acquired at the same setting as the previous session, except a 2x2 binning of the CCD which acquire image at the speed of 20 fps under 44 ms exposure.

The bouton regions and their surrounding homogeneous background region (**Figure 4.4 A & B**, respectively) were selected with the use of ImageJ software (NIH). Fluorescence values (**Figure 4.4 C**) in those roi were then corrected for photobleaching as described in the previous session (**Figure 4.4 D**). The net fluorescence (F) was then calculated by subtracting the value of photobleaching corrected background roi from photobleaching corrected bouton roi. The fluorescence values (F) were then subtracted and divided by the baseline fluorescence before stimulation (F0) i.e. $\delta F=(F-F0)/F0$ to yield the factional fluorescent changes (δF;**Figure 4.4 E**).

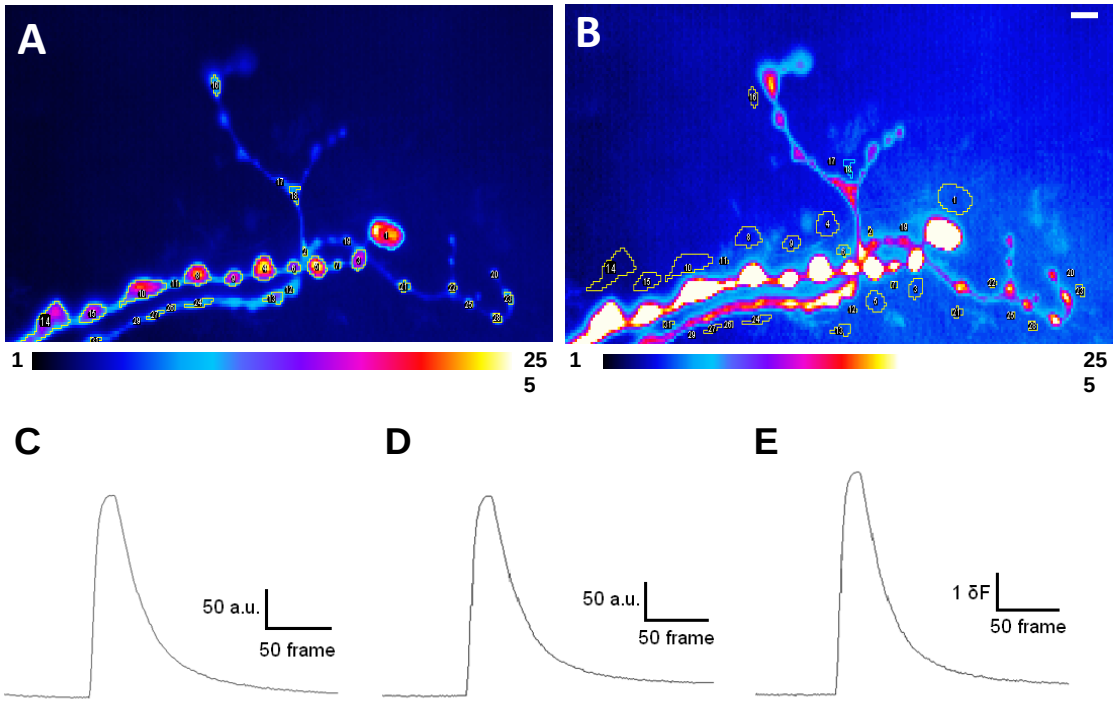

Figure 4.4: Quantitative calcium imaging and the estimation of calcium concentration in the presynaptic boutons of *Drosophila* NMJ

A-B Pseudo color images of an example NMJ with marked bouton (**A**) and background (**B**) regions. **C** Example raw fluorescence trace of bouton roi in response to 40Hz stimulation. **D** Linear photobleachinging corrected fluorescence trace from (**C**). **E** Fractional fluorescence changes (δF).

4.5.2.1. Calculation of Calcium concentration

The estimation of the peak intracellular calcium concentration rise upon stimulation was conducted by the method described by (Maravelli et al., 2000), which calculates the change in calcium concentration $\Delta[Ca^{2+}]$ by:

$$\frac{\Delta[Ca^{2+}]}{K_D} = \frac{F_{max}}{F_0}(1 - R_f^{-1})\frac{\delta F}{(\delta F_{max} - \delta F)\delta F_{max}}$$

Equation 4.2: Change in calcium concentration

and the resting calcium concentration $[Ca^{2+}]_{rest}$ by:

$$\frac{[Ca^{2+}]_{rest}}{K_D} = \frac{(1 - R_f^{-1})}{\delta F_{max}} - R_f^{-1}$$

Equation 4.3: Resting Calcium Concentration

where

- Fmax stands for the maximal fluorescence when GCaMP6m is saturated with calcium
- F0 stands for the basal fluorescence of GCaMP6m before any stimulation
- Rf stands for the dynamic range of GCaMP6m
- δF stands for factional fluorescent changes i.e. ΔF-F0)/F0
- δFmax stands for the maximum value of δF when GCaMP6m is saturated with calcium
- KD stands for the dissociation constant of GCaMP6m, which is 167nM (Chen et al., 2013)

4.5.2.2. Analysis of Calcium rise and decay kinetics

To dissect the kinetics of calcium rise and decay in response to various stimulation frequencies, the tau value is extracted by fitting a single first order exponential function 'c+a*(1-exp(-x/tau)' on the 10 to 90% rise and 'c+a*exp(-x/tau)' on the 90 to 20% decay region of δF (**Figure 4.5 A**) with the use of custom-written program script in Matlab R2012a (MathWorks). The exemplar best fitted curves for rise and decay were shown on **Figure 4.5 B & C** respectively, blue trace is the δF region to be fitted, and the orange curve draws the fitted function.

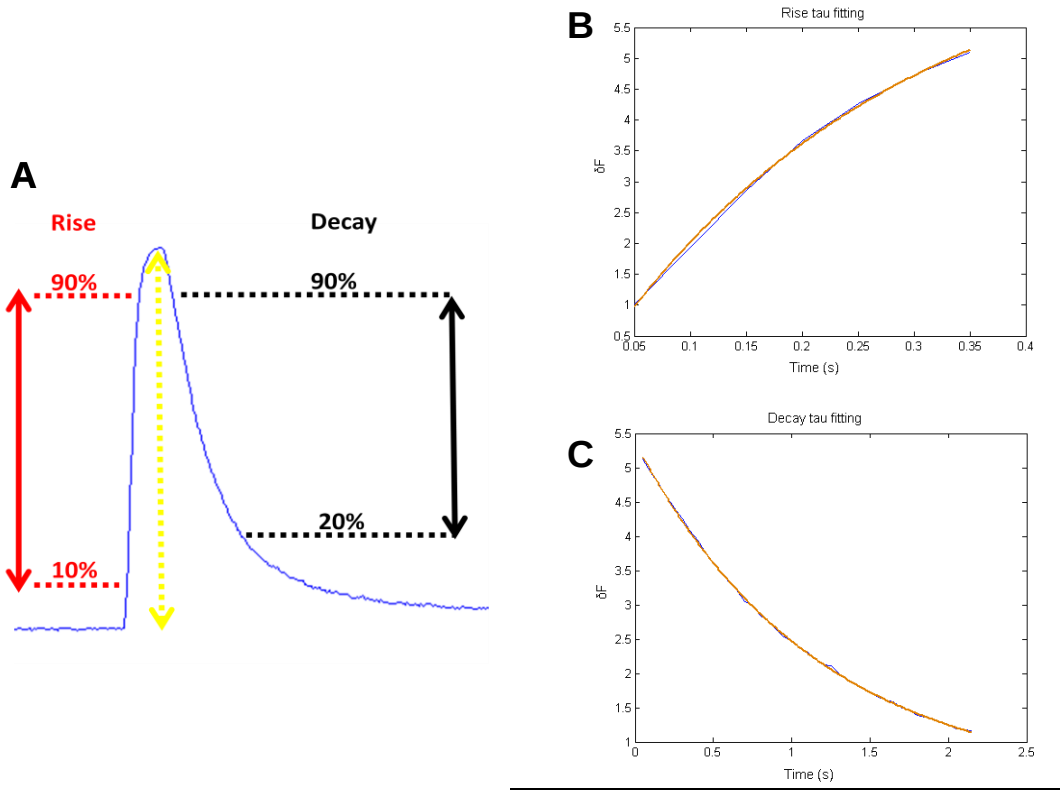

Figure 4.5: Extraction of Calcium rise and decay tau

A Extraction of the 10 to 90% rise and 90 to 20% decay region from an example δF traces in response to 40Hz stimulation. **B-C** Example fitting of a single first order exponential function to the rise **B** and decay tau region **C** on the δF in **A**, blue trace is the δF region to be fitted, and the orange curve denote the fitted function. **B** Example fit of 'c+a*(1-exp(-x/tau)' on the 10 to 90% rise region. **C** Example fit of 'c+a*exp(-x/tau)' on the 90 to 20% decay region.

4.6. Statistics

Data was expressed as mean ± SEM of the indicated n numbers. Sample size for experiments with two means was estimated according to (Suresh and Chandrashekara, 2012) to yield a statistical power of 0.8 with an alpha-level of 0.05. Normal distribution of the data points in each sample was analyzed with the Shapiro-Wilk-Test. Normally-distributed samples were analyzed using unpaired or paired two-tailed Student's t-tests. Samples with non-normally distributed data points were analyzed by two-tailed Mann-Whitney-U-Tests. Level of significance is marked with asterisks: * $p > 0.05$; *$p < 0.05$; ** $p < 0.01$; *** $p < 0.001$.

5. RESULTS

5.1. AKT controls the functional status of the presynaptic vesicle release machinery in rat hippocampal neurons

An earlier study in our laboratory has found that the ubiquitous kinase AKT dynamically regulates spontaneous vesicle release at the glutamatergic synapses of *Drosophila* neuromuscular junctions (NMJ; Ge*, Leung* et al., *under revision*). Interestingly, the PI3K/AKT signaling pathway and the vesicular release machineries are evolutionarily highly conserved, and AKT has been shown to localize in pre- and postsynaptic terminals of mammalian synapses (Majumdar et al., 2011; Smillie and Cousin, 2012; Huang et al., 2013). In addition, AKT has been repeatedly determined as a risk gene for neurological diseases such as Schizophrenia (Zheng et al., 2012) and Autism Spectrum Disorders (ASD; Ebert and Greenberg, 2013). Our identification of a novel synaptic role of AKT at *Drosophila* NMJs and its potential high degree of conservation in the mammalian system might implicate an intriguing new mechanism that could be responsible for several human disease conditions. We were therefore interested to investigate whether the identified synaptic role of AKT in *Drosophila* applies to mammalian central synapses.

5.1.1. AKT regulates spontaneous vesicle release at excitatory and inhibitory synapses of cultured rat hippocampal neurons

To measure spontaneous vesicle release at the mammalian synapse, whole cell current clamp recordings were performed on primary cultures of rat hippocampal neurons (11-14 days *in vitro*, DIV) in order to reveal miniature excitatory postsynaptic potentials (mEPSPs). Recording solutions contained, unless stated otherwise, 1μM Tetrodotoxin (TTX), which blocks the voltage-gated fast sodium channel-induced action potentials. Similar synaptic effects of the PI3K/AKT signaling as seen at *Drosophila* NMJs were observed: acute AKT inhibition (by 50μM MK-2206) resulted in a strong increase in mEPSP-frequency (**Figure 5.1 A-B**), whereas limiting the availability of PIP_3 for AKT membrane anchorage (detail mechanism see **Introduction 3.4.1**) via inhibition of PI3K (by 50μM LY-294002) resulted in more subtle but still significant increases. Conversely,

blockage of PIP3 phosphatase, PTEN (by 120nM VO-OHPIC) decreased the rate of mEPSPs (**Figure 5.1 B**). Well in line with the mechanism in *Drosophila* NMJs, this regulation of spontaneous vesicle release is independent of extracellular calcium: bathing the neurons in calcium free ACSF containing 1mM of calcium chelator EGTA, resulted in the same robust increase in the rate of mEPSPs after AKT blockade (**Figure 5.1 C-D**) as in the presence of calcium (**Figure 5.1 A-B**)

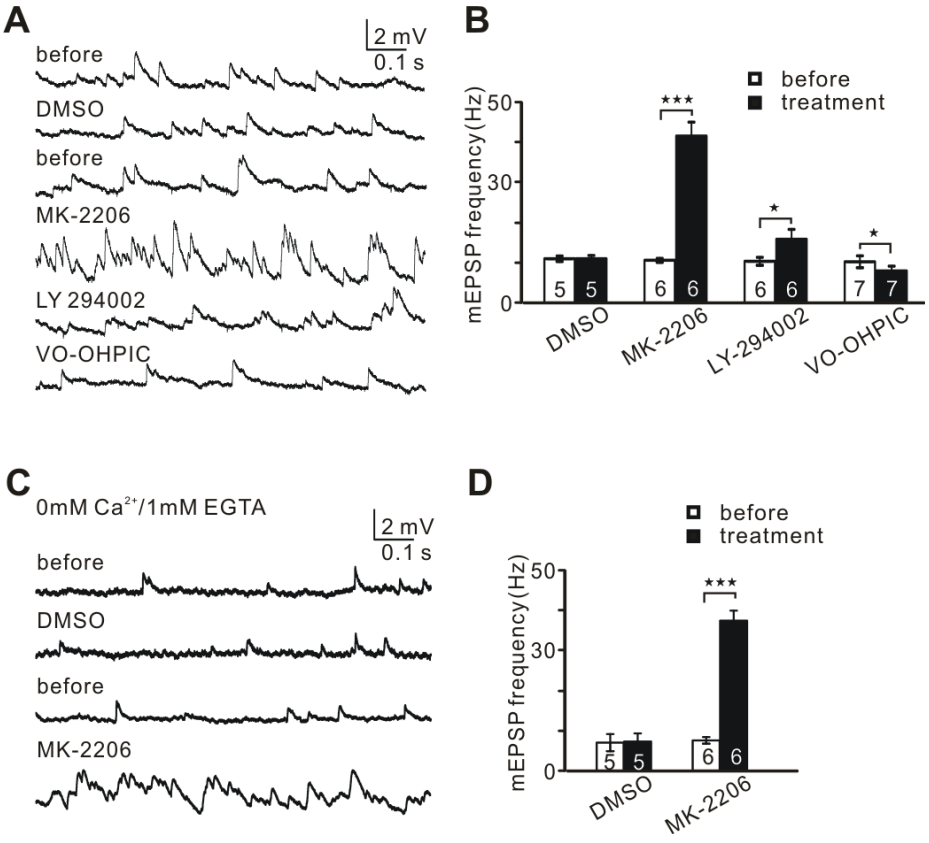

Figure 5.1: AKT regulates spontaneous vesicle release in hippocampal neurons and is independent of extracellular calcium

A & C Representative traces of whole cell current clamp recordings of miniature excitatory postsynaptic potentials (mEPSPs) from primary rat hippocampal neuron cultures under the indicated conditions. **B** Under physiological extracellular calcium concentration (2.4mM), inhibition of AKT (MK-2206) or PI3K (LY-294002) significantly enhanced the rate of mEPSPs. The opposite was observed under the inhibition of PTEN (VO-OHPIC), where mEPSP frequency was reduced. **D** Under extracellular calcium free condition (0mM $CaCl_2$ and 1mM EGTA), inhibition of AKT (MK-2206) also significantly enhanced the rate of mEPSPs, at an extent comparable to that measured under normal calcium (**B**). Data denote means ± S.E.M collected from the indicated number of cells. *p<0.05; **p<0.01; ***p<0.001 by two-tailed Student's paired *t*-tests.

This data from excitatory hippocampal synapses closely resembles the results from glutamatergic synapses of *Drosophila* NMJs (Ge*, Leung* et al., *under revision*) suggesting that the AKT-dependent mechanism of regulating the functional status of vesicle release machineries is evolutionarily conserved.

We next asked whether the AKT-mechanism is confined to glutamatergic synapses or whether it is potentially a universal mechanism acting on all vesicle release machineries independently of the nature of its contained neurotransmitter. We therefore turned our attention to inhibitory, GABAergic synapses, which apart from the transmitter have several differences in synaptic architecture compared to their excitatory counterparts (Bialer and White, 2010; van Spronsen and Hoogenraad, 2010).

Recordings of miniature inhibitory postsynaptic potentials (mIPSPs) were performed under the blockage of glutamatergic inputs by 50μM APV (a competitive antagonist at the glutamate binding site of NMDA receptors; Olney et al., 1991) and 20μM DNQX (a competitive kainate, quisqualate (non-NMDA) glutamate receptor antagonist; Honore et al., 1988). In addition, in order to favor the visualization of mIPSPs in our voltage recording, we reduced the Cl^- ion concentration in the internal solution of the patch electrode to 0.5mM resulting in a more negative equilibrium potential for Cl^- ions of -150mV as determined by Nernst Equation (Nernst, 1888) due to the enhanced the electrochemical force for driving Cl^- ions into the cell. To confirm that the observable voltage transients (arrows in **Figure. 5.2A**) are indeed due to spontaneous GABAergic transmission we applied the potent $GABA_A$ receptor antagonist Bicucullin (Bowery et al., 1981; Johnston, 2013). We found that the principal role of AKT for vesicle release machineries was also preserved at Bicucullin-sensitive GABAergic synapses: inhibition of AKT via MK-2206-treatment resulted in a significant increase in the rate of mIPSPs whereas solvent alone did not (**Figure 5.2 A-B**). However, the degree of the mIPSP frequency increase was obviously lower than that observed for mEPSPs (about two-fold versus about 4-10 fold).

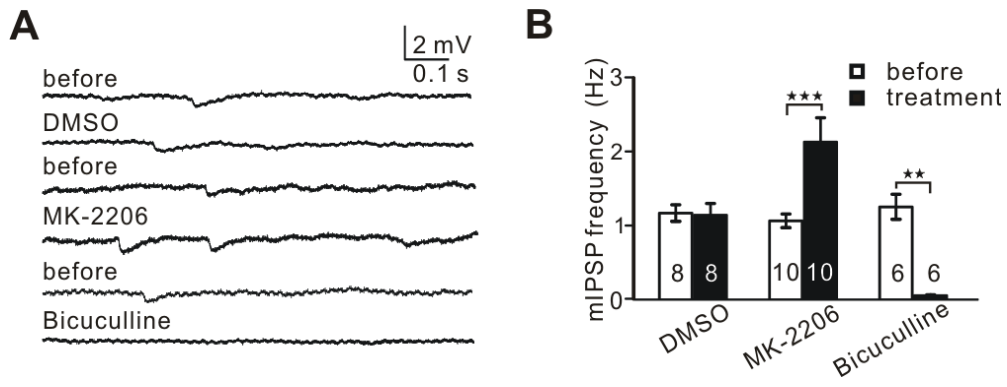

Figure 5.2: AKT regulates inhibitory spontaneous vesicle release in hippocampal neurons

A Representative miniature inhibitory postsynaptic potentials (mIPSPs)-traces recorded in rat hippocampal cultured neurons under the indicated conditions. **B** The rate of Bicucullin-sensitive mIPSPs was significantly enhanced by AKT-inhibition (MK-2206). Data denotes means ± S.E.M collected from the indicated number of cells. *p<0.05; **p<0.01; ***p<0.001 by two-tailed Student's paired *t*-tests, except the non-normally distributed data set of MK-2206 and Bicuculline, which is performed by two-tailed Mann-Whitney-U-Tests.

One explanation could be that the number of GABAergic synapses on the recorded neurons is apparently much lower than excitatory synapses as indicated by the almost ten-fold lower basal mIPSP frequency than mEPSPs. In addition, AKT has been shown to phosphorylate $GABA_A$ receptors resulting in their increased localization to synapses (Serantes et al., 2006). Inhibition of AKT may therefore lead to a reduction of $GABA_A$ receptor localization in postsynaptic membranes and hence to fewer functional GABAergic synapses. This could well suppress the degree of mIPSP-rate increase.

Taken together, our data from rat hippocampal neurons and *Drosophila* NMJs (Ge*, Leung* et al., *under revision*) demonstrates that the AKT-dependent functional switch of vesicle release machineries is an evolutionarily conserved mechanism that seems to be shared across different types of synapses with different transmitter identities.

5.1.2. The AKT-mediated functional mode switch of vesicle release machineries affects spontaneous and evoked vesicle release in rat hippocampal neurons

Our results show that AKT activity modulates spontaneous vesicle release across types of synaptic identities indicating that it may represent a fundamental property of all vesicle release machineries. We therefore asked whether this mechanism may also affect action potential evoked vesicle release. Conventional membrane potential recording at the cell body is not a favorable approach to solve this question, owing to the complexity of multi axonal-dentritic connections at the hippocampal network. Added to that, the accuracy of the eEPSP-amplitude recordings from postsynaptic neurons will suffer from the substantial baseline jitter during high frequency spontaneous vesicle release. We therefore decided to quantify the amount of presynaptic vesicle release by expressing the vesicularly targeted pH-sensitive GFP pHluorin in hippocampal neurons (Miesenbock et al., 1998). The luminal pH of synaptic vesicles is substantially lower than that of the extracellular environment (pH5.5 versus pH7.4) resulting in an efficient quenching of the fluorescence of pHluorin within the lumen of presynaptic vesicles, and fluorescence upon vesicle fusion with the plasma membrane (Miesenbock et al., 1998). Imaging the fluorescence changes induced by stimulating cultured neurons in the presence or absence of the AKT blocker MK-2206 would allow us to assess the role of AKT in evoked vesicle release.

We infected hippocampal neurons (400-600 cells/ mm^2) with a recombinant adeno-associated virus (rAAV) carrying an expression cassette for SypHluorin2x: synaptophysin with two phluorins incorporated into its second intravesicular loop (Zhu et al., 2009). Imaging was performed after at least 10 days of infection (DIV 17-21) for optimal SypHluorin (2x) expression. After this time period the exogenous expression of pHluorin-tagged synaptophysin typically distributes widely across vesicle pools (Kwon and Chapman, 2011).

Phluorin-imaging was performed by capturing image data according to and in experimental order of the following three paradigms:

1. **F0**: The basal fluorescence after 10 mins of drug treatment (DMSO control or MK-2206). Images were recorded at 5 frames per second (fps) with 192 ms exposure/frame (**Figure 5.3 A & B**, upper left panel).

2. $\mathbf{F_{peak20Hz}}$: The maximum fluorescence value after 10 seconds 20Hz field stimulation (delivered by a pair of 10mm spacing parallel silver bath electrodes that deliver 200 bipolar pulses (1ms,10 mA) at 20 Hz). Images were recorded at 5 fps with 192 ms exposure/frame (**Figure 5.3 A & B**, upper right panel).

3. $\mathbf{F_{pH5.5}}$: The minimum residual fluorescence, when surface SypHluorin2x is quenched at pH5.5. Images were recorded after 5-7 mins superfusion of ACSF at pH5.5 at 0.2 fps with 192 ms exposure/frame (**Figure 5.3 A & B** lower left panel).

4. $\mathbf{F_{NH4Cl}}$: The maximum fluorescence from all expressed SypHluorin2x by alkalization of all vesicles in the synaptic terminal. Images were recorded at 02 fps with 192 ms exposure/frame after 5-7 mins superfusion of ACSF containing 50mM ammonium chloride (NH_4Cl), which leads to a general alkalization of all vesicles. (**Figure 5.3 A & B** lower right panel).

In each captured frame, 900-1300 of synaptic puncta were identified (by image thresholding combined with manual correction using ImageJ software, (for details see **Materials and Methods 4.5.1**). Briefly, the fluorescence signals of each of these regions were 1) corrected for photobleaching, 2) transformed into factional fluorescence changes $\delta F=(F-F0)/F0$ and 3) averaged into a single data point per frame. The factional fluorescence response (averaged value from all identified synaptic puncta of a single frame or time point) across the stimulation time course from 9-10 independent experiments were temporally aligned and plotted as means ± SEM over time (**Figure 5.3 C**).

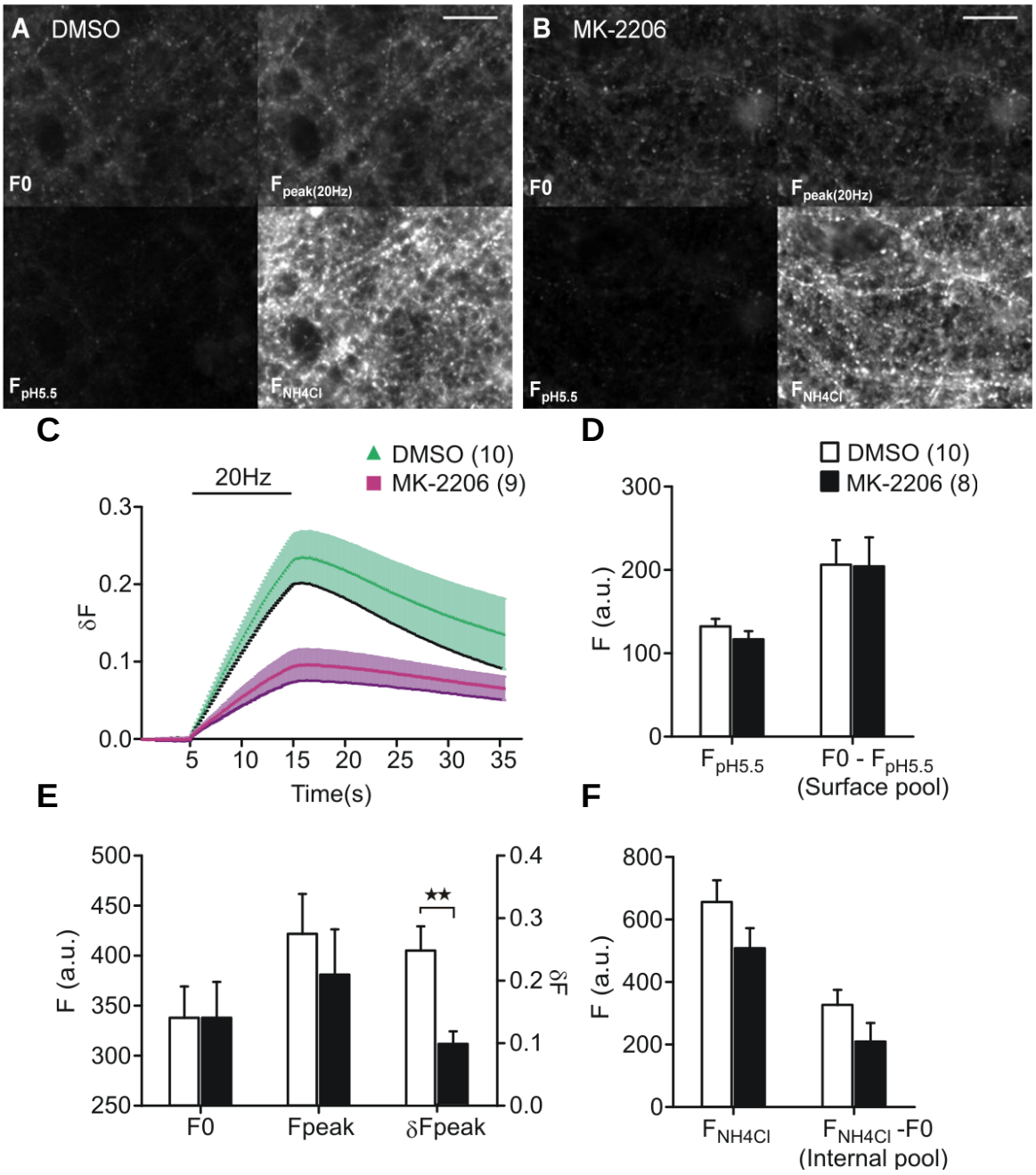

Figure 5.3: Stimulation evoked vesicle release is impaired by AKT inhibition in hippocampal cultured neurons

A-B Representative images of the hippocampal neuronal culture after 10mins of DMSO (**A**) or MK-2206 (**B**) treatment. The basal fluorescence before stimulation (F0, upper left panel), peak fluorescence change after 200 stimulations at 20Hz ($F_{peak20Hz}$, upper right panel), residual fluorescent at pH5.5 ($F_{pH5.5}$, lower left panel), and the fluorescence when all vesicles were alkalinize by ammonium chloride (F_{NH4Cl}, lower right panel) were captured. **C** Fractional fluorescent change (δF) at the course of 200 stimulation pulses at 20Hz. MK-2206 treated synapses elicited lowered δF response compared to the DMSO control. **E** Raw value of F0 and

peak fluorescence resulted from 20Hz stimulation (F_{peak}), as well as the photobleaching corrected fractional fluorescent rise peak (δF_{peak}) that is significantly reduced by AKT-inhibition. **D** No observable difference were found in the surface pool size, which was reflected by F0 - $F_{pH5.5}$ (where surface SypHluorin2x is quenched). **F** Internal pool size was represented by F_{NH4Cl} (which represent total pool) - F0 (which represent surface pool). The value from MK-2206 treated synapses was apparently reduced, potentially due to more severe photobleaching owing to slower endocytosis, as observed from the dampened decay slope in (**C**). Scale bar: 20µm. Data denote means ± S.E.M collected from the indicated number of imaged cultures. *p<0.05; **p<0.01; ***p<0.001 by two-tailed Student's t-tests

Our analysis revealed a significantly reduced averaged total evoked vesicle release under AKT inhibition compared to control treated cells (**Figure 5.3 E**). This reduction was not due to potential differences in the expression or localization of SypHluorin as indicated by the similar F0, $F_{pH5.5}$ and F_{NH4Cl} signals under both experimental conditions and the thereof derived similar surface and internal fluorophor-pool sizes (**Figure 5.3 D & F**).

Taken together, the AKT-dependent enhancement of spontaneous vesicle release and the observed simultaneous impairment of evoked release in rat hippocampal neurons suggest that AKT is not a general regulator of the fusogenicity of vesicle release machineries of these synapses. AKT activity appears to maintain release machineries in a tightly clamped mode that suppresses spontaneous vesicle fusion and favors action potential triggered evoked vesicle release. Conversely, reduced AKT activity apparently loosens the clamping of release machinery, which favor spontaneous vesicle fusion and hamper action potential triggered evoked release.

5.1.3 AKT activity impairs successive evoked vesicle release at *Drosophila* NMJs

Given the findings at the mammalian central synapses, we wished to examine whether AKT regulates evoked and spontaneous vesicle release in opposing directions also at *Drosophila* NMJs, the system in which we made our original AKT-related findings (Ge*, Leung* et al., *under revision*). Owing to the massive contractions of muscles upon AKT inhibition, evoked vesicle release was measured at *Drosophila* NMJs not by pHluorin imaging but by electrophysiological recordings of evoked excitatory

junctional potentials (eEJPs). The high sensitivity of electrophysiological recordings allowed us to examine the effects of AKT activity on evoked release during both single pulse nerve stimulation (1Hz, **Figure 5.4**) and higher frequency stimulation (30Hz, **Figure 5.5**).

Experiments were conducted in hemolymph-like saline (HL3; Stewart et al., 1994) containing 20mM [Mg^{2+}] and 0.5mM [Ca^{2+}]. Lower extracellular calcium concentration than the physiological condition (1.5mM [Ca^{2+}]) was employed to reduce the amplitudes of eEJPs in order to minimize the effect of "non-linear summation" (McLachlan and Martin, 1981) and thereby increase the accuracy of eEJP-amplitude analyses. The amplitudes of eEJPs were recorded under AKT inhibition (50μM MK-2206), activation (240nM VO-OHPIC) or solvent control (0.1% DMSO). Miniature junctional potential (mEJPs) amplitudes were also monitored in order to control for the potential postsynaptic effect of AKT activity, such as postsynaptic glutamate receptor GluRIIA subunits localization (Lee et al., 2013a). After 25 mins of drug treatment (**Figure 5.4 A**) the rates of mEJPs were strongly increased under AKT-blockade (**Figure 5.4 B-C**) and their amplitudes were slightly, but significantly reduced (**Figure 5.4 D**). At this time point the amplitudes of isolated eEJPs showed no differences compared to the other treatments (**Figure 5.4 E & F**), suggesting that the efficiency of isolated evoked vesicle release is unaltered under AKT blockade.

We then analyzed the efficiency of evoked vesicle release under an extended (5 mins) high frequency (30Hz) train of action potentials (**Figure 5.5**). Interestingly, inhibition of AKT resulted in a rapid and increasingly strong reduction of eEJP amplitudes during the course of the high frequency stimulation until reaching plateau after 3 mins of stimulation (**Figure 5.5 A-C**). Therefore, AKT inhibition does substantially influence evoked vesicle release during high frequency nerve stimulation.

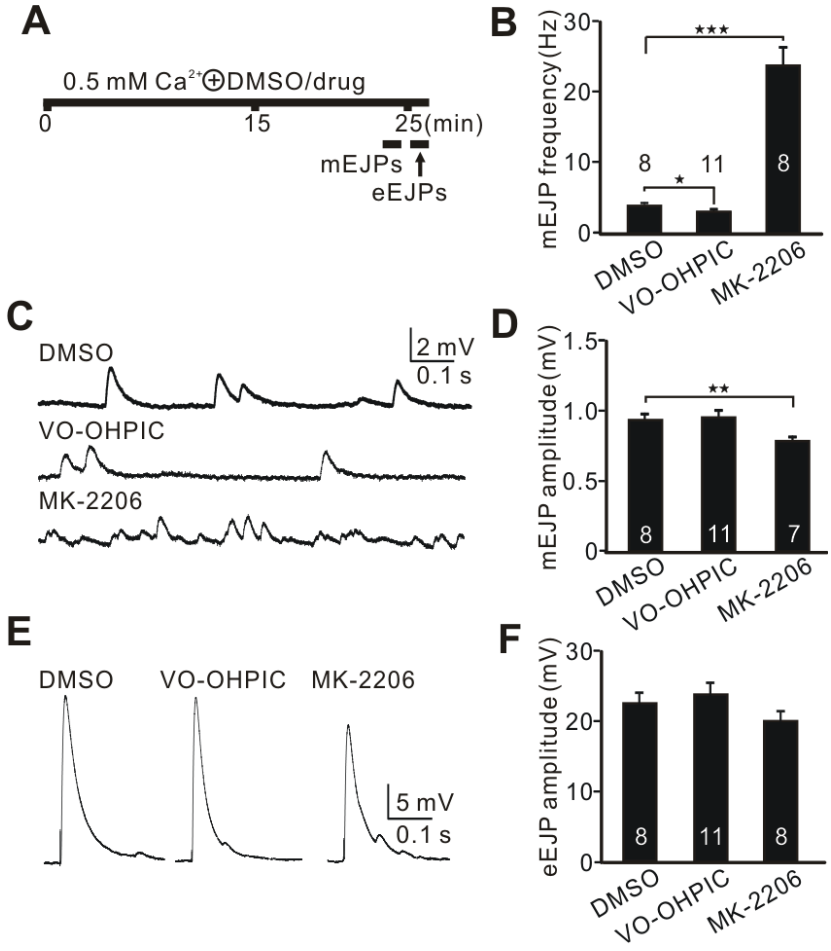

Figure 5.4 Single stimulation induced evoked vesicle release in *Drosophila* NMJ does not show significant alternation with AKT activity

A Schematic illustration of the experimental protocol. **C & E** Representative traces of mEJP (**C**) and eEJPs (**E**) as well as respective mean data of the mEJP frequencies (**B**), mEJP amplitudes (**D**) and eEJP amplitudes (**F**) recorded after 25 min of the indicated treatment. Acute inhibition of PTEN (VO-OHPIC) significantly reduced the rate of mEJPs (**B**) but had no effect on mEJP- or eEJP-amplitudes (**D** and **F** respectively). AKT inhibition (MK-2206) strongly enhanced the mEJP-frequency (**B**) and reduced the mEJP-amplitudes (**D**), but did not significantly alter eEJP amplitudes (**F**). Data denoted means ± S.E.M collected from the indicated number of cells. *p<0.05; **p<0.01; ***p<0.001 by two-tailed Student's *t*-tests

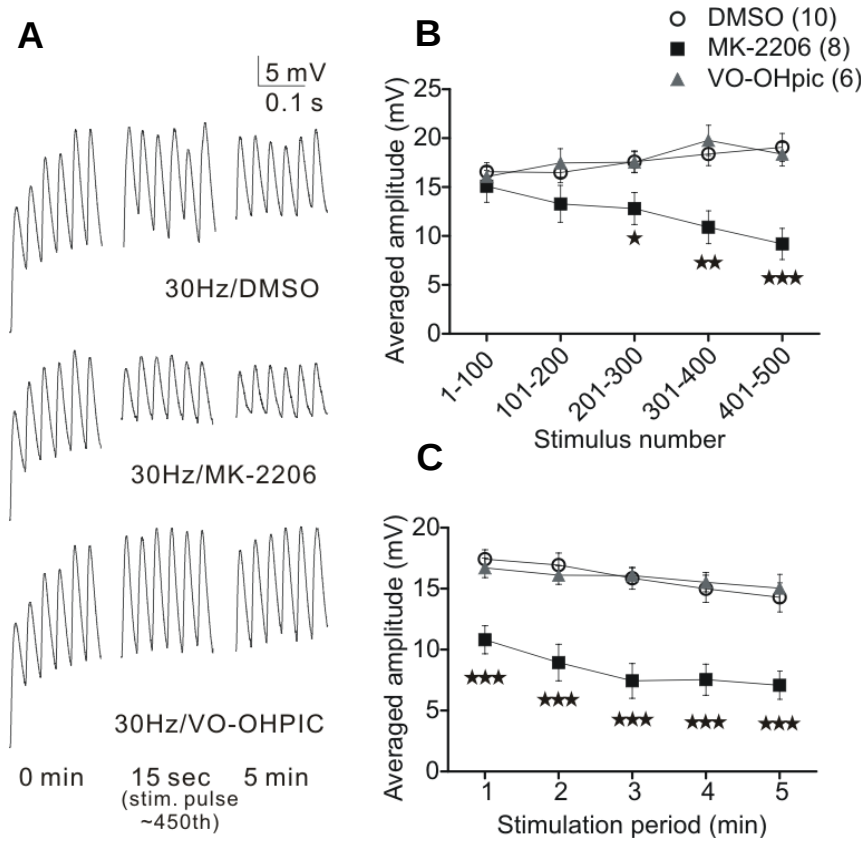

Figure 5.5: Sustained high frequency evoked vesicle release in Drosophila NMJ was hampered under AKT inhibition

A Representative traces of eEJPs at the beginning (0 mins, left column), 15 seconds (middle column) and 5 mins (right column) of 30Hz stimulation under the indicated treatments. **B** Averaged eEJP amplitude of the first to fifth hundred stimulations. Significant reduction of eEJP amplitude by AKT inhibition (MK-2206) was observed starting from the 200-300th stimulation pulse. **C** One minute binning of eEJP amplitude over the course of 5 mins 30Hz stimulation. AKT inhibition (MK-2206) induced progressive reduction of eEJP amplitude in the first 3 mins of 30Hz stimulation. Data denoted means ± S.E.M collected from the indicated number of cells. *p<0.05; **p<0.01; ***p<0.001 by two-tailed Student's t-tests

Interpreting from those results, the functional shift of the release machinery towards spontaneous release only lowered the efficiency of evoke release at repeated events, AKT activity is indeed exhibiting no direct effect on evoke release and is specific for spontaneous events. One reason for the reduction in subsequent evoked amplitude could be the role played by AKT activity in vesicle endocytosis (Barbieri et al., 1998; as observed from the attenuated fluorescence decay in MK-2206 treated synapse observed in our experiment **Figure 5.3 C**), impairment of which may reduce the recycling and

availability of readily releasable vesicle for successive evoke release. Other speculations could be that impaired AKT activity may alter the affinity or desensitization/dissociation kinetics of the components in the release machinery, which do not affect isolated release but temporally tight repeated evoked release. Further investigations would be required to clarify the above issues.

5.1.3. Acute inhibition of AKT transforms spontaneous spiking into robust bursting activity in hippocampal neuronal network

AKT inactivity appeared to affect evoked vesicle release in a use-dependent manner. Moreover, the impairment of AKT activity tends to drive the release machinery towards spontaneous release at both excitatory and inhibitory synapses, with more pronounced effects at the former than the latter synapses. Given these prominent effects of AKT on vesicle release, we wondered whether the spiking behavior of neurons within a complex neuronal network is also affected by AKT.

Strikingly, we found that the rather irregular spontaneous spiking activity of single action potentials within hippocampal neuronal networks (upper panel in **Figure 5.6 A**) transformed into oscillating bursts of three or more clustered action potentials within minutes of applying blockers of PI3K or AKT (lower two panels in **Figure 5.6 A**). Intriguingly, the timing of this spiking-to-bursting transition happened in parallel to the increases in the rates of spontaneous vesicle release (**Figure 5.1 B**) indicating that increased network noise (i.e. enhanced spontaneous vesicle release) might over-sensitize the networks' firing behavior. Interestingly, while both the blockade of PI3K or AKT resulted in enhanced bursting with similar overall duration of cell depolarization (**Figure 5.6 D**), the bursting pattern achieved with each of the treatments was obviously different. PI3K blockade (which elicited a moderate increase in the rate of mEPSPs **Figure 5.1 B**) resulted in a concomitant clustering of additional spikes into short and rather irregular bursts (middle panel- **Figure 5.6 A**), whereas AKT blockade (which massively increased mEPSP rates **Figure 5.1 B**) yielded robust and longer lasting bursts and inter-burst pauses (lower panel **Figure 5.6 A**).

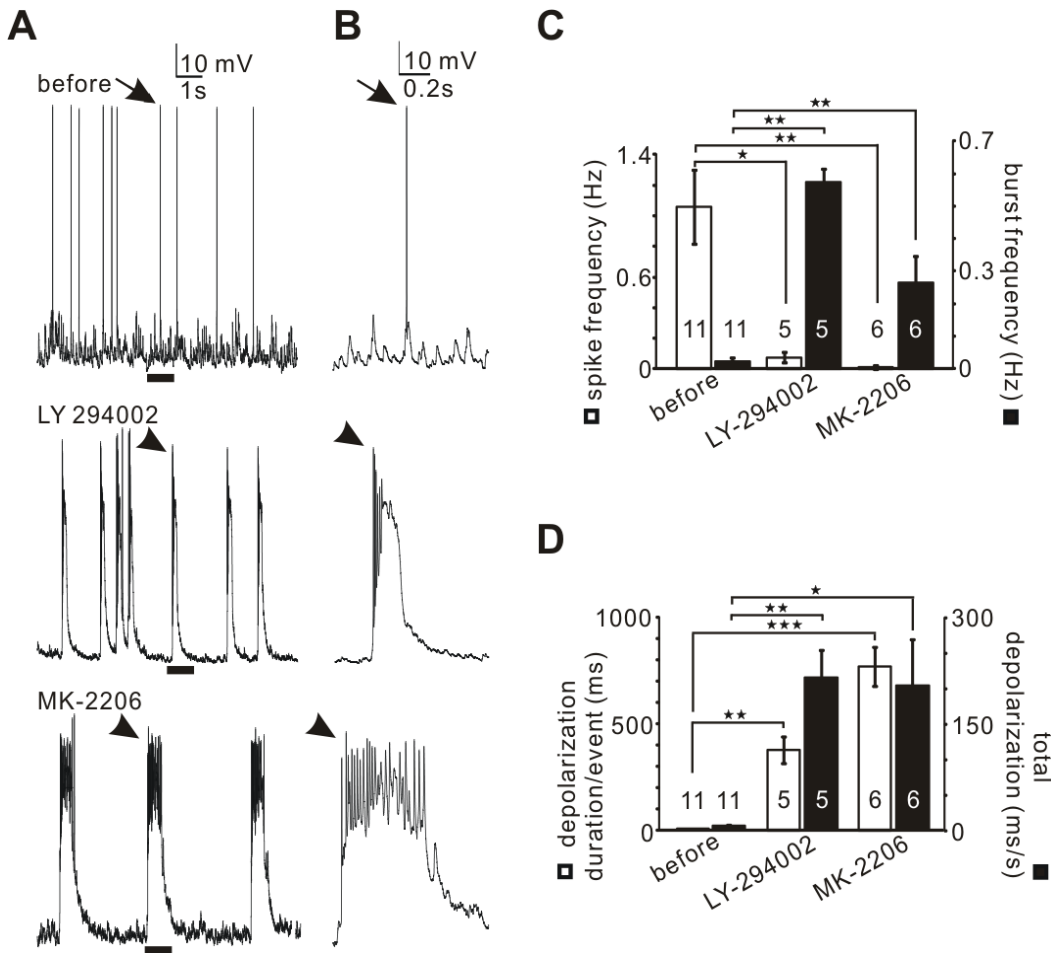

Figure 5.6: Inhibition of AKT induce bursting activity in hippocampal neuronal network

A Representative membrane potential recordings of hippocampal neuronal firing activities. **B** Five-times temporal magnification of the underlined region (black bar) in **A**. Note that the irregular spontaneous spiking of single action potentials (arrows in **A & B**) was transformed to a robust oscillating bursting of clustered action potentials (arrow heads) when AKT or PI3K were inhibited (MK-2206 or LY-294002, respectively). **C** Occurrence of single spikes was reduced by both AKT and PI3K inhibition (white bars), which were replaced by bursting behavior that occurred at typical frequencies (black bars). **D** The duration of depolarization per event (spike or burst) was substantially increased by both drugs, with that of LY-294002 being shorter than MK-2206 (white bars). Both AKT and PI3K inhibition strongly enhanced neuronal excitativity as indicated by the significant elongation of depolarization duration (black bars). Data denoted means ± S.E.M collected from the indicated number of cells. *p<0.05; **p<0.01; ***p<0.001 by two-tailed paired Student's *t*-tests

How the rate of mEPSPs is related to the here observed different bursting behaviors is currently unclear, but since those bursting appear and disappear with the changes in mEPSP rates upon drug treatment and washout (data not shown, n = 2-3), it seems likely that the mEPSP rates exert a direct influence on the neuronal firing behavior. These sharp changes in spiking behavior may affect many aspects of neuronal network functions, such as network plasticity and signal processing in general.

5.1.4. rAAV-shRNA mediated specific knockdown of Synaptotagmin1 does not impair AKT inhibition induced spontaneous vesicle release

Synaptotagmin1 (Syt1), the classical calcium sensor that is required for evoked vesicle release (Fernandez-Chacon et al., 2001; Sorensen et al., 2003), works in conjunction with complexin as a key component of the vesicle fusion clamp (Sollner et al., 1993a; Tang et al., 2006; Huntwork and Littleton, 2007; Xu et al., 2013). Syt1 is the most abundant Syt isoform at mammalian synapses (Takamori et al., 2006; Weingarten et al., 2014; Wilhelm et al., 2014). Disruption of Syt1 function was shown to enhance spontaneous vesicle fusion, and obstruct evoked vesicle release (DiAntonio et al., 1993; Littleton et al., 1993; Geppert et al., 1994; Nishiki and Augustine, 2004b; Maximov and Sudhof, 2005). At *Drosophila* NMJs, we have shown that knocking down of Syt1 abolished the mEJP frequency rise upon AKT inhibition (Ge*, Leung* et al., *under revision*). This finding suggested that Syt1 is a key effector to translate the activity of AKT onto the vesicular clamping machinery. We therefore wished to assess whether this role of Syt1 in mediating the synaptic effects of AKT on vesicle release machineries is conserved in the mammalian system.

To knockdown Syt1 in rat hippocampal neurons, we generated recombinant adeno-associated virus (rAAV) particle that carry an expression cassette for small hairpin RNA (shRNA; Klugmann et al., 2005) targeting specifically against Syt1. The shSyt1 sequence (5′-GAGCAAATCCAGAAAGTGCAA-3′) that has been utilized in repeated publications (Xu et al., 2007; Yang et al., 2010; Bacaj et al., 2013) was used. For details of the generation of rAAV-particles see **Materials and methods 4.2.** A non-targeting scramble shRNA sequence (5′-GTGCCAAGACGGGTAGTCA-3′; shSCR) that showed

no observable morphological or physiological effect on neurons (Mauceri et al., 2011) was used as control. All shRNA expression was driven by the mouse RNA polymerase III U6 promoter (Miyagishi and Taira, 2002). The expression construct also contain the mCherry reporter control by the neuron-specific calcium/calmodulin-dependent protein kinase (CaMKII) promoter. The rAAV subtype we used exhibits a specific infection towards neurons over glia (Xu et al., 2001) and has a typical infection efficiency of 75-85% in rat hippocampal neurons (data not shown).

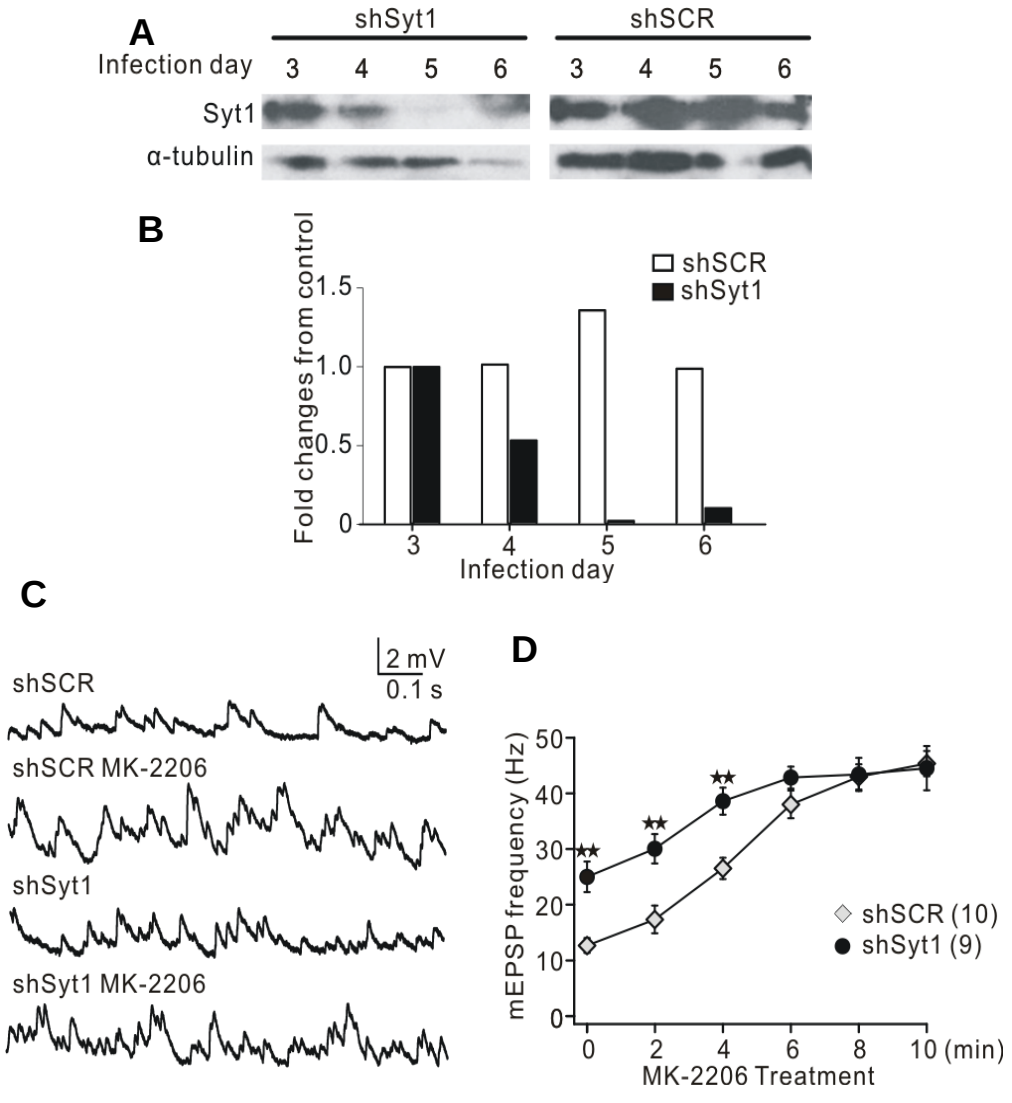

Figure 5.7: rAAV-shRNA mediates specific knockdown of Synaptotagmin1 does not impair AKT inhibition induced spontaneous vesicle release

A Western blot analysis illustrating the effective knockdown of Synaptotagmin (Syt1) starting from the 5th day of rAAV infection. α-tubulin was used as a loading control. **B** Quantification of Syt1 expression levels from the western blot results in **A**, reflecting an almost complete abolishment of Syt1 protein expression on the 5th day of rAAV infection. **C** Representative mEPSP recordings from cells infected with rAAV carrying shSyt1 or non-targeting sequence (shSCR), before and after AKT blockage by MK-2206. **D** Syt1 knockdown significantly increased basal mEPSP frequency. In contrast to the *Drosophila* NMJ system, knocking down of Syt1 in hippocampal neurons did not block the mEPSP frequency increase towards AKT-inhibition, the highest mEPSP rate shows no difference to the control. Data denote means ± S.E.M collected from the indicated number of cells. *p<0.05; **p<0.01; ***p<0.001 by two-tailed Student's t-tests

Knockdown (KD) of Syt1 was shown to be effective starting at day 5 of virus infection (**Figure 5.7 A & B**) western blot performed by Marlena Lübke B.Sc.), this infection time point was therefore implemented for the testing of Syt1-KD on our cultures. Consistent with reported observations from other laboratories (DiAntonio et al., 1993; Littleton et al., 1993; Geppert et al., 1994; Nishiki and Augustine, 2004b; Maximov and Sudhof, 2005), the mEPSP frequency was about two-fold higher in cultures treated with rAAV-shSyt1 (**Figure 5.7 C & D**). This observation supports the idea that a Syt1-KD weakens the clamp of the vesicle fusion machinery (Chicka et al., 2008). However, knocking down Syt1 from the mammalian vesicle release machinery did not eliminate its sensitivity towards AKT inhibition (**Figure 5.7 C & D**) as it did in *Drosophila* (Ge*, Leung* et al., *under revision*). Although it is not excluded that the expression of the shSyt1 construct is not as strong as in *Drosophila*, this finding indicates that at mammalian synapses, Syt1 is not the only crucial translator of AKT's activity into the vesicular clamping machinery. This is consistent with the reported differences in the role of Syt1 and Complexin at invertebrate and vertebrate synapses (Huntwork and Littleton, 2007; Maximov et al., 2009; Xue et al., 2009). Nevertheless, those results demonstrated the effectiveness of rAAV-shRNA for the KDs of specific synaptic target molecules in rat hippocampal neurons.

5.1.5. rAAV-shRNA mediates specific knockdown of AKT1 or AKT3

The *Drosophila* genome has only one AKT related gene (Franke et al., 1994), whereas three AKT genes were found in mammalian genomes (Alessi and Cohen, 1998; Coffer et al., 1998) giving rise to three AKT isoforms: AKT1/PKBα, AKT2/PKBβ, and AKT3/PKBγ with distinct spatial and temporal expression patterns (Zinda et al., 2001; Gonzalez and McGraw, 2009b). As mentioned in the introduction (**Introduction 3.5**), each of these isoforms was reported to perform both unique and common functions in cells (Chen et al., 2001; Cho et al., 2001; Brazil et al., 2002; Nicholson and Anderson, 2002). So far, we have collected data of AKT inhibition using the blocker MK-2206 that targeted all isoforms (Hirai et al., 2010), we therefore wish to discriminate the effects contribute by different AKT isoforms on spontaneous vesicle release. AKT1, the ubiquitously expressed isoform; as well as AKT3, the isoform predominantly expressed in the brain were first brought to test.

rAAV virus particles carrying shRNA that targets either rat AKT1 (5′-ACAACTCAGGTGCTGAGGA-3′) or AKT3 (5′-ATAATATTGGAGAGGAAGA-3′;Katome et al., 2003) were produced. To test the effectiveness and specificity of our rAAV-shRNAs, the expression of AKT1 and AKT3 proteins was analyzed on day 8 and 10 post-infection (**Figure 5.8 A & C;** western blot performed by Marlena Lübke B.Sc.). Both of the infection period reduced the expression of AKT1 and AKT3 was effectively and specifically (**Figure 5.8 A, D)**. In addition, the silencing of AKT1 was accompanied by an almost equivalent compensatory up-regulation of AKT3 at day 8 post infection (**Figure 5.8 A-C**). Similarly, the AKT3-KD was apparently compensated by a corresponding up-regulation of AKT1. However, after 10 days of virus infection, the compensatory up-regulation of the not-targeted AKT isoform dropped back to normal while the silencing of the targeted isoforms were almost complete (**Figure 5.8 D-F**). These results show that those rAAV-shRNAs were highly effective in the specific silencing of AKT1 or AKT3 at rat hipppocampal neurons. The western blot data suggest that AKT1 and AKT3 may be functionally linked such that the silencing of one is compensated by a transient stronger expression of the other.

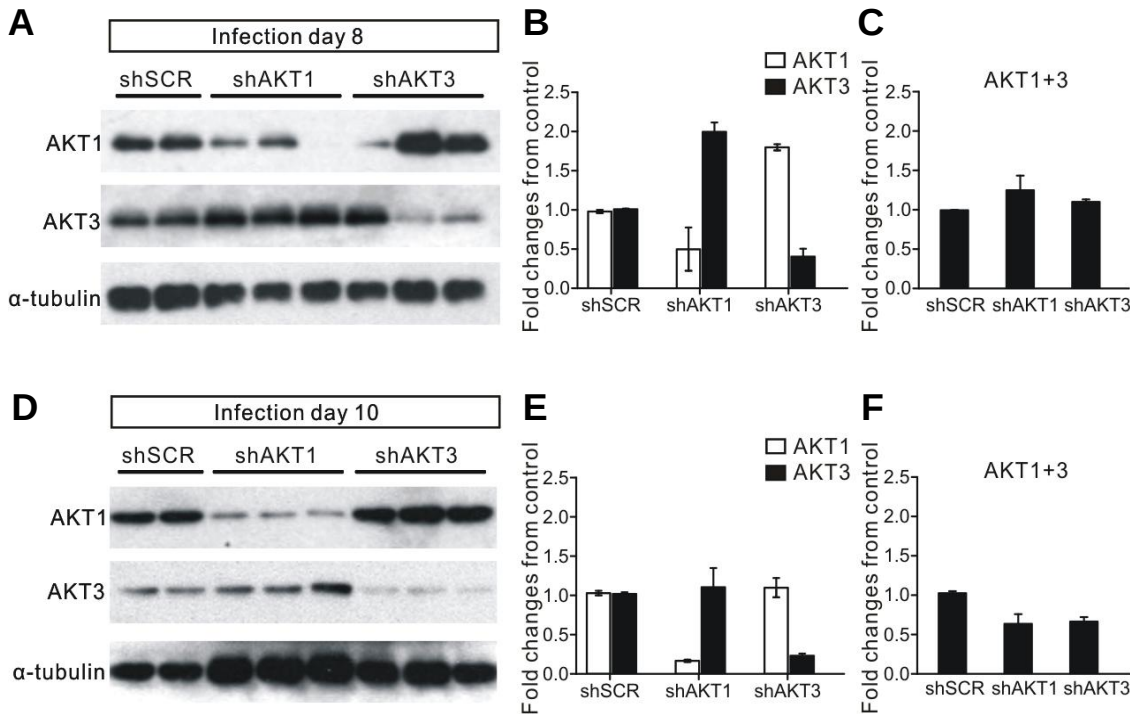

Figure 5.8: rAAV-shRNA mediates specific knockdown of AKT1 or AKT3

A & C Western blot analysis indicating effective and specific AKT1 or AKT3 knockdown by shRNA carrying rAAV at infection day 8 (**A**) and 10 (**C**). α-tubulin was used as loading control. **B & D** Quantification of AKT1 and AKT3 expression levels from the western blot results in **A & C** respectively. Intensity proportion of protein bands were first referenced to the first lane of sh-SCR control and then normalized to the level of α-tubulin in each lane. Data denote means ± S.E.M.

5.1.6. AKT1 or AKT3 knockdown exhibit opposite effects on spontaneous vesicle release in hippocampal neuronal culture

Since the shRNA KDs were effective on rAAV infection day 8, and a portion of culture cells were appeared unhealthy at infection day 10, we examined the physiological effects of our KDs on mEPSPs primarily on day 8 post infection. Surprisingly, silencing either of the two isoforms elicited opposite effects on the basal mEPSP frequencies: cultures infected with rAAV-shAKT1 exhibited a significantly reduced rate of mEPSP, whereas AKT3-KD enhanced the basal mEPSP rate (**Figure 5.9 A & B,** time point 0).

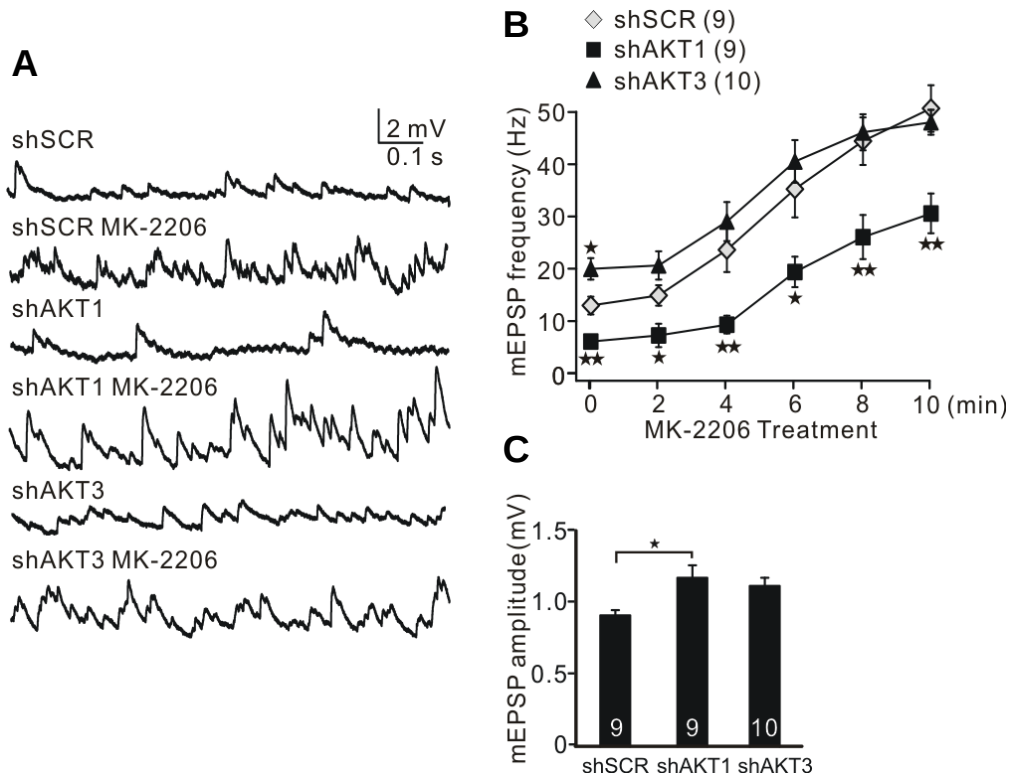

Figure 5.9: AKT1 or 3 knockdown exhibit opposite effects on spontaneous vesicle release in hippocampal neuronal culture

A Representative mEPSP recordings from cells infected with rAAV expressing the indicated shRNA sequence before and after AKT blockage by MK-2206. **B** Knockdown of AKT1 results in reduced mEPSP frequency at drug treatment time 0 min, there is still responsiveness towards AKT-inhibition (MK-2206), but the frequency rise is lowered throughout the treatment time. Knockdown of AKT3 increased mEPSP frequency, but the sensitivity towards AKT-inhibition was not significantly different from control. **C** knocking down of both AKT1 or AKT3 manifested apparent increase in mEPSP amplitude, of which the elevation by the AKT1 knockdown is significant compared to control. Data denote means ± S.E.M collected from the indicated number of cells. *p<0.05; **p<0.01; ***p<0.001 by two-tailed Student's *t*-tests.

In addition, when we applied the AKT blocker (MK-2206), the AKT3-KD cells behaved similarly to control cells. AKT1-KD was also responsive to the AKT blocker, but the mEPSP-frequency rise was lowered throughout the treatment time, and plateau at a lower frequency compared to those of AKT3-KD or control cells (**Figure 5.9 B**). The sensitivity of AKT1-KD to MK-2206 treatment may due to incomplete shRNA-mediated KDs. Longer duration of AKT level reduction may also enhance the expression of its

downstream molecules that subject the system to be more sensitive towards AKT inhibition.

Since AKT has been reported to affect the postsynaptic glutamate receptor localization (Lee et al., 2013a) we also analyzed the amplitude of mEPSP in our recordings. Interestingly, AKT1 or AKT3 KD both manifested apparent increase in mEPSP amplitude, of which the elevation by the AKT1 KD was significant compared to scramble control (**Figure 5.9 C**). The concentration of postsynaptic receptor did not show a reduction in our existing data, whether there is a change in the number of synapse or postsynaptic receptor clusters are however remained to be elucidated. If those synaptic properties were not changed, the reduced sensitivity of AKT1-KD under MK-2206 treatment may point towards AKT1 as the isoform responsible for the modulation of vesicle release machinery. However, RNAi-mediated KDs of *Drosophila* AKT resulted in an increased basal mEJP rate (Ge*, Leung* et al., *under revision*), acute pan-AKT inhibition also increase mEPSP frequency in hippocampal neurons (**Figure 5.1 B**). The reduced basal mEPSP-frequency in AKT1-KD appears to contradict the phenotypes of reduced activity of pan-AKT. The increased rate of mEPSP in AKT3-KD seems to correlate with the effect of acute pan-AKT inhibition instead. In addition to the potential adaptive response of the synapses towards extended duration of AKT decline, an alternative explanation could be the potential functional redundancy of the two isoforms (Lee et al., 2011c) and the compensatory up-regulation of one isoform when the other is down-regulated. Since the kinase activity of AKT3 is substantially higher (~15fold; Cristiano et al., 2006) then AKT1, AKT1-KD (and compensation overexpression of AKT3) may resemble an overall enhancement of AKT kinase activity, which exhibit a lower rate of spontaneous release and reduced sensitivity to AKT pharmacological inhibition, while AKT3-KD may resemble an overall reduction of kinase activity, which leads to an elevation of spontaneous vesicle release. Nevertheless, the validity of this reasoning would be examined after the functional role of AKT2 was explored.

5.2. Experimental input for the construction of three-dimensional mathematical model of calcium dynamics in *Drosophila* NMJ boutons

Our laboratory has established a joint collaborative project with the theoretical group of Prof. Gillian Queisser (Goethe-Universität Frankfurt), in which a detailed three-dimensional mathematical model of presynaptic vesicle dynamics of the synaptic bouton of *Drosophila* NMJ was developed (M. M. Knodel, 2014). This mathematical model provides a framework for reconstructing the physical dynamics of other biological players in relation to their functional outcome. The first player that came into our interest is calcium, which is the key signal that trigger presynaptic vesicle release and modulate numerous cellular signaling processes. To theoretically reconstruct the calcium dynamics of *Drosophila* NMJ bouton, we established a collaborative effort with Martin Stepniewski (AG Prof. Gillian. Queisser, Goethe-Universität Frankfurt) who is responsible for the building of the theoretical model. To ensure this model reflect the realistic biological condition, this second part of project provide experimental data to validate and adjust the corresponding mathematical parameters.

Here, the glutamatergic synapses of *Drosophila* NMJ boutons were chosen to overcome the experimental limitations posed by the complexity of mammalian synapses. The calcium dynamics in *Drosophila* NMJ boutons was dissected in two experimental approaches. First, the electrophysiological measurement of paired-pulse eEJPs ratio provides data for accessing the calcium dynamics within the active zones of all boutons in an NMJ. Second, quantitative life calcium imaging using a genetically expressed GCaMP6m indicator provides data for estimating the calcium dynamics within individual bouton (Takamori et al., 2006).

5.2.1. Calcium dynamics at *Drosophila* NMJ active zone

In response to a pair of tight temporally spaced stimulation pulses, postsynaptic response towards the second pulse is affected by a number of synaptic factors, which gives rise to a larger or smaller response over the first pulse, referred as paired-pulse facilitation (PPF) or paired-pulse depression (PPD) respectively. The ratio between the postsynaptic response amplitude of the second pulse over the first (paried-pulse ratio,

PPR) has an inverse relationship with the initial release probability (Dobrunz and Stevens, 1997), and is a function of the availability of readily releasable pool vesicles (contributing PPD) and residual calcium (contributing PPF). According to the residual calcium hypothesis for PPF (Katz and Miledi, 1968; Zucker, 1989), there is a distinct time window that the calcium influx from an action potential persists in the presynaptic bouton. When a second action potential arrives within that time window, calcium builds up leading to an augmented vesicle release. This augmentation is probably due to a larger calcium microdomain to reach more distant vesicles, or a higher calcium concentration in the microdomain that increase the probability of triggering vesicle release. Assumed unlimited availability of readily releasable vesicles, the response amplitude to the first pulse can be estimated by $A_1 = k([Ca^{2+}]_{influx})^4$, to the second pulse $A_2 = k([Ca^{2+}]_{residual} + [Ca^{2+}]_{influx})^4$ (where k is a constant). The ratio of residual to influx calcium concentration can then be approximated by $[Ca^{2+}]_{residual}/[Ca^{2+}]_{influx} = \sqrt[4]{A_2/A_1} - 1$, i.e. $\sqrt[4]{PPR} - 1$. Since the release probability and the readily releasable pool of *Drosophila* NMJ bouton has been described in our first collaborative project (M. M. Knodel, 2014), the contribution of those two parameters on PPR can be isolated, which allow us to compute the $[Ca^{2+}]_{residual}$ to $[Ca^{2+}]_{influx}$ ratio. The $[Ca^{2+}]_{influx}$ per release site can be derived from the $[Ca^{2+}]_{influx}$ of the entire bouton collected from the next session (**Results 5.2.2**), which can be used to extract the $[Ca^{2+}]_{residual}$ for the interpretation of calcium buffering properties and export kinetics.

In this experiment, the motor nerve was stimulated at a frequency of 0.1Hz with pairs of stimuli that were separated by 25/50/75/100 ms, which results in pairs of accordingly spaced evoked excitatory junctional potentials (eEJPs; **Figure 5.10 A**). The PPRs were analyzed in a range of extracellular calcium concentration ($[Ca^{2+}]_{ex}$): 0.5, 0.75, 1 and 1.5mM (**Figure 5.10 B & C**).

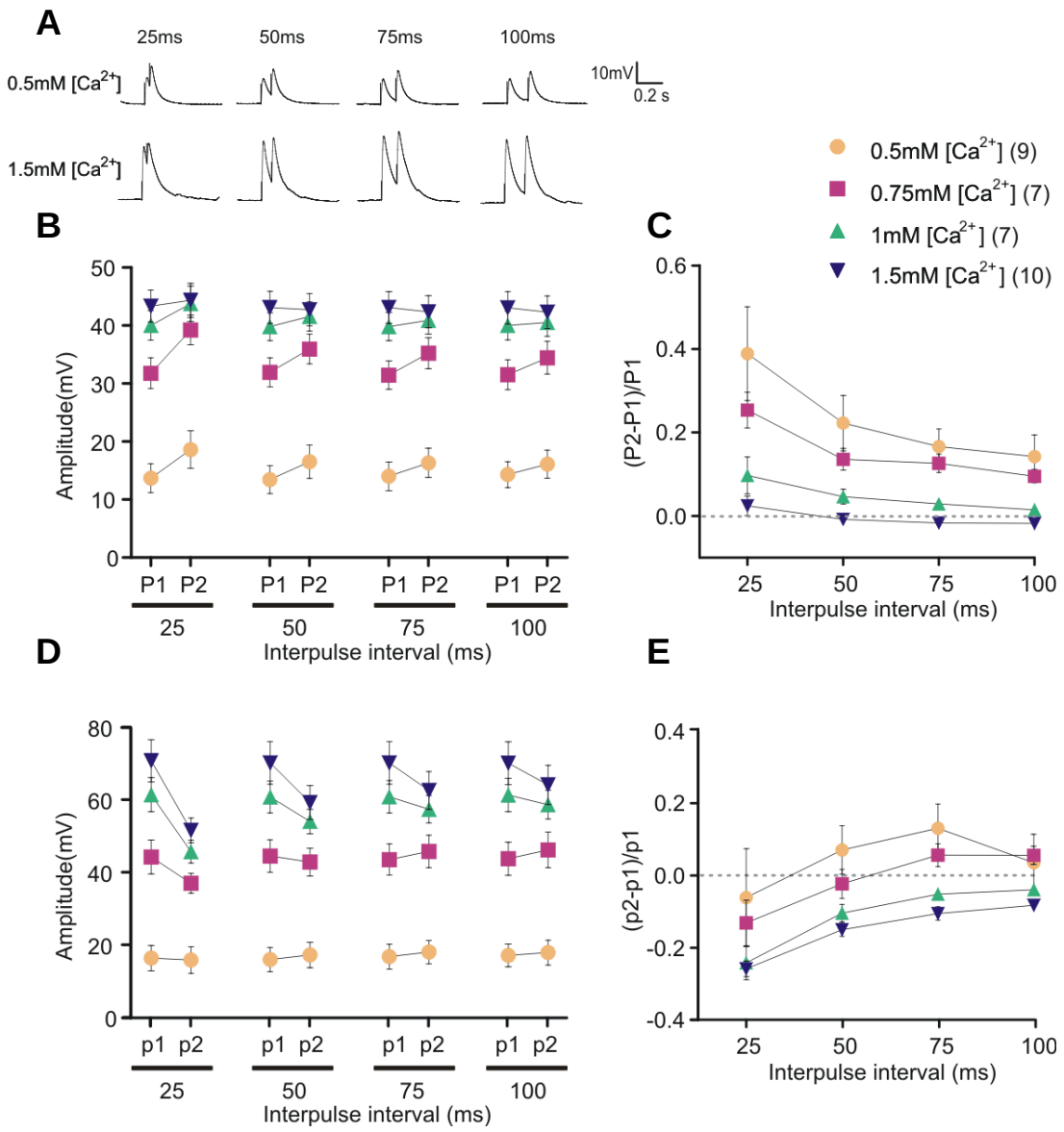

Figure 5.10: Estimation of Calcium buffering capacity and export kinetics in *Drosophila* NMJ boutons by measurement of paired pulse ratio

A Representative eEJP pairs in response to paired pulse stimulation in the indicated calcium concentration and inter-pulse interval. **B** The mean amplitude of eEJPs elicited by the first (P1) and the second stimulation pulse (P2). **C** Mean paired-pulse ratios (PPR) calculated from unadjusted eEJPs amplitude (P2-P1)/P1. **D** Adjusted mean amplitude of the pair of eEJPs. To enhance the precision of the PPR value, the eEJPs were corrected by two factors: 1) An estimated decay phase of the first eEJP was used as the baseline for the calculation of the amplitude of the second eEJP. 2) Both first and second eEJPs amplitudes were corrected for non-linear summation. **E** Resultant adjusted paired pulse ratio. Paired-pulse facilitation (PPF, positive PPR values) was observed at lower [Ca2+]ex (0.5-0.75mM) and longer inter-pulse interval (50-100ms). At 0.5mM [Ca2+]ex, as interpulse interval increase from 75 to 100ms, the positive PPR

value started approaching zero, indicating a clearance of calcium within the active zone at 75-100ms. Data denote means ± S.E.M collected from the indicated number of cells.

At all inter-pulse intervals, the values of PPR increase with decreasing $[Ca^{2+}]_{ex}$. This is consistent with the notion that the larger the $[Ca^{2+}]_{ex}$, the more is the vesicle released by the first pulse, and the less availability of readily releasable vesicles at the arrival of the second pulse. Moreover, the difference of PPR between $[Ca^{2+}]_{ex}$ reduced with increasing paired pulse interval. This also agrees with the rationale that the sooner the second pulse arrive after the first pulse, the less complete clearance of residual calcium, and therefore elicited larger number of vesicle release.

In addition to the analysis of PPR by conventional method, we opt to enhance the precision by correcting two factors: 1) the amplitude of the second eEJPs (P2) that overlay on the first eEJP (P1) and 2) non-linear summation. Since the P2 overlaps with the P1, the calculation of the P2 amplitude by simply subtracting the peak potential value by the baseline potential before the two pulses arrive do not reflect the true P2 amplitude. The baseline potential of P2 was therefore extracted from the potential contributed by P1 instead. To obtain the real baseline potential of P2, the decay phase of P1 was first fitted by linear or single order exponential function. The fitted curve was then extrapolated to estimate the baseline contributed by P1, where the adjusted P2 amplitude was calculated (for details see **Materials and Methods 4.4.2.1**). Secondly, both amplitudes of P1 and P2 were corrected for non-linear summation that arise from the non-linearity between eEJP and the number of released vesicle. To this end, the Martin correction factor (McLachlan and Martin, 1981), which adjusts for the leakage conductance and membrane capacitance, was employed for the correction of non-linear summation of quanta, yielding the corrected pair of amplitudes (**Figure 5.10 D**).

Same as the unadjusted PPRs (**Figure 5.10 C**), the values of adjusted PPR generally increase with decreasing $[Ca^{2+}]_{ex}$ (**Figure 5.10 E**). However, different from the unadjusted PPRs, the adjusted PPR values generally increased with the duration of the paired pulse interval instead. And a PPD (negative PPR values) instead of PPF (positive PPR values) was observed at all higher $[Ca^{2+}]_{ex}$ (1-1.5mM) and short inter-pulse interval

(25ms). From this adjusted PPR data, the release probability of vesicle induced by high $[Ca^{2+}]_{ex}$ appeared to be larger, the first pulse appeared to have recruited most readily releasable vesicles, which limited their availability for the second pulse. Since the replenishment of readily releasable vesicle is a time dependent process, the availability of readily releasable vesicle for the second pulse reduced with shorter duration of inter-pulse interval. In the above cases, the reduced availability of the readily releasable vesicle has limited the action of residual calcium build up. Nonetheless, at 0.5mM $[Ca^{2+}]_{ex}$, when the inter-pulse interval reduces from 75ms to 100ms, the value of PPR started to drop and approaching zero value, indicating a clearance of residual calcium by around 100ms.

Since we have obtained the release probability, the vesicles pool size and the kinetic terms of vesicle diffusion in our first collaborative project, incorporating those parameters together with the current PPR data (adjusted or unadjusted) would allow us to estimate the of calcium buffering properties and calcium export kinetics.

5.2.2. Quantitative Calcium imaging and the estimation of Calcium concentration in the presynaptic boutons of *Drosophila* NMJ

To image the calcium dynamics within *Drosophila* boutons in response to nerve stimulation, we employed the calcium sensor GCaMP6m (Chen et al., 2013) that was expressed in the *Drosophila* NMJ motoneurons by the $elav^{C155}$ pan neuronal Gal4-driver. NMJ bouton calcium fluorescence was recorded at HL3 solution with 1.5mM $CaCl_2$ and 2 mM $MgCl_2$. Throughout the image recording, 7mM Glutamate was incorporated in the HL3 solution to desensitize the postsynaptic glutamate receptors. This receptors desensitization approach is able to block postsynaptic muscle contractions without influencing presynaptic calcium dynamics (Macleod et al., 2004).

The peak intracellular calcium concentration rise upon stimulation was estimated using the method described by (Maravelli et al., 2000), which calculates the change in calcium concentration $\Delta[Ca^{2+}]$ by:

$$\frac{\Delta[Ca^{2+}]}{K_D} = \frac{F_{max}}{F_0}(1 - R_f^{-1})\frac{\delta F}{(\delta F_{max} - \delta F)\delta F_{max}}$$

and the resting calcium concentration $[Ca^{2+}]_{rest}$ by:

$$\frac{[Ca^{2+}]_{rest}}{K_D} = \frac{(1 - R_f^{-1})}{\delta F_{max}} - R_f^{-1}$$

where

- Fmax stands for the maximal fluorescence when GCaMP6m is saturated with calcium
- F0 stands for the basal fluorescence of GCaMP6m before any stimulation
- Rf stands for the dynamic range of GCaMP6m
- δF stands for factional fluorescent changes i.e. ΔF-F0)/F0
- δFmax stands for the maximum value of δF when GCaMP6m is saturated with calcium
- KD stands for the dissociation constant of GCaMP6m, which is 167nM (Chen et al., 2013)

The *in vivo* dynamic range (Rf) of GCaMP6m was obtained experimentally from the value of Fmax and Fmin (Rf =Fmax/Fmin). Fmax refers to the maximal fluorescence when GCaMP6m is saturated with calcium. It was measured at 2 seconds of 300Hz of nerve stimulation (**Figure 5.11 C**). Here, high frequency stimulation instead of ionomycin application was used for the determination of Fmax because ionomycin treatment induces severe twitching of muscle, which destroys the imaging of NMJ bouton. Nevertheless, though not perfectly comparable, the value of Fmax determined by high frequency stimulation yield a good 94% of that obtained from the ionomycin method (Albantakis and Lohmann, 2009). Fmin refers to the minimal fluorescence when calcium is taken out from the GCaMP6m. This value was obtained by 40mins incubation of 1mM EGTA and 200µM BAPTA-AM in calcium free HL3(**Figure 5.11** D). Under those conditions, the *in vivo* Rf of GCaMP6m in *Drosophila* NMJ bouton was found to be 20.48 ± 1.02 (134 boutons, 8 NMJ; **Figure 5.11** E).

The peak fluorescence change in response to one stimulus (ΔF_1) of a single bouton was expressed in factional fluorescent changes δF_1 i.e. δF_1=(ΔF-F0)/F0, where F0 is the basal fluorescence before stimulation (**Figure 5.11 B**). The δFmax value of the corresponding bouton was obtained from the maximum fluorescence response towards 2 seconds of 300Hz stimulation (**Figure 5.11 C**). Computing from the above values, the peak rise in calcium concentration triggered by a single stimulation ($\Delta[Ca^{2+}]_{1Hz}$) was

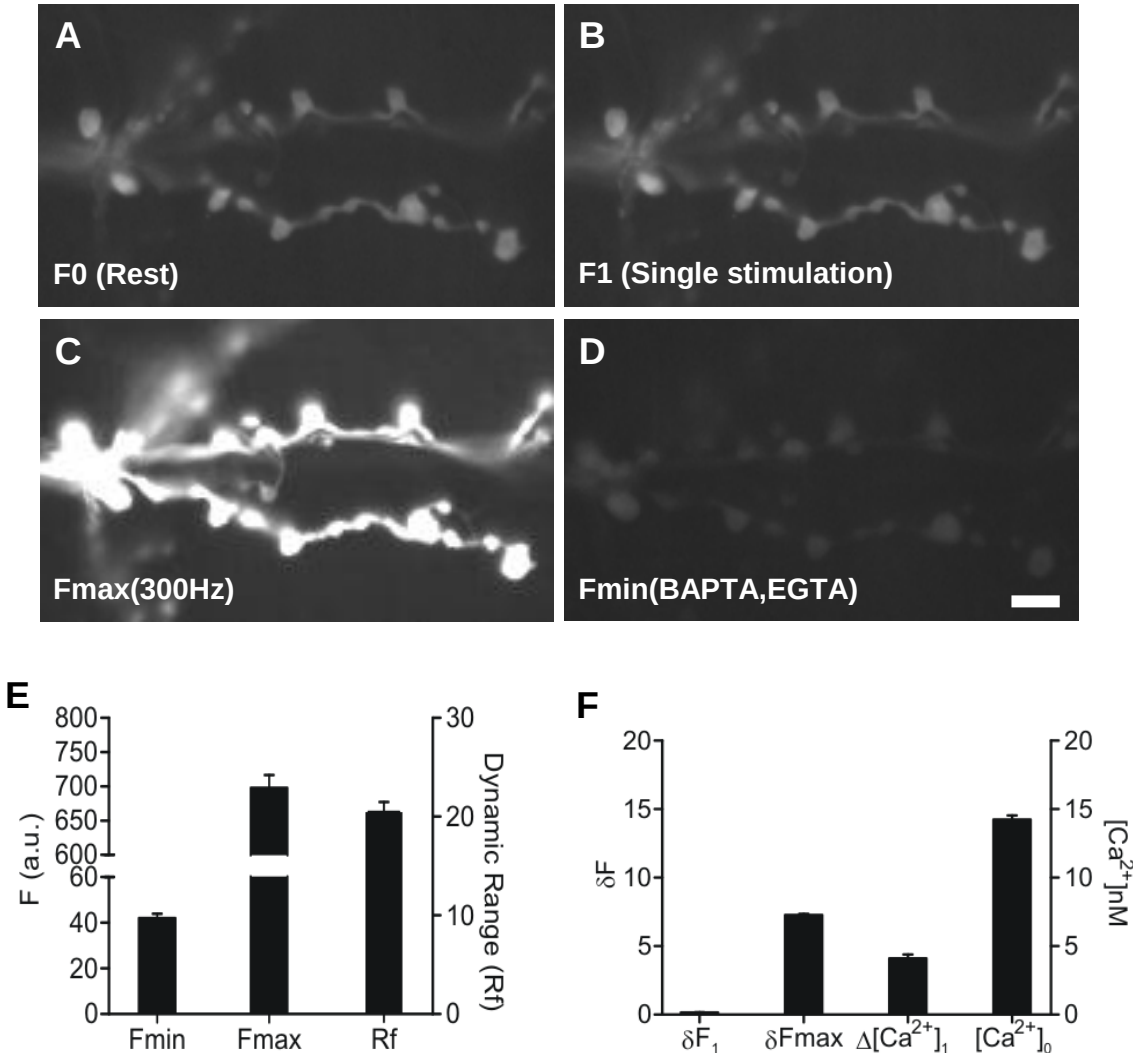

Figure 5.11: Quantitative calcium imaging and the estimation of calcium concentration in the presynaptic boutons of *Drosophila* NMJ

A-D Images of an example NMJ (muscle 6/7) undergoing experimental conditions that were used for the estimation of calcium concentrations within boutons: **A** Resting condition before stimulation (F0); **B** Peak fluorescent after a single stimulation (F_1); **C** Maximum fluorescence value (Fmax) after 300Hz stimulation to achieve GCaMP6m sensor saturation; and **D** Minimum fluorescence (Fmin) after incubation with the calcium chelator BAPTA-AM and EGTA, to obtain the residual fluorescence of the GCaMP6m sensor when calcium is chelated away. **E** The averaged Fmin and Fmax values, where the *in vivo* dynamic range (Rf) of GCaMP6m derived from. **F** The calculated values of peak fractional fluorescent change after a single stimulation (δF_1) and maximum fractional fluorescent change (δFmax) which were used to estimate the peak calcium change of an average bouton after one stimulation pulse ($\Delta[Ca^{2+}]_1$) and the calcium concentration at rest ($[Ca^{2+}]_0$). Data denote means ± S.E.M collected from the indicated number of cells. Scale bar: 5µm

estimated to be 4.11 ± 0.28 nM (118 boutons, 8 NMJs) and resting calcium concentration ($[Ca^{2+}]_0$) to be 14.24 ± 0.29nM (217boutons, 13NMJs), as summarized in (**Figure 5.11 F**).

5.2.3. Calcium rise triggered by single stimulation in the entire bouton is negatively correlated with bouton size

The study from our first collaborative project demonstrated that the release probability and bouton size (that governs the number of release site and size of vesicle pool) determines the limits of firing frequency (M. M. Knodel, 2014). To investigate the relationship between calcium concentration bouton size, correlation analysis was performed on the data from **Figure 5.11**. An inverse relationship was observed from the scatter plot of single stimulation induced peak calcium rise $\Delta[Ca^{2+}]_1$ and the bouton area (**Figure 5.12 A**), the correlation was significant indicated from the Pearson's correlation coefficient (Pearson r =0.523; **Table 5.1**). On the other hand, no significant relationship was shown between the resting calcium concentration and the bouton area, as observed from the parallel distribution of the data points along the x-axis in **Figure 5.12 B** and the close to zero Pearson r value (**Table 5.1**).

The simplest explanation for the negative relationship between bouton size and calcium rise is the reduction in surface area to volume ratio. Assuming all boutons are spherical, the surface area of a sphere=$4\pi r^2$, volume=$(4\ \pi r^3)/3$, surface area to volume ratio can then be given as 3/r, the bouton area can therefore be transformed into the reciprocal of radius. This transformation achieved a linear relationship with $\Delta[Ca^{2+}]_1$ (**Figure 5.12 C**). By fitting a simple linear regression model, the relationship of $\Delta[Ca^{2+}]_1$ and bouton radius were found to be: $\Delta[Ca^{2+}]_1$=2.86/radius+0.43, when expressed in surface area to volume ratio (sav): $\Delta[Ca^{2+}]_1$=0.95sav+0.43. This linear relationship suggest that the calcium rise induced by single stimulation is at a large degree dependent on the surface area to volume ratio at *Drosophila* NMJ bouton.

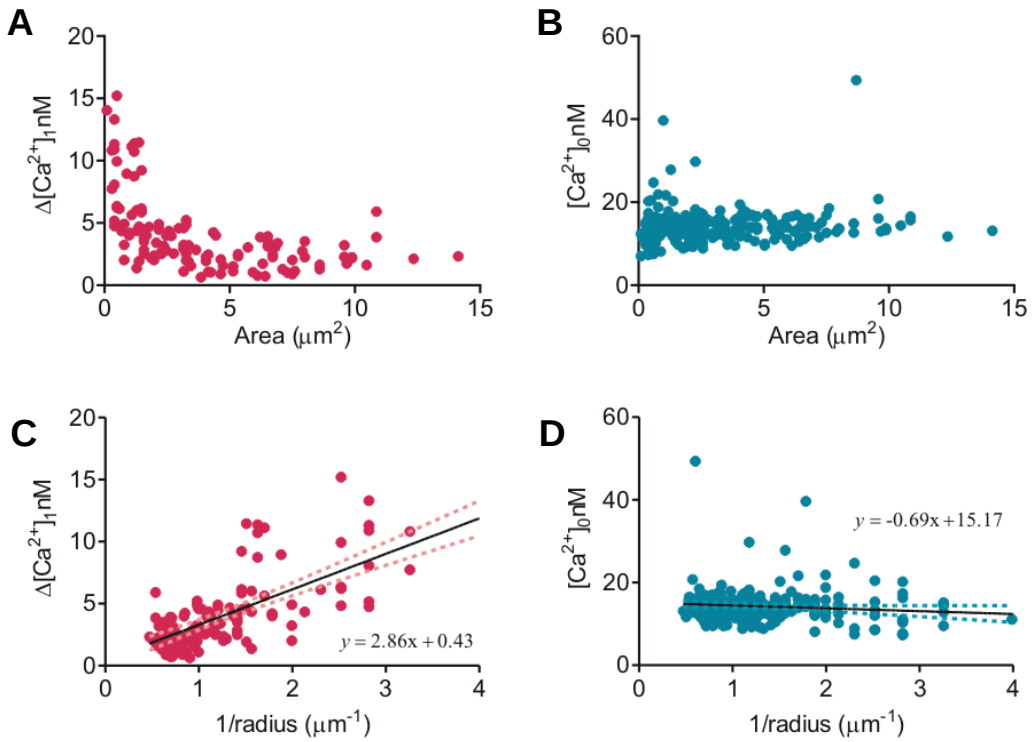

Figure 5.12: Peak calcium rise of the entire bouton triggered by single stimulation exhibit inverse correlation with bouton size

A-D Scatter plot of the intra boutonal calcium concentration against bouton size expressed in bouton area or 1/radius. **A** Peak rise in calcium concentration from single stimulation ($\Delta[Ca^{2+}]_1$) manifest a negative relationship with bouton area. **C** $\Delta[Ca^{2+}]_1$ varies linearly to 1/radius, which reflects the surface area to volume ratio. **B & D** No relationship was observed between the resting calcium concentration ($[Ca^{2+}]_0$) and bouton area (**B**) nor radius (**D**). Dotted curve (pink in **C** and green in **D**) denoted the 95% confidence intervals of the fitted line (black).

Table 5.1: Correlation and linear regression analysis of the relationship between Calcium concentration and bouton size

	Peak rise upon single stimulation $\Delta[Ca^{2+}]_1$	**Resting concentration $[Ca^{2+}]_0$**
Correlation with bouton area (Pearson r)	**-0.523** (p-value < 0.001)	**0.0846** (p-value > 0.05)
Correlation with reciprocal of bouton radius (Pearson r)	**0.7284** (p-value < 0.001)	**-0.1244** (p-value > 0.05)
Slope (value differ from 0)	**2.86 ± 0.25** (p-value < 0.001)	**-0.69 ± 0.37** (p-value 0.0638)
Y-intercept when X=0.0	**0.43 ± 0.38**	**15.17 ± 0.57**
X-intercept when Y=0.0	-0.1499	21.91
Goodness of fit	r^2=0.5305	r^2=0.01546

5.2.4. Calcium dynamics were optimized in different bouton types to serve different physiological firing frequencies

As demonstrated from the previous section, the calcium concentration rise in response to individual stimuli is negatively correlated with bouton size. Size seems to be an important feature for the physiological functioning of boutons, because two bouton types of different sizes (Type 1b:big, Type 1s:small) in the *Drosophila* NMJs have been shown to be specialized for different firing frequencies (M. M. Knodel, 2014). These two bouton types originate from two distinct motor neurons. They both harbor multiple glutamatergic release sites that disperse at strict nearest-neighborhood relationship (Atwood et al., 1993; Meinertzhagen et al., 1998; Sigrist et al., 2003). The release probability of type 1b (diameter 3 μm) is substantially lower (5%) than that of type 1s (diameter 2 μm) boutons (40%). The bigger sized type 1b bouton accommodates more release sites and serves optimally for sustained bouts of synaptic activity (natural firing frequency ramp from 20-40-20Hz; M. M. Knodel, 2014). Whilst the smaller sized type 1s bouton harbors fewer release sites and is only reliable for short trains of stimulation (natural firing frequency below 20Hz; Kurdyak et al., 1994; Lnenicka and Keshishian, 2000; M. M. Knodel, 2014).

We were therefore interested to examine the calcium dynamics at the two types of bouton at their physiological firing frequencies. Fluorescence responses towards one second of 10, 20, 40, 60Hz nerve stimulation were recorded at the *Drosophila* NMJs where both bouton types are visible on the same image plane (**Figure 5.13 A**, **E-H**). To dissect the kinetics of calcium rise and decay in response to various stimulation frequencies, the tau value is extracted by fitting a single exponential function on the respective rise and decay regions – for details cf. **Materials and methods 4.5.2.2**. As depicted in **Figure 5.13 B-C**, type 1s boutons exhibit a quicker rise and slower decay over type 1b boutons at all frequencies, in general 40-50% shorter for rise tau and 10-20% longer decay tau, meaning a faster rise then decay kinetics for 1s boutons.

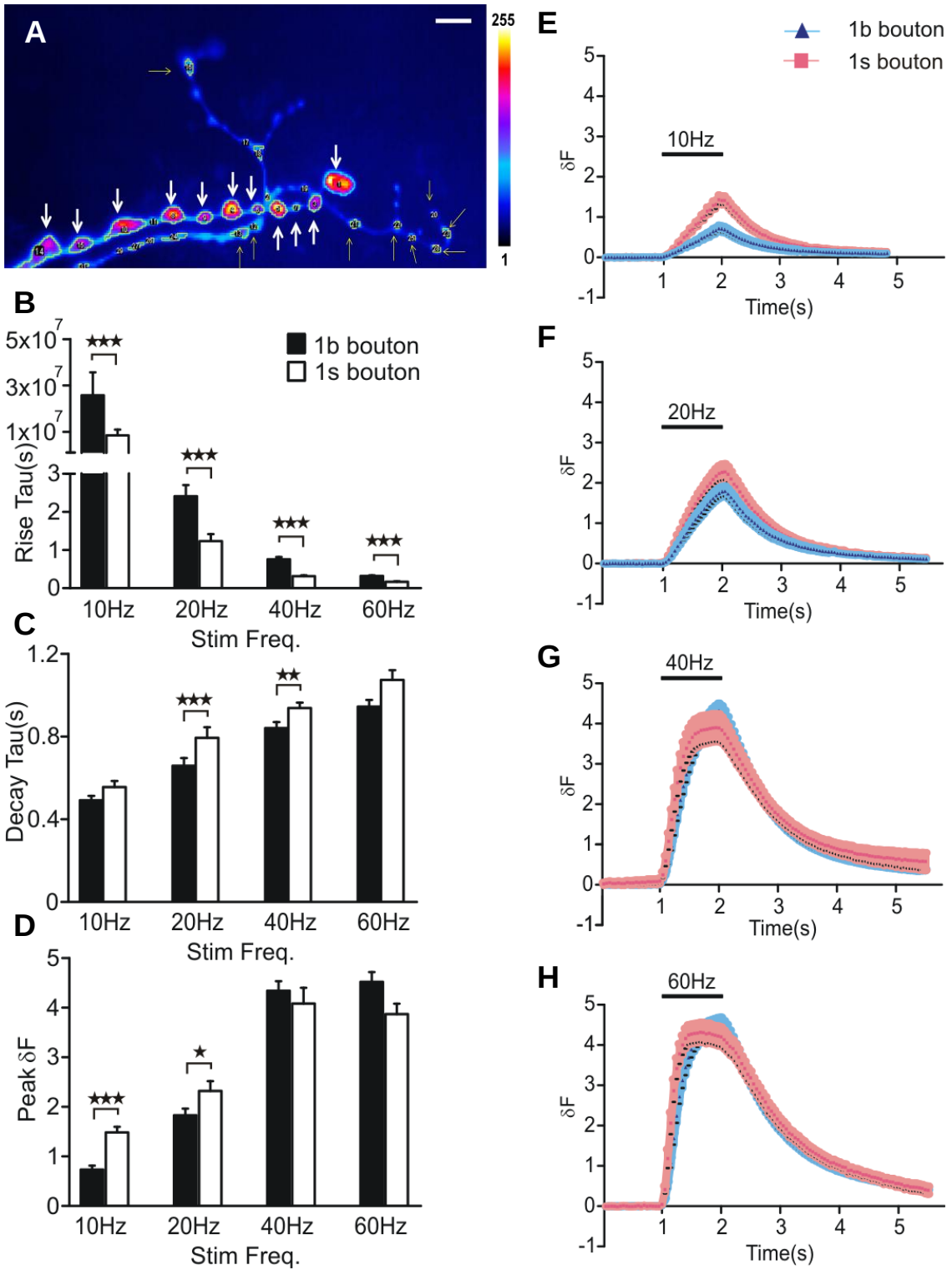
A
255
1
B
1b bouton
1s bouton
Rise Tau(s)
10Hz
20Hz
40Hz
60Hz
Stim Freq.
C
Decay Tau(s)
D
Peak δF
E
1b bouton
1s bouton
10Hz
δF
Time(s)
F
20Hz
G
40Hz
H
60Hz

Figure 5.13: Calcium dynamics of type 1b and type 1s boutons at different stimulation frequencies at physiological range

(**A**) Pseudo color images of an example NMJ (muscle 6/7) with marked bouton regions, white and yellow arrows highlight type 1b and type 1s boutons, respectively. (**B-C**) Time-constants of intracellular calcium rise (**B**) and decay (**C**) at type 1b and 1s boutons triggered by one second of nerve stimulation at the indicated frequencies (30-40 1b boutons; 20-301s boutons; 4 NMJs). Note that the rise time differences between 1s and 1b boutons are highest at 10 Hz stimulation. At all frequencies 1s boutons tend to show faster rise time constants and slightly slower decay time constants. (**D**) Average peak intracellular fluorescence changes at the corresponding stimulations. The peak rise is significantly higher in 1s boutons at lower stimulation frequency (10 and 20Hz), but level off compared to the 1b boutons at stronger stimulation (40 and 60Hz). (**E-H**) Mean normalized fluorescence changes (± SEM) of 1b and 1s boutons (blue and pink, respectively) upon a 1 second stimulation at 10Hz (**E**), 20Hz (**F**), 40Hz (**G**) and 60Hz (**H**). Scale bar: 5µm. Data denote means ± S.E.M collected from the indicated number of cells. *p<0.05; **p<0.01; ***p<0.001 by two-tailed Student's *t*-tests

Interestingly, type 1s bouton processes a substantially higher peak rise in calcium fluorescence within the range of their natural firing frequencies (10 & 20Hz, **Figure 5.13 D**). Despite a faster fluorescence rise in 1s boutons at all frequencies, saturation kicks in earlier at 40 and 60Hz stimulation (**Figure 5.13 G-H**, pink trace). Domination of calcium peak rise is taken over by type 1b bouton at 40 and 60Hz, the type 1b bouton natural firing range (40 & 60Hz, **Figure 5.13 D**).

Taken together, type 1s boutons are able to support faster calcium rise at all frequencies, but are limiting in the peak rise in calcium at prolonged high frequency stimulation. Type 1b bouton, on the other hand, is only capable to attain slower calcium rise kinetics, but allows larger peak calcium rise during longer duration of high frequency firing. The calcium dynamics of the two bouton type appeared to be specifically tuned for their prevailing firing patterns.

5.2.5. Relationship between bouton size and Calcium dynamics changes with stimulation frequency

The major anatomical difference between the two bouton types is their size. To access whether bouton size influence calcium dynamics at different stimulation frequencies, we extracted data of 1b and 1s boutons and analyzed the relationship

between the reciprocal of radius (surface area to volume ratio) and the calcium dynamics at different stimulation frequencies. We first found that the relationship between calcium rise tau and reciprocal of the radius were increasingly negative as stimulation frequency increase, an increasing negative relationship between bouton size and speed of calcium rise was observed as stimulation frequency increase (**Figure 5.14 A**), which becomes significant at 40-60Hz stimulation frequency (**Figure 5.14 D**). On the other hand, the decay tau shows no significant relationship with bouton size (**Figure 5.14 B & E**), bouton size appeared to exert no influence on calcium clearance. The resultant peak calcium rise (reflected by δF) showed a positive correlation with 1/radius at 10Hz stimulation but not at higher stimulation frequencies (**Figure 5.14 C & F**), demonstrating a negative correlation of peak calcium rise and bouton size that is refined at low frequency firing condition.

In summary, size of a bouton appeared to exhibit a negative relationship with calcium build up at low stimulation frequency (10Hz). This negative relationship was not observed at higher stimulation frequencies despite the speed of calcium rise at higher stimulation frequencies (40-60Hz) is negatively related with bouton size. This may due to the plateauing of calcium build up in smaller bouton after 1 second of stimulation at higher frequency. Interestingly, type 1s bouton exhibit slower calcium decay kinetics than the 1b boutons (**Figure 5.13 C**), but this difference did not appear to relate with bouton size (**Figure 5.14 E**). The faster calcium rise kinetics of type 1s (**Figure 5.13 B**) is also not explainable by size differences at lower stimulation frequency (10-20Hz, **Figure 5.14 D**). Smaller sized bouton favors calcium build up during low frequency stimulation, the smaller sized architecture of 1s boutons may be significant for physiological functioning at the lower frequency firing (below 20Hz) it specialized. Bigger bouton size attenuated calcium rise kinetics at high stimulation frequency (40-60Hz) but did not affect the calcium build up at those frequency ranges, this property may also serve the functioning of bigger sized 1b boutons that specialized at sustained high frequency firing (20-40Hz).

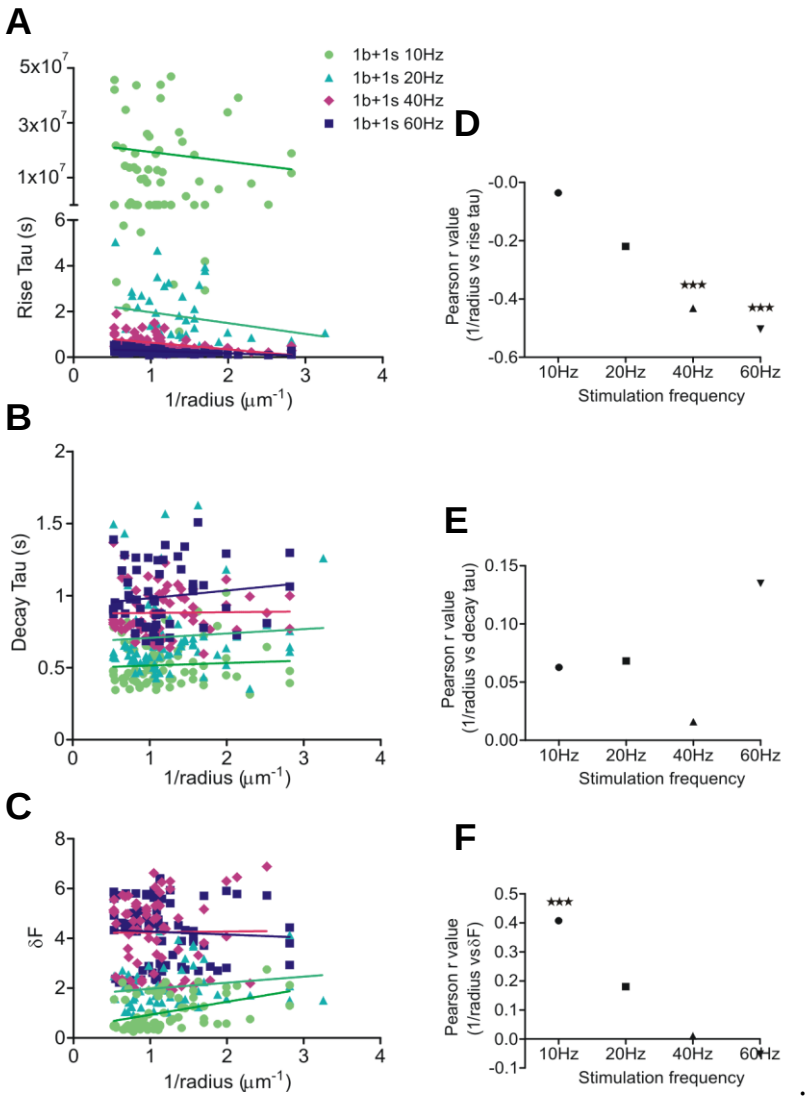

Figure 5.14: Relationship between bouton size and Calcium dynamics changes with stimulation frequency

A-C Scatter plot of calcium dynamics: rise tau (**A**), decay tau (**B**) and peak fractional fluorescence change (**C**) against the reciprocal of bouton radius. The best fit line computed from the linear regression of the 10Hz, 20Hz, 40Hz and 60Hz data sets were colored green, blue, pink and deep blue respectively. **A** Rise tau of all stimulation frequencies shows a negative relationship with 1/radius. **D** As the stimulation frequency increases, the correlation coefficient Pearson r value reflecting the relationship between the rise tau and reciprocal of bouton radius becomes increasingly negative. The correlation is significant at 40Hz and 60Hz of stimulation, showing a negative relationship between the speed of calcium rise and bouton size at high frequency stimulation. **B** Data of decay tau versus 1/radius disperse evenly along the x,y-axis, **E** Close to zero Pearson r value all stimulation frequencies demonstrated the lack of correlation between decay tau and bouton size. **C** Scattered data of peak fractional fluorescence change (δF) versus 1/radius. **F** Correlation between δF and 1/radius was shown significant at 10Hz stimulation, the significant correlation was lost at higher stimulation frequency.

6. DISCUSSION

6.1. A novel acute action of AKT in spontaneous vesicle release at mammalian central synapse

This study is an extension of an earlier finding in our laboratory, where we uncovered the regulatory role of AKT on spontaneous vesicle release in *Drosophila* NMJ (Ge*, Leung* et al., *under revision*). Here we show that this modulatory pathway is conserved in the mammalian central synapse, where the acute effect of AKT on the vesicle release machinery has never been reported before. Since acute pharmacological inhibition of AKT results in elevation of spontaneous vesicle release in both excitatory and inhibitory synapses, this conservation across species and synaptic identities infers that this dynamic modulation by AKT maybe a fundamental property of vesicle release machineries.

Interestingly, the AKT regulated spontaneous release pathway is independent of extracellular calcium. A recent study shows that stochastic opening of voltage-activated calcium channels (VACCs) accounts for approximately 50% of all spontaneous release at rat cultured hippocampal glutamatergic synapses. The AKT regulated pathway may contribute at least part of the yet unresolved mechanism of spontaneous release, where conformational change of the members in the vesicle release machinery is independent of the calcium binding.

Our observed enhancement in spontaneous release but inhibition of high frequency stimulated evoke release under hypo-AKT activity suggested that AKT activity may act as a functional switch of the clamping mode of release machinery. Under this model, AKT activity serves to maintain the vesicle machinery at a tightly clamped mode that is not favoring spontaneous release, this reserve the availability of the presynaptic vesicles for evoked transmission, importance of which being prominent during high frequency stimulation.

The activity of AKT is regulated by a multitude of signaling paths (for review see Hanada et al., 2004) including intense neuronal activity (Smillie and Cousin, 2012) and spill-over glutamate activated presynaptic metabotropic glutamate receptors (Lin et al.,

2011). In both cases the activity of presynaptic AKT is stimulated, when applied to our model, those signals may effectuate local suppression of spontaneous vesicle release, thereby reduce uncorrelated "noise" in the neuronal network and strengthen synaptic efficacy by homeostatic regulation (Sutton and Schuman, 2006; Kavalali et al., 2011).

When the AKT activity is low, the vesicle machinery is loosely clamped, which leads to an augmented spontaneous release. This potentially trigger 1) recurrent activity of a neuronal network by dendritic summation of spontaneous quanta (Carter and Regehr, 2002; Sharma and Vijayaraghavan, 2003); 2) in the presence of postsynaptic target, a reduction in synaptic efficacy by homeostatic plasticity (Sutton and Schuman, 2006; Kavalali et al., 2011); 3) in the absence of postsynaptic target, local synaptic terminal growth (Choi et al., 2014).

Our study also demonstrated the activity of AKT depends on its membrane association via PIP3 (generated by PI3K, degraded by PTEN). Localized microdomains of PIP3 and AKT were observed in axons, which are involved in the formation of axonal F-actin patches, filopodia, and axon branches (Ketschek and Gallo, 2010). PIP3 were also reported to accumulate in spines where it regulates spinule formation during structural long-term potentiation (Ueda and Hayashi, 2013). Interestingly, in *Drosophila* NMJs, PIP3 has been shown to form small local patches at presynaptic release sites where they appear to be involved in clustering the SNARE-protein Syntaxin1A (Khuong et al., 2013). These release-site-associated PIP3-patches may serve in positioning the AKT on individual vesicle release machineries and thus modulate their functional properties. Owing to the mosaic nature of membrane lipids, the distribution of PIP3 may be dynamically regulated depending on the localization and activity of PI3K and PTEN. Interestingly, recent studies have inferred the dynamic nature of the vesicle machinery in terms of forms of vesicle release. It was found that a large portion (~70%) of synapses in hippocampal neurons serve both spontaneous and evoked vesicle release, while the remaining synapses exhibit a preference for spontaneous or evoked release (Kavalali, 2014). Similarly in *Drosophila* NMJs, both non specialized and specialized release site for spontaneous and/or evoked vesicle release were observed, where some exhibit consistently high rates (around 2 events per min) of spontaneous release and others

displays substantially lower rates or even absence of spontaneous release (Melom et al., 2013; Peled et al., 2014). However, the reason for how those release sites exhibit a spectrum of preference for the two forms of release is unknown. Our finding may offer a well fitting mechanism to explain this intriguing property of the vesicle release machinery.

6.2. Potential molecular players in the AKT modulated spontaneous release in mammalian system

In *Drosophila* NMJ, synaptotagmin 1(Syt1) knockdown abolished the sensitivity of spontaneous release frequency towards AKT-blockade, showing that Syt1 is required to translate AKT's activity onto the fusion clamp (Ge*, Leung* et al., *under revision*). However, this dominant role is not observed in the rat hippocampal synapse in the current study.

In fact, both *Drosophila* and mammalian Syt1 lack the canonical AKT-consensus motif R-X-R-X-X-(S/T) (Alessi et al., 1996a). Furthermore, the conserved sites of mammalian Syt1 that have been recently shown to be phosphorylated (Vrljic et al., 2011) do not display similarity to the AKT-consensus motif. Thus, direct phosphorylation of Syt1 by AKT seems unlikely, intermediate kinases may involve in translating the AKT activity on the vesicle release machinery, while at the more complex mammalian system, additional component of the vesicle fusion machinery may be involved.

The *Drosophila melanogaster* genome contains only 7 Syts genes (Lloyd et al., 2000), while 16 genes encoding Syts were identified in the mammalian genome (Sudhof, 2002). Within the 8 calcium binding Syts, Syt2 and Syt9 were capable of rescuing the Syt1 knockout phenotype (Xu et al., 2007). Among the 16 Syts, Syt2 resembles Syt1 the most by sequence (76% sequence identity in mice) and function (Maximov and Sudhof, 2005; Liu et al., 2009; Wierda and Sorensen, 2014). However, Syt2 is primarily expressed in fast transmitting synapses (such as the auditory system or the neuromuscular junction), whereas Syt9 is primarily expressed in the limbic system (Xu et al., 2007) which infers a functional significance in hippocampal neurons. It is possible that at our

Syt1 knockdown hippocampal neurons, the increase in spontaneous release under AKT inhibition is due to functional compensation by homologous molecules like Syt2 or Syt9.

The availability of bioinformatics tools will allow us to screen for functionally interesting AKT targets. Peptide library screening has provided detail information of the AKT preferred substrate (Obata et al., 2000; Hutti et al., 2004). This matrix of data were utilized by programs like Scansite (http://scansite.mit.edu; Yaffe et al., 2001), which instead of identifying just a simple consensus sequence, calculate the likelihood of amino acid sequence surrounding the phosphorylation site to be favored by the kinases. This approach will be instrumental for isolating potential AKT substrate as well as its target residues in our future work.

6.3. Oscillating burst activity induced by AKT inhibition in hippocampal neurons

An intriguing observation in this study is that inhibitions of either AKT or PI3K both induce oscillating burst behavior at the neurons of the hippocampal culture network. The duration of the burst seems to correlate with the frequency of spontaneous neurotransmission. The inhibition of PI3K (which elicited more subtle increase in spontaneous vesicle release) induces bursting of shorter duration, whereas inhibition of AKT (which elicited prominent augmentation in spontaneous vesicle release) induced robust extensive bursts. Moreover, acute inhibition of AKT results in elevation of excitatory and inhibitory neurotransmitter release by 4-fold and 2-fold respectively. Low level of AKT activity seems to favor the enhancement of excitatory spontaneous vesicle release to a greater extent. Therefore, the bursting of the neuron may arise, at least in part, from the overcharge of excitatory tone. Since dendritic integration of spontaneous quanta (Sharma and Vijayaraghavan, 2003) can modulate electrical activity of a neuron, it is likely that down regulation of AKT may increase noise in a signal processing network. Stepping further into our speculation, even if the initial discordance of spontaneous release is small, extra noises may be amplified by feedback connections and exert a global influence on network activity.

Isolated spikes and various bursting patterns are thought to involve in different forms of behaviorally relevant information processing (Harris et al., 2001). Hippocampal place cells, for example, exhibit complex spike bursts that are spatially tuned (Harvey et al., 2009; Epsztein et al., 2011). While single isolated spikes are not always successful to be transmitted between neurons, high-frequency bursts of action potentials are transmitted more reliably (Lisman, 1997; Izhikevich et al., 2003) and are more likely to induce synaptic plasticity (Paulsen and Sejnowski, 2000). Provided the prominent functional variations between different spiking behaviors, it is not difficult to conceive that alterations of spiking properties have been associated with neurological disorders (Walker et al., 2008).

6.4. Potential role of AKT isoforms on spontaneous vesicle release

Here we have reported an AKT isoform specificity in this study, where recombinant adeno-associated virus (rAAV)-shRNA mediated knockdown of the ubiquitously expressed AKT isoform, AKT1, reduced the rate of spontaneous vesicle release, while silencing the predominantly brain expressed AKT3 elicited an increase.

Those two isoforms seems to exert their effect differently. The most interesting possible cause could be the differences in kinase activity. Although the AKT isoforms exhibit limited substrates specificity, several molecules are phosphorylated differently by the two isoforms. For example, AKT1 but not AKT3 is essential for tuberous sclerosis complex 2 (TSC2) phosphorylation (Brognard et al., 2007), whereas AKT3 but not AKT1 is important for the activation of mammalian target of rapamycin complex 1/ p70-S6 kinase 1 (mTORC1/S6K1) pathway in brain (Easton et al., 2005) and phosphorylation of the cell cycle inhibitor p27 (Brognard et al., 2007). Furthermore, AKT3 seems to be the most sensitive isofrom to the PTEN signal, as the reduction of PTEN level in melanocytes appears to activate AKT3 but not AKT1 or AKT2 (Stahl et al., 2004; Gonzalez and McGraw, 2009a).

The other potential reason for the observed isoform specificity is the differential cellular expression pattern and thus the site of the isoform action. Although the AKT

isoform expression level is cell type specific (Lee et al., 2011c), AKT1 is generally expressed at the cytoplasm and plasma membrane, while AKT3 at the nuclear membrane (Gonzalez and McGraw, 2009a; Santi and Lee, 2009). The difference in localization may allow the isoforms to access a divergent set of target substrates. However, the quantitative distribution of the AKT isoforms at the hippocampal neuron, especially at the case of specific isoform knockdown has not been examined yet, which would be accomplished in subsequent experiments.

From the site of action, AKT1 seems to be the higher probable candidate for exerting function on the vesicle release machinery. Indeed, AKT1 was shown to be genetically associated with schizophrenia (Emamian et al., 2004). Although the potential participation of the other isoforms cannot be ruled out (Birnbaum, 2004; Freyberg et al., 2010), the protein level of AKT1 but not AKT2 or AKT3 was shown to be reduced in the hippocampus and frontal cortex of postmortem schizophrenic samples (Emamian et al., 2004). Also, AKT1 knockout mice were shown to be impaired attenuation of startle response by prepulse inhibition, a behavioral signature of schizophrenia (Arguello and Gogos, 2008).

However, the effect of AKT1 knockdown is the opposite of acute AKT inhibitors treatment. Since the rAAV-shRNA mediate knockdown is a rather slow process that takes at least 8 days to significantly suppress the isoform expression, the phenotypic outcome could be an orchestrated result of a plethora of misregulated pathways. Moreover, the surge of excitability may induce excitotoxic injury and change in synaptic efficacy (Benes, 1999; Pozo and Goda, 2010). The impact of the specific isoform knockdown on the number of synapse and postsynaptic receptor cluster are remained to be confirmed.

A result that baffled us is that both AKT1 and AKT3 knockdown did not abolish the sensitivity towards pharmacological AKT inhibition. One possibility is the incomplete knockdown of the AKT isoforms, where the majority of the isoform that are still expressed may exist at their active (phosphorylated) form which may be sufficient for maintaining the vesicle release machinery in clamped mode and thus being responsive to the inhibitor treatment. The other possibility is both isoforms are not or only partially

responsible for the regulation of the vesicle release machinery. If both AKT1 and AKT3 are ruled out, then it is likely that AKT2 is indeed the isoform that is responsible. Compared to AKT1 and AKT3, the specific activity of this isoform includes the phosphorylation of mouse double minute 2 homolog (MDM2; Brognard et al., 2007) but less intensive phosphorylation of glycogen synthase kinase 3α (GSK3α) and forkhead family of transcription factors: FoxO1/3a (Lee et al., 2011c). However, the effect of AKT2 knockdown on spontaneous vesicle release has not been examined in this study yet, which will be one of the key question to address in the near future.

In the case of partial responsibility of the AKT1 and AKT3 isoform, all three isoforms may contribute to the modulation of spontaneous vesicle release. The AKT isoforms are indeed having limited in vivo substrate specificity (Lee et al., 2011c). For instance, the three AKT isoforms contribute additively to the extent of FoxO1/3a phosphorylation. If functional redundancy exist between isoforms, the existence of non-silenced isoforms may be sufficient to keep the vesicle release machinery in tighter clamped mode and therefore remains sensitive to AKT inhibitors treatment. Since we have observed a compensation expression of the AKT1 and AKT3 isoforms at the virus infection day 8, the opposite effect of AKT1 or AKT3 knockdown on spontaneous vesicle release can be explained by the redundant kinase action between the isoforms. Owing to the substantially higher (~15fold) kinase activity of AKT3 over AKT1, if they share the same action on the vesicle release machinery and are overexpressed when one of the isoform is silenced, AKT 1 knockdown (and compensation overexpression of AKT3) may resemble an overall enhancement of AKT kinase activity, which exhibit a lower rate of spontaneous release. While AKT3 knockdown may resemble an overall suppression of kinase activity, which leads to an elevation of spontaneous vesicle release that is in line with the effect of acute pharmacological inhibition. Nevertheless, the validity of this reasoning would be examined after the functional role of AKT2 was explored.

6.5. Prospect of the current finding towards the understanding of human neurological diseases

Interestingly, many neurotransmitters and psychoactive molecules, such as endocannabinoids (Wenner, 2013), caffeine (Simkus and Stricker, 2002), ketamine (the NMDA receptor blocker; Autry et al., 2011; Nosyreva et al., 2013; Gideons et al., 2014) and nicotine (Radcliffe et al., 1999) are modulators of the spontaneous release signals (Prestwich et al., 1987; Lena et al., 1993; Radcliffe et al., 1999; Grillner et al., 2000; Barazangi and Role, 2001; Simkus and Stricker, 2002; Lambe et al., 2003). While many clinically applied antipsychotic drugs seem to converge on the enhancement of AKT signaling (Emamian et al., 2004; Freyberg et al., 2010). These lines of studies evident the psychological effect of selective interference of spontaneous neurotransmitter release at mature synaptic networks, which confers therapeutic potential of targeting the AKT pathway against psychiatric disorders (Gideons et al., 2014).

Importantly, misregulation of AKT activity was reported to be associated with Schizophrenia (Emamian et al., 2004; Thiselton et al., 2008; Freyberg et al., 2010; Mathur et al., 2010; Emamian, 2012; Ripke et al., 2014), Autism spectrum disorder (Ebert and Greenberg, 2013), Bipolar disease (Toyota et al., 2003; Karege et al., 2010) and other mental disorders (Eldar-Finkelman, 2002; Ebert and Greenberg, 2013). While speculations generally point to the effect of AKT on the cell survival, protein synthesis and neuronal wiring (Emamian, 2012; Ebert and Greenberg, 2013), our results demonstrated that AKT has a direct synaptic role in neurotransmitter release with acute action on neuronal firing. The robust effect of AKT on vesicle release machinery may alter the signal transmission and processing of a neuronal network, and thus may contribute more directly to the etiology of those psychological disorders than so far assumed.

Intriguingly, imbalance between excitatory and inhibitory synaptic transmission are shown to cause circuit dysfunction and are implicated in the disease etiology of Autism Spectrum Disorders (ASD) and schizophrenia (Kehrer et al., 2008; Gogolla et al., 2009). The delicate balance between excitatory and inhibitory tone is thought to be crucial to the functioning of rhythmic network activity, such as gamma and theta band

activity (Bartos et al., 2007), changes in those oscillatory patterns may leads to pathological outcome. For example, reduced gamma activity, which may have a causal relationship with diminished GABA signals (Lewis et al., 2005; Bartos et al., 2007) were found in schizophrenics (Kwon et al., 1999; Lee et al., 2001; Clementz et al., 2003; Spencer et al., 2008), which may hinder the differentiation of intrinsic versus extrinsic signals (Behrendt, 2003). Moreover, reduced inhibitory input and connectivity (Singer, 1993; Just et al., 2004; Welsh et al., 2005; Rippon et al., 2007; Uhlhaas and Singer, 2007), as well as disrupted gamma-oscillations were also reported in ASD (Grice et al., 2001; Brown et al., 2005), which may alter the synchronicity between different brain regions and signal-to-noise processing problems. Our proven effect of misregulated AKT on the alternation of excitatory and inhibitory spontaneous vesicle release seems to align well with the etiology of those disorders. Furthermore, since the AKT1 and AKT3 appeared to elicit opposite effect on spontaneous vesicle release, any differences in the relative expression of AKT1 and AKT3 between excitatory and inhibitory neurons may offer a provocative insight into disease mechanism.

To test the potential involvement of the AKT synaptic function in cognitive functioning, we established a collaboration with the laboratory of Prof. Peter Gass (Central Institute of Mental Health Mannheim) to analyze the behavioral outcome of acute AKT inhibition in rodent. Since we have successfully generated rAAV-shRNA that are effective to silence endogenous AKT1 or AKT3 isoforms and alter the rate of spontaneous vesicle release *in vitro*, such viruses would be a potential tool for *in vivo* studies.

6.6. Three-dimensional mathematical modeling of calcium dynamics at *Drosophila* NMJ boutons

This second project is part of a collaborative effort to build a three-dimensional mathematical model of calcium dynamics at the synaptic bouton of *Drosophila* NMJ. Despite the many technical revolutions to overcome diffraction limited resolution in microscopy, super-resolution technology (e.g stimulated emission depletion (STED), photoactivated light microscopy (PALM) or structured illumination microscopy (SIM))

still bear limitations in three-dimensional space and time resolution, which hampers the precision in accessing the fast physiological processes in living cells. The availability of highly precise mathematical model enhances robustness in investigating complex biological events in extreme resolution. However, the degree to which the theoretical model recapitulates the realistic biological circumstances is always a matter of concern. To this end, we provided experimental data for the validation and adjustment of this theoretical model to achieve adequate alignment with the actual biological events. The experimentally proven mathematical model would be a robust tool for the detail analysis of the temporal-spatial interplay between calcium regulating and calcium dependent molecules during physiological function. Here we would discuss the preliminary observation from the experimental data, while the real finding of this collaborative project remains to be confirmed after incorporation into the computational model.

Through the electrophysiological measurement of paired-pulse ratio (PPRs), we found that complete clearance of residual calcium from a single stimulation at is achieved by around 75-100ms. While quantitative calcium life imaging estimated the peak rise in calcium concentration of the entire bouton triggered by a single stimulation ($\Delta[Ca^{2+}]_{1Hz}$) to be 4.11 ± 0.28 nM and resting calcium concentration ($[Ca^{2+}]_0$) to be 14.24 ± 0.29nM. It was further demonstrated that $\Delta[Ca^{2+}]_{1Hz}$ is negatively correlated with the bouton size, and express a linear relationship with the bouton surface area to volume ratio. Since the *Drosophila* NMJ contain two differently sized bouton types (Type 1b:big, Type 1s:small) which specialized in disparate firing frequencies (Type 1b:20-40Hz, Type 1s:below 20Hz), to explore the influence of calcium dynamics in different bouton dimensions on physiological firing, the calcium dynamics at various stimulation frequencies were compared between the bouton types. Here were found that type 1s boutons are able to support faster calcium rise speed at all stimulation frequencies (10/20/40/60Hz), it facilitate larger peak calcium rise at lower stimulation frequencies (10-20Hz) but not prolonged high frequency stimulation (40-60Hz). Type 1b bouton, on the other hand, exhibit slower calcium rise kinetics, but allows larger peak calcium rise during longer duration of high frequency firing (40-60Hz). The peak calcium rise at low stimulation frequencies (10Hz) appears to correlate with the size of the bouton, which can explain the larger peak calcium rise in type 1s boutons. However, the type 1s boutons' faster calcium

rise kinetics at lower stimulation frequency (10-20Hz) and slower calcium decay kinetics at all frequencies did not appear to relate with bouton size. Other calcium regulatory mechanism maybe employed by the two bouton types to elicit the variation in calcium dynamics at different stimulation frequencies. For example, type 1b terminals harbor more intraterminal mitochondria, and abundant subsynaptic reticulum around or beneath the boutons, while the 1s accommodate fewer intraterminal mitochondria, and less developed subsynaptic reticulum (Atwood et al., 1993b). The abundant calcium sinks in type 1b boutons may play a more crucial role in the speed of calcium clearance.

7. REFERENCES

Adler EM, Augustine GJ, Duffy SN, Charlton MP (1991) Alien intracellular calcium chelators attenuate neurotransmitter release at the squid giant synapse. J Neurosci 11:1496-1507.

Akerboom J, Rivera JD, Guilbe MM, Malave EC, Hernandez HH, Tian L, Hires SA, Marvin JS, Looger LL, Schreiter ER (2009) Crystal structures of the GCaMP calcium sensor reveal the mechanism of fluorescence signal change and aid rational design. J Biol Chem 284:6455-6464.

Albantakis L, Lohmann C (2009) A simple method for quantitative calcium imaging in unperturbed developing neurons. J Neurosci Methods 184:206-212.

Alessi DR, Cohen P (1998) Mechanism of activation and function of protein kinase B. Curr Opin Genet Dev 8:55-62.

Alessi DR, Caudwell FB, Andjelkovic M, Hemmings BA, Cohen P (1996a) Molecular basis for the substrate specificity of protein kinase B; comparison with MAPKAP kinase-1 and p70 S6 kinase. FEBS letters 399:333-338.

Alessi DR, Andjelkovic M, Caudwell B, Cron P, Morrice N, Cohen P, Hemmings BA (1996b) Mechanism of activation of protein kinase B by insulin and IGF-1. EMBO J 15:6541-6551.

Altomare DA, Guo K, Cheng JQ, Sonoda G, Walsh K, Testa JR (1995) Cloning, chromosomal localization and expression analysis of the mouse Akt2 oncogene. Oncogene 11:1055-1060.

Andreae LC, Fredj NB, Burrone J (2012) Independent vesicle pools underlie different modes of release during neuronal development. J Neurosci 32:1867-1874.

Angleson JK, Betz WJ (2001) Intraterminal Ca(2+) and spontaneous transmitter release at the frog neuromuscular junction. J Neurophysiol 85:287-294.

Aoto J, Nam CI, Poon MM, Ting P, Chen L (2008) Synaptic signaling by all-trans retinoic acid in homeostatic synaptic plasticity. Neuron 60:308-320.

Arguello PA, Gogos JA (2008) A signaling pathway AKTing up in schizophrenia. J Clin Invest 118:2018-2021.

Atluri PP, Regehr WG (1998) Delayed release of neurotransmitter from cerebellar granule cells. J Neurosci 18:8214-8227.

Atwal JK, Massie B, Miller FD, Kaplan DR (2000) The TrkB-Shc site signals neuronal survival and local axon growth via MEK and P13-kinase. Neuron 27:265-277.

Atwood HL, Karunanithi S (2002) Diversification of synaptic strength: presynaptic elements. Nat Rev Neurosci 3:497-516.

Atwood HL, Govind CK, Wu CF (1993a) Differential ultrastructure of synaptic terminals on ventral longitudinal abdominal muscles in Drosophila larvae. J Neurobiol 24:1008-1024.

Atwood HL, Govind CK, Wu CF (1993b) Differential ultrastructure of synaptic terminals on ventral longitudinal abdominal muscles in Drosophila larvae. Journal of neurobiology 24:1008-1024.

Augustine GJ, Charlton MP (1986) Calcium dependence of presynaptic calcium current and post-synaptic response at the squid giant synapse. J Physiol 381:619-640.

Augustine GJ, Adler EM, Charlton MP (1991) The calcium signal for transmitter secretion from presynaptic nerve terminals. Ann N Y Acad Sci 635:365-381.

Augustine GJ, Santamaria F, Tanaka K (2003) Local calcium signaling in neurons. Neuron 40:331-346.

Autry AE, Adachi M, Nosyreva E, Na ES, Los MF, Cheng PF, Kavalali ET, Monteggia LM (2011) NMDA receptor blockade at rest triggers rapid behavioural antidepressant responses. Nature 475:91-95.

Bacaj T, Wu D, Yang X, Morishita W, Zhou P, Xu W, Malenka RC, Sudhof TC (2013) Synaptotagmin-1 and synaptotagmin-7 trigger synchronous and asynchronous phases of neurotransmitter release. Neuron 80:947-959.

Bading H, Greenberg ME (1991) Stimulation of protein tyrosine phosphorylation by NMDA receptor activation. Science 253:912-914.

Baines RA, Bate M (1998) Electrophysiological development of central neurons in the Drosophila embryo. J Neurosci 18:4673-4683.

Baird GS, Zacharias DA, Tsien RY (1999) Circular permutation and receptor insertion within green fluorescent proteins. Proc Natl Acad Sci U S A 96:11241-11246.

Barazangi N, Role LW (2001) Nicotine-induced enhancement of glutamatergic and GABAergic synaptic transmission in the mouse amygdala. J Neurophysiol 86:463-474.

Barbieri MA, Kohn AD, Roth RA, Stahl PD (1998) Protein kinase B/akt and rab5 mediate Ras activation of endocytosis. J Biol Chem 273:19367-19370.

Barrett EF, Stevens CF (1972) The kinetics of transmitter release at the frog neuromuscular junction. J Physiol 227:691-708.

Bartos M, Vida I, Jonas P (2007) Synaptic mechanisms of synchronized gamma oscillations in inhibitory interneuron networks. Nat Rev Neurosci 8:45-56.

Behrendt RP (2003) Hallucinations: synchronisation of thalamocortical gamma oscillations underconstrained by sensory input. Conscious Cogn 12:413-451.

Bellacosa A, Testa JR, Staal SP, Tsichlis PN (1991) A retroviral oncogene, akt, encoding a serine-threonine kinase containing an SH2-like region. Science 254:274-277.

Bellacosa A, Kumar CC, Di Cristofano A, Testa JR (2005) Activation of AKT kinases in cancer: implications for therapeutic targeting. Adv Cancer Res 94:29-86.

Bellen HJ BV (2000) The Neuromuscular Junction. In Drosophila protocols. . Cold Spring Harbor Laboratory Press.

Benes FM (1999) Evidence for altered trisynaptic circuitry in schizophrenic hippocampus. Biol Psychiatry 46:589-599.

Bennett MK, Calakos N, Scheller RH (1992) Syntaxin: a synaptic protein implicated in docking of synaptic vesicles at presynaptic active zones. Science 257:255-259.

Betz A, Thakur P, Junge HJ, Ashery U, Rhee JS, Scheuss V, Rosenmund C, Rettig J, Brose N (2001) Functional interaction of the active zone proteins Munc13-1 and RIM1 in synaptic vesicle priming. Neuron 30:183-196.

Bhave SV, Ghoda L, Hoffman PL (1999) Brain-derived neurotrophic factor mediates the anti-apoptotic effect of NMDA in cerebellar granule neurons: signal transduction cascades and site of ethanol action. J Neurosci 19:3277-3286.

Bialer M, White HS (2010) Key factors in the discovery and development of new antiepileptic drugs. Nat Rev Drug Discov 9:68-82.

Bijur GN, Jope RS (2003) Rapid accumulation of Akt in mitochondria following phosphatidylinositol 3-kinase activation. J Neurochem 87:1427-1435.

Birnbaum MJ (2004) On the InterAktion between hexokinase and the mitochondrion. Dev Cell 7:781-782.

Blatow M, Caputi A, Burnashev N, Monyer H, Rozov A (2003) Ca2+ buffer saturation underlies paired pulse facilitation in calbindin-D28k-containing terminals. Neuron 38:79-88.

Borst JG, Sakmann B (1996) Calcium influx and transmitter release in a fast CNS synapse. Nature 383:431-434.

Bowery NG, Doble A, Hill DR, Hudson AL, Shaw JS, Turnbull MJ, Warrington R (1981) Bicuculline-insensitive GABA receptors on peripheral autonomic nerve terminals. Eur J Pharmacol 71:53-70.

Bracher A, Kadlec J, Betz H, Weissenhorn W (2002) X-ray structure of a neuronal complexin-SNARE complex from squid. The Journal of biological chemistry 277:26517-26523.

Brachtendorf S, Eilers J, Schmidt H (2015) A use-dependent increase in release sites drives facilitation at calretinin-deficient cerebellar parallel-fiber synapses. Front Cell Neurosci 9:27.

Brand AH, Perrimon N (1993) Targeted gene expression as a means of altering cell fates and generating dominant phenotypes. Development 118:401-415.

Brazil DP, Park J, Hemmings BA (2002) PKB binding proteins. Getting in on the Akt. Cell 111:293-303.

Broadie K, Bellen HJ, DiAntonio A, Littleton JT, Schwarz TL (1994) Absence of synaptotagmin disrupts excitation-secretion coupling during synaptic transmission. P Natl Acad Sci USA 91:10727-10731.

Brognard J, Sierecki E, Gao T, Newton AC (2007) PHLPP and a second isoform, PHLPP2, differentially attenuate the amplitude of Akt signaling by regulating distinct Akt isoforms. Mol Cell 25:917-931.

Brose N (2008) For better or for worse: complexins regulate SNARE function and vesicle fusion. Traffic 9:1403-1413.

Brose N, Hofmann K, Hata Y, Sudhof TC (1995) Mammalian homologues of Caenorhabditis elegans unc-13 gene define novel family of C2-domain proteins. J Biol Chem 270:25273-25280.

Brown C, Gruber T, Boucher J, Rippon G, Brock J (2005) Gamma abnormalities during perception of illusory figures in autism. Cortex 41:364-376.

Brunet A, Bonni A, Zigmond MJ, Lin MZ, Juo P, Hu LS, Anderson MJ, Arden KC, Blenis J, Greenberg ME (1999) Akt promotes cell survival by phosphorylating and inhibiting a Forkhead transcription factor. Cell 96:857-868.

Bucurenciu I, Kulik A, Schwaller B, Frotscher M, Jonas P (2008) Nanodomain coupling between Ca2+ channels and Ca2+ sensors promotes fast and efficient transmitter release at a cortical GABAergic synapse. Neuron 57:536-545.

Budnik V (1996) Synapse maturation and structural plasticity at Drosophila neuromuscular junctions. Curr Opin Neurobiol 6:858-867.

Byrne JH, Shapiro E, Dieringer N, Koester J (1979) Biophysical mechanisms contributing to inking behavior in Aplysia. J Neurophysiol 42:1233-1250.

Calleja V, Alcor D, Laguerre M, Park J, Vojnovic B, Hemmings BA, Downward J, Parker PJ, Larijani B (2007) Intramolecular and intermolecular interactions of protein kinase B define its activation in vivo. PLoS biology 5:e95.

Carbone E, Lux HD (1984) A low voltage-activated, fully inactivating Ca channel in vertebrate sensory neurones. Nature 310:501-502.

Cardone MH, Roy N, Stennicke HR, Salvesen GS, Franke TF, Stanbridge E, Frisch S, Reed JC (1998) Regulation of cell death protease caspase-9 by phosphorylation. Science 282:1318-1321.

Carter AG, Regehr WG (2002) Quantal events shape cerebellar interneuron firing. Nat Neurosci 5:1309-1318.

Catterall WA (2011) Voltage-gated calcium channels. Cold Spring Harb Perspect Biol 3:a003947.

Catterall WA, Perez-Reyes E, Snutch TP, Striessnig J (2005) International Union of Pharmacology. XLVIII. Nomenclature and structure-function relationships of voltage-gated calcium channels. Pharmacol Rev 57:411-425.

Chapman ER, Hanson PI, An S, Jahn R (1995) Ca2+ regulates the interaction between synaptotagmin and syntaxin 1. The Journal of biological chemistry 270:23667-23671.

Chen TW, Wardill TJ, Sun Y, Pulver SR, Renninger SL, Baohan A, Schreiter ER, Kerr RA, Orger MB, Jayaraman V, Looger LL, Svoboda K, Kim DS (2013) Ultrasensitive fluorescent proteins for imaging neuronal activity. Nature 499:295-300.

Chen WS, Xu PZ, Gottlob K, Chen ML, Sokol K, Shiyanova T, Roninson I, Weng W, Suzuki R, Tobe K, Kadowaki T, Hay N (2001) Growth retardation and increased apoptosis in mice with homozygous disruption of the Akt1 gene. Genes Dev 15:2203-2208.

Chen X, Tomchick DR, Kovrigin E, Arac D, Machius M, Sudhof TC, Rizo J (2002) Three-dimensional structure of the complexin/SNARE complex. Neuron 33:397-409.

Chicka MC, Hui E, Liu H, Chapman ER (2008) Synaptotagmin arrests the SNARE complex before triggering fast, efficient membrane fusion in response to Ca2+. Nat Struct Mol Biol 15:827-835.

Cho H, Mu J, Kim JK, Thorvaldsen JL, Chu Q, Crenshaw EB, 3rd, Kaestner KH, Bartolomei MS, Shulman GI, Birnbaum MJ (2001) Insulin resistance and a diabetes mellitus-like syndrome in mice lacking the protein kinase Akt2 (PKB beta). Science 292:1728-1731.

Choi BJ, Imlach WL, Jiao W, Wolfram V, Wu Y, Grbic M, Cela C, Baines RA, Nitabach MN, McCabe BD (2014) Miniature neurotransmission regulates Drosophila synaptic structural maturation. Neuron 82:618-634.

Choi JC, Park D, Griffith LC (2004) Electrophysiological and morphological characterization of identified motor neurons in the Drosophila third instar larva central nervous system. J Neurophysiol 91:2353-2365.

Chong ZZ, Li F, Maiese K (2005) Activating Akt and the brain's resources to drive cellular survival and prevent inflammatory injury. Histol Histopathol 20:299-315.

Chouhan AK, Zhang J, Zinsmaier KE, Macleod GT (2010) Presynaptic mitochondria in functionally different motor neurons exhibit similar affinities for Ca2+ but exert little influence as Ca2+ buffers at nerve firing rates in situ. J Neurosci 30:1869-1881.

Christie JM, Chiu DN, Jahr CE (2010) Ca(2+)-dependent enhancement of release by subthreshold somatic depolarization. Nat Neurosci 14:62-68.

Chung C, Kavalali ET (2006) Seeking a function for spontaneous neurotransmission. Nat Neurosci 9:989-990.

Clementz BA, Dzau JR, Blumenfeld LD, Matthews S, Kissler J (2003) Ear of stimulation determines schizophrenia-normal brain activity differences in an auditory paired-stimuli paradigm. Eur J Neurosci 18:2853-2858.

Coffer PJ, Jin J, Woodgett JR (1998) Protein kinase B (c-Akt): a multifunctional mediator of phosphatidylinositol 3-kinase activation. The Biochemical journal 335 (Pt 1):1-13.

Cristiano BE, Chan JC, Hannan KM, Lundie NA, Marmy-Conus NJ, Campbell IG, Phillips WA, Robbie M, Hannan RD, Pearson RB (2006) A specific role for AKT3 in the genesis of ovarian cancer through modulation of G(2)-M phase transition. Cancer Res 66:11718-11725.

Cross DA, Alessi DR, Cohen P, Andjelkovich M, Hemmings BA (1995) Inhibition of glycogen synthase kinase-3 by insulin mediated by protein kinase B. Nature 378:785-789.

Crossley CA (1978) The morphology and development of the Drosophila muscular system. In: The Genetics and Biology of Drosophila.

Cummings DD, Wilcox KS, Dichter MA (1996) Calcium-dependent paired-pulse facilitation of miniature EPSC frequency accompanies depression of EPSCs at hippocampal synapses in culture. J Neurosci 16:5312-5323.

Datta SR, Brunet A, Greenberg ME (1999) Cellular survival: a play in three Akts. Genes Dev 13:2905-2927.

Datta SR, Dudek H, Tao X, Masters S, Fu H, Gotoh Y, Greenberg ME (1997) Akt phosphorylation of BAD couples survival signals to the cell-intrinsic death machinery. Cell 91:231-241.

Davletov BA, Sudhof TC (1993) A single C2 domain from synaptotagmin I is sufficient for high affinity Ca2+/phospholipid binding. The Journal of biological chemistry 268:26386-26390.

Deak F, Xu Y, Chang WP, Dulubova I, Khvotchev M, Liu X, Sudhof TC, Rizo J (2009) Munc18-1 binding to the neuronal SNARE complex controls synaptic vesicle priming. J Cell Biol 184:751-764.

Deitcher DL, Ueda A, Stewart BA, Burgess RW, Kidokoro Y, Schwarz TL (1998) Distinct requirements for evoked and spontaneous release of neurotransmitter are

revealed by mutations in the Drosophila gene neuronal-synaptobrevin. J Neurosci 18:2028-2039.

Deng L, Kaeser PS, Xu W, Sudhof TC (2011) RIM proteins activate vesicle priming by reversing autoinhibitory homodimerization of Munc13. Neuron 69:317-331.

Desai RC, Vyas B, Earles CA, Littleton JT, Kowalchyck JA, Martin TF, Chapman ER (2000) The C2B domain of synaptotagmin is a Ca(2+)-sensing module essential for exocytosis. J Cell Biol 150:1125-1136.

DiAntonio A, Parfitt KD, Schwarz TL (1993) Synaptic transmission persists in synaptotagmin mutants of Drosophila. Cell 73:1281-1290.

DiAntonio A, Petersen SA, Heckmann M, Goodman CS (1999) Glutamate receptor expression regulates quantal size and quantal content at the Drosophila neuromuscular junction. J Neurosci 19:3023-3032.

Diehl JA, Cheng M, Roussel MF, Sherr CJ (1998) Glycogen synthase kinase-3beta regulates cyclin D1 proteolysis and subcellular localization. Genes Dev 12:3499-3511.

Dobrunz LE, Stevens CF (1997) Heterogeneity of release probability, facilitation, and depletion at central synapses. Neuron 18:995-1008.

Dodge FA, Jr., Rahamimoff R (1967) Co-operative action a calcium ions in transmitter release at the neuromuscular junction. J Physiol 193:419-432.

Dolphin AC (2009) Calcium channel diversity: multiple roles of calcium channel subunits. Curr Opin Neurobiol 19:237-244.

Downward J (1998) Mechanisms and consequences of activation of protein kinase B/Akt. Curr Opin Cell Biol 10:262-267.

Dudek H, Datta SR, Franke TF, Birnbaum MJ, Yao R, Cooper GM, Segal RA, Kaplan DR, Greenberg ME (1997) Regulation of neuronal survival by the serine-threonine protein kinase Akt. Science 275:661-665.

Dulubova I, Khvotchev M, Liu S, Huryeva I, Sudhof TC, Rizo J (2007) Munc18-1 binds directly to the neuronal SNARE complex. Proc Natl Acad Sci U S A 104:2697-2702.

Dulubova I, Sugita S, Hill S, Hosaka M, Fernandez I, Sudhof TC, Rizo J (1999) A conformational switch in syntaxin during exocytosis: role of munc18. The EMBO journal 18:4372-4382.

Dummler B, Tschopp O, Hynx D, Yang ZZ, Dirnhofer S, Hemmings BA (2006) Life with a single isoform of Akt: mice lacking Akt2 and Akt3 are viable but display impaired glucose homeostasis and growth deficiencies. Mol Cell Biol 26:8042-8051.

Dunlap K, Luebke JI, Turner TJ (1995) Exocytotic Ca2+ channels in mammalian central neurons. Trends Neurosci 18:89-98.

Easton RM, Cho H, Roovers K, Shineman DW, Mizrahi M, Forman MS, Lee VM, Szabolcs M, de Jong R, Oltersdorf T, Ludwig T, Efstratiadis A, Birnbaum MJ (2005) Role for Akt3/protein kinase Bgamma in attainment of normal brain size. Mol Cell Biol 25:1869-1878.

Ebert DH, Greenberg ME (2013) Activity-dependent neuronal signalling and autism spectrum disorder. Nature 493:327-337.

Eldar-Finkelman H (2002) Glycogen synthase kinase 3: an emerging therapeutic target. Trends Mol Med 8:126-132.

Emamian ES (2012) AKT/GSK3 signaling pathway and schizophrenia. Frontiers in molecular neuroscience 5:33.

Emamian ES, Hall D, Birnbaum MJ, Karayiorgou M, Gogos JA (2004) Convergent evidence for impaired AKT1-GSK3beta signaling in schizophrenia. Nature genetics 36:131-137.

Emptage NJ, Reid CA, Fine A (2001) Calcium stores in hippocampal synaptic boutons mediate short-term plasticity, store-operated Ca2+ entry, and spontaneous transmitter release. Neuron 29:197-208.

Engelman JA, Luo J, Cantley LC (2006) The evolution of phosphatidylinositol 3-kinases as regulators of growth and metabolism. Nat Rev Genet 7:606-619.

Epsztein J, Brecht M, Lee AK (2011) Intracellular determinants of hippocampal CA1 place and silent cell activity in a novel environment. Neuron 70:109-120.

Ermolyuk YS, Alder FG, Surges R, Pavlov IY, Timofeeva Y, Kullmann DM, Volynski KE (2013) Differential triggering of spontaneous glutamate release by P/Q-, N- and R-type Ca2+ channels. Nat Neurosci 16:1754-1763.

Espinosa F, Kavalali ET (2009) NMDA receptor activation by spontaneous glutamatergic neurotransmission. J Neurophysiol 101:2290-2296.

Fakler B, Adelman JP (2008) Control of K(Ca) channels by calcium nano/microdomains. Neuron 59:873-881.

Fatt P, Katz B (1952) Spontaneous subthreshold activity at motor nerve endings. J Physiol 117:109-128.

Fatt p K, B (1950) Some observations on biological noise. Nature 166:597-598.

Fedchyshyn MJ, Wang LY (2005) Developmental transformation of the release modality at the calyx of Held synapse. J Neurosci 25:4131-4140.

Fernandez-Busnadiego R, Asano S, Oprisoreanu AM, Sakata E, Doengi M, Kochovski Z, Zurner M, Stein V, Schoch S, Baumeister W, Lucic V (2013) Cryo-electron tomography reveals a critical role of RIM1alpha in synaptic vesicle tethering. J Cell Biol 201:725-740.

Fernandez-Chacon R, Konigstorfer A, Gerber SH, Garcia J, Matos MF, Stevens CF, Brose N, Rizo J, Rosenmund C, Sudhof TC (2001) Synaptotagmin I functions as a calcium regulator of release probability. Nature 410:41-49.

Frank T, Rutherford MA, Strenzke N, Neef A, Pangrsic T, Khimich D, Fejtova A, Gundelfinger ED, Liberman MC, Harke B, Bryan KE, Lee A, Egner A, Riedel D, Moser T (2010) Bassoon and the synaptic ribbon organize Ca(2)+ channels and vesicles to add release sites and promote refilling. Neuron 68:724-738.

Franke TF, Tartof KD, Tsichlis PN (1994) The SH2-like Akt homology (AH) domain of c-akt is present in multiple copies in the genome of vertebrate and invertebrate eucaryotes. Cloning and characterization of the Drosophila melanogaster c-akt homolog Dakt1. Oncogene 9:141-148.

Freyberg Z, Ferrando SJ, Javitch JA (2010) Roles of the Akt/GSK-3 and Wnt signaling pathways in schizophrenia and antipsychotic drug action. The American journal of psychiatry 167:388-396.

Fuson KL, Montes M, Robert JJ, Sutton RB (2007) Structure of human synaptotagmin 1 C2AB in the absence of Ca2+ reveals a novel domain association. Biochemistry 46:13041-13048.

Galli T, Haucke V (2004) Cycling of synaptic vesicles: how far? How fast! Sci STKE 2004:re19.

Gariepy J, Hodges RS (1983) Primary sequence analysis and folding behavior of EF hands in relation to the mechanism of action of troponin C and calmodulin. FEBS Lett 160:1-6.

Geppert M, Goda Y, Hammer RE, Li C, Rosahl TW, Stevens CF, Sudhof TC (1994) Synaptotagmin I: a major Ca2+ sensor for transmitter release at a central synapse. Cell 79:717-727.

Gerber SH, Rah JC, Min SW, Liu X, de Wit H, Dulubova I, Meyer AC, Rizo J, Arancillo M, Hammer RE, Verhage M, Rosenmund C, Sudhof TC (2008) Conformational switch of syntaxin-1 controls synaptic vesicle fusion. Science 321:1507-1510.

Gideons ES, Kavalali ET, Monteggia LM (2014) Mechanisms underlying differential effectiveness of memantine and ketamine in rapid antidepressant responses. Proc Natl Acad Sci U S A 111:8649-8654.

Gielow ML, Gu GG, Singh S (1995) Resolution and pharmacological analysis of the voltage-dependent calcium channels of Drosophila larval muscles. J Neurosci 15:6085-6093.

Giraudo CG, Eng WS, Melia TJ, Rothman JE (2006) A clamping mechanism involved in SNARE-dependent exocytosis. Science 313:676-680.

Glitsch MD (2008) Spontaneous neurotransmitter release and Ca2+--how spontaneous is spontaneous neurotransmitter release? Cell Calcium 43:9-15.

Goda Y, Stevens CF (1994) Two components of transmitter release at a central synapse. P Natl Acad Sci USA 91:12942-12946.

Gogolla N, Leblanc JJ, Quast KB, Sudhof TC, Fagiolini M, Hensch TK (2009) Common circuit defect of excitatory-inhibitory balance in mouse models of autism. J Neurodev Disord 1:172-181.

Gonzalez E, McGraw TE (2009a) Insulin-modulated Akt subcellular localization determines Akt isoform-specific signaling. Proc Natl Acad Sci U S A 106:7004-7009.

Gonzalez E, McGraw TE (2009b) The Akt kinases: isoform specificity in metabolism and cancer. Cell Cycle 8:2502-2508.

Gorczyca M, Augart C, Budnik V (1993) Insulin-like receptor and insulin-like peptide are localized at neuromuscular junctions in Drosophila. J Neurosci 13:3692-3704.

Goswami SP, Bucurenciu I, Jonas P (2012) Miniature IPSCs in hippocampal granule cells are triggered by voltage-gated Ca2+ channels via microdomain coupling. J Neurosci 32:14294-14304.

Gracheva EO, Hadwiger G, Nonet ML, Richmond JE (2008) Direct interactions between C. elegans RAB-3 and Rim provide a mechanism to target vesicles to the presynaptic density. Neurosci Lett 444:137-142.

Grice SJ, Spratling MW, Karmiloff-Smith A, Halit H, Csibra G, de Haan M, Johnson MH (2001) Disordered visual processing and oscillatory brain activity in autism and Williams syndrome. Neuroreport 12:2697-2700.

Grider MH, Park D, Spencer DM, Shine HD (2009) Lipid raft-targeted Akt promotes axonal branching and growth cone expansion via mTOR and Rac1, respectively. J Neurosci Res 87:3033-3042.

Grillner P, Berretta N, Bernardi G, Svensson TH, Mercuri NB (2000) Muscarinic receptors depress GABAergic synaptic transmission in rat midbrain dopamine neurons. Neuroscience 96:299-307.

Groffen AJ, Martens S, Diez Arazola R, Cornelisse LN, Lozovaya N, de Jong AP, Goriounova NA, Habets RL, Takai Y, Borst JG, Brose N, McMahon HT, Verhage M (2010) Doc2b is a high-affinity Ca2+ sensor for spontaneous neurotransmitter release. Science 327:1614-1618.

Gu H, Jiang SA, Campusano JM, Iniguez J, Su H, Hoang AA, Lavian M, Sun X, O'Dowd DK (2009) Cav2-type calcium channels encoded by cac regulate AP-independent neurotransmitter release at cholinergic synapses in adult Drosophila brain. J Neurophysiol 101:42-53.

Guan B, Hartmann B, Kho YH, Gorczyca M, Budnik V (1996) The Drosophila tumor suppressor gene, dlg, is involved in structural plasticity at a glutamatergic synapse. Curr Biol 6:695-706.

Guertin DA, Stevens DM, Thoreen CC, Burds AA, Kalaany NY, Moffat J, Brown M, Fitzgerald KJ, Sabatini DM (2006) Ablation in mice of the mTORC components raptor, rictor, or mLST8 reveals that mTORC2 is required for signaling to Akt-FOXO and PKCalpha, but not S6K1. Dev Cell 11:859-871.

Gundelfinger ED, Kessels MM, Qualmann B (2003) Temporal and spatial coordination of exocytosis and endocytosis. Nat Rev Mol Cell Biol 4:127-139.

Hagler DJ, Jr., Goda Y (2001) Properties of synchronous and asynchronous release during pulse train depression in cultured hippocampal neurons. Journal of neurophysiology 85:2324-2334.

Han W, Rhee JS, Maximov A, Lao Y, Mashimo T, Rosenmund C, Sudhof TC (2004) N-glycosylation is essential for vesicular targeting of synaptotagmin 1. Neuron 41:85-99.

Han Y, Kaeser PS, Sudhof TC, Schneggenburger R (2011) RIM determines Ca(2)+ channel density and vesicle docking at the presynaptic active zone. Neuron 69:304-316.

Hanada M, Feng J, Hemmings BA (2004) Structure, regulation and function of PKB/AKT--a major therapeutic target. Biochimica et biophysica acta 1697:3-16.

Hanson PI, Roth R, Morisaki H, Jahn R, Heuser JE (1997) Structure and conformational changes in NSF and its membrane receptor complexes visualized by quick-freeze/deep-etch electron microscopy. Cell 90:523-535.

Hardingham GE, Arnold FJ, Bading H (2001) Nuclear calcium signaling controls CREB-mediated gene expression triggered by synaptic activity. Nature neuroscience 4:261-267.

Harris KD, Hirase H, Leinekugel X, Henze DA, Buzsaki G (2001) Temporal interaction between single spikes and complex spike bursts in hippocampal pyramidal cells. Neuron 32:141-149.

Harvey CD, Collman F, Dombeck DA, Tank DW (2009) Intracellular dynamics of hippocampal place cells during virtual navigation. Nature 461:941-946.

Hata Y, Slaughter CA, Sudhof TC (1993) Synaptic vesicle fusion complex contains unc-18 homologue bound to syntaxin. Nature 366:347-351.

Hefft S, Jonas P (2005) Asynchronous GABA release generates long-lasting inhibition at a hippocampal interneuron-principal neuron synapse. Nat Neurosci 8:1319-1328.

Hirai H, Sootome H, Nakatsuru Y, Miyama K, Taguchi S, Tsujioka K, Ueno Y, Hatch H, Majumder PK, Pan BS, Kotani H (2010) MK-2206, an allosteric Akt inhibitor, enhances antitumor efficacy by standard chemotherapeutic agents or molecular targeted drugs in vitro and in vivo. Mol Cancer Ther 9:1956-1967.

Hoang B, Chiba A (2001) Single-cell analysis of Drosophila larval neuromuscular synapses. Dev Biol 229:55-70.

Hobson RJ, Liu Q, Watanabe S, Jorgensen EM (2011) Complexin maintains vesicles in the primed state in C. elegans. Curr Biol 21:106-113.

Honore T, Davies SN, Drejer J, Fletcher EJ, Jacobsen P, Lodge D, Nielsen FE (1988) Quinoxalinediones: potent competitive non-NMDA glutamate receptor antagonists. Science 241:701-703.

Howlett E, Lin CC, Lavery W, Stern M (2008) A PI3-kinase-mediated negative feedback regulates neuronal excitability. PLoS genetics 4:e1000277.

Hsia AY, Malenka RC, Nicoll RA (1998) Development of excitatory circuitry in the hippocampus. J Neurophysiol 79:2013-2024.

Huang W, Zhu PJ, Zhang S, Zhou H, Stoica L, Galiano M, Krnjevic K, Roman G, Costa-Mattioli M (2013) mTORC2 controls actin polymerization required for consolidation of long-term memory. Nat Neurosci 16:441-448.

Huntwork S, Littleton JT (2007) A complexin fusion clamp regulates spontaneous neurotransmitter release and synaptic growth. Nat Neurosci 10:1235-1237.

Hutti JE, Jarrell ET, Chang JD, Abbott DW, Storz P, Toker A, Cantley LC, Turk BE (2004) A rapid method for determining protein kinase phosphorylation specificity. Nature methods 1:27-29.

Hyun T, Yam A, Pece S, Xie X, Zhang J, Miki T, Gutkind JS, Li W (2000) Loss of PTEN expression leading to high Akt activation in human multiple myelomas. Blood 96:3560-3568.

Inoki K, Li Y, Zhu T, Wu J, Guan KL (2002) TSC2 is phosphorylated and inhibited by Akt and suppresses mTOR signalling. Nat Cell Biol 4:648-657.

Izhikevich EM, Desai NS, Walcott EC, Hoppensteadt FC (2003) Bursts as a unit of neural information: selective communication via resonance. Trends Neurosci 26:161-167.

Jacinto E, Facchinetti V, Liu D, Soto N, Wei S, Jung SY, Huang Q, Qin J, Su B (2006) SIN1/MIP1 maintains rictor-mTOR complex integrity and regulates Akt phosphorylation and substrate specificity. Cell 127:125-137.

Jahn R, Scheller RH (2006) SNAREs--engines for membrane fusion. Nat Rev Mol Cell Biol 7:631-643.

Jahn R, Lang T, Sudhof TC (2003) Membrane fusion. Cell 112:519-533.

Jahr CE, Stevens CF (1990) Voltage dependence of NMDA-activated macroscopic conductances predicted by single-channel kinetics. J Neurosci 10:3178-3182.

Jan LY, Jan YN (1976a) L-glutamate as an excitatory transmitter at the Drosophila larval neuromuscular junction. J Physiol 262:215-236.

Jan LY, Jan YN (1976b) Properties of the larval neuromuscular junction in Drosophila melanogaster. J Physiol 262:189-214.

Jaworski J, Spangler S, Seeburg DP, Hoogenraad CC, Sheng M (2005) Control of dendritic arborization by the phosphoinositide-3'-kinase-Akt-mammalian target of rapamycin pathway. J Neurosci 25:11300-11312.

Jensen K, Lambert JD, Jensen MS (2000) Tetanus-induced asynchronous GABA release in cultured hippocampal neurons. Brain research 880:198-201.

Jia XX, Gorczyca M, Budnik V (1993) Ultrastructure of neuromuscular junctions in Drosophila: comparison of wild type and mutants with increased excitability. J Neurobiol 24:1025-1044.

Jin J, Anthopoulos N, Wetsch B, Binari RC, Isaac DD, Andrew DJ, Woodgett JR, Manoukian AS (2001) Regulation of Drosophila tracheal system development by protein kinase B. Dev Cell 1:817-827.

Johansen J, Halpern ME, Johansen KM, Keshishian H (1989) Stereotypic morphology of glutamatergic synapses on identified muscle cells of Drosophila larvae. J Neurosci 9:710-725.

Johnston GA (2013) Advantages of an antagonist: bicuculline and other GABA antagonists. Br J Pharmacol 169:328-336.

Jorquera RA, Huntwork-Rodriguez S, Akbergenova Y, Cho RW, Littleton JT (2012) Complexin controls spontaneous and evoked neurotransmitter release by regulating the timing and properties of synaptotagmin activity. J Neurosci 32:18234-18245.

Jun K, Piedras-Renteria ES, Smith SM, Wheeler DB, Lee SB, Lee TG, Chin H, Adams ME, Scheller RH, Tsien RW, Shin HS (1999) Ablation of P/Q-type Ca(2+) channel currents, altered synaptic transmission, and progressive ataxia in mice lacking the alpha(1A)-subunit. P Natl Acad Sci USA 96:15245-15250.

Just MA, Cherkassky VL, Keller TA, Minshew NJ (2004) Cortical activation and synchronization during sentence comprehension in high-functioning autism: evidence of underconnectivity. Brain : a journal of neurology 127:1811-1821.

Kaeser-Woo YJ, Yang X, Sudhof TC (2012) C-terminal complexin sequence is selectively required for clamping and priming but not for Ca2+ triggering of synaptic exocytosis. J Neurosci 32:2877-2885.

Kaeser PS, Regehr WG (2013) Molecular mechanisms for synchronous, asynchronous, and spontaneous neurotransmitter release. Annu Rev Physiol 76:333-363.

Kaeser PS, Deng L, Wang Y, Dulubova I, Liu X, Rizo J, Sudhof TC (2011) RIM proteins tether Ca2+ channels to presynaptic active zones via a direct PDZ-domain interaction. Cell 144:282-295.

Kamiya H, Umeda K, Ozawa S, Manabe T (2002) Presynaptic Ca2+ entry is unchanged during hippocampal mossy fiber long-term potentiation. J Neurosci 22:10524-10528.

Karege F, Perroud N, Schurhoff F, Meary A, Marillier G, Burkhardt S, Ballmann E, Fernandez R, Jamain S, Leboyer M, La Harpe R, Malafosse A (2010) Association of AKT1 gene variants and protein expression in both schizophrenia and bipolar disorder. Genes Brain Behav 9:503-511.

Katome T, Obata T, Matsushima R, Masuyama N, Cantley LC, Gotoh Y, Kishi K, Shiota H, Ebina Y (2003) Use of RNA interference-mediated gene silencing and adenoviral overexpression to elucidate the roles of AKT/protein kinase B isoforms in insulin actions. J Biol Chem 278:28312-28323.

Katz B, Miledi R (1968) The role of calcium in neuromuscular facilitation. J Physiol 195:481-492.

Kavalali ET (2014) The mechanisms and functions of spontaneous neurotransmitter release. Nat Rev Neurosci 16:5-16.

Kavalali ET, Chung C, Khvotchev M, Leitz J, Nosyreva E, Raingo J, Ramirez DM (2011) Spontaneous neurotransmission: an independent pathway for neuronal signaling? Physiology (Bethesda) 26:45-53.

Kawasaki F, Felling R, Ordway RW (2000) A temperature-sensitive paralytic mutant defines a primary synaptic calcium channel in Drosophila. J Neurosci 20:4885-4889.

Kawasaki F, Collins SC, Ordway RW (2002) Synaptic calcium-channel function in Drosophila: analysis and transformation rescue of temperature-sensitive paralytic and lethal mutations of cacophony. J Neurosci 22:5856-5864.

Kawasaki F, Zou B, Xu X, Ordway RW (2004) Active zone localization of presynaptic calcium channels encoded by the cacophony locus of Drosophila. J Neurosci 24:282-285.

Kazuyoshi Itoh AK, Shoko Nishihara (2013) Electrophysiological recording in the Drosophila larval muscle. In.

Kehrer C, Maziashvili N, Dugladze T, Gloveli T (2008) Altered Excitatory-Inhibitory Balance in the NMDA-Hypofunction Model of Schizophrenia. Frontiers in molecular neuroscience 1:6.

Ketschek A, Gallo G (2010) Nerve growth factor induces axonal filopodia through localized microdomains of phosphoinositide 3-kinase activity that drive the formation of cytoskeletal precursors to filopodia. J Neurosci 30:12185-12197.

Khuong TM, Habets RL, Kuenen S, Witkowska A, Kasprowicz J, Swerts J, Jahn R, van den Bogaart G, Verstreken P (2013) Synaptic PI(3,4,5)P3 is required for Syntaxin1A clustering and neurotransmitter release. Neuron 77:1097-1108.

Khvotchev M, Dulubova I, Sun J, Dai H, Rizo J, Sudhof TC (2007) Dual modes of Munc18-1/SNARE interactions are coupled by functionally critical binding to syntaxin-1 N terminus. J Neurosci 27:12147-12155.

Kim MH, Korogod N, Schneggenburger R, Ho WK, Lee SH (2005) Interplay between Na+/Ca2+ exchangers and mitochondria in Ca2+ clearance at the calyx of Held. J Neurosci 25:6057-6065.

Kim SM, Kumar V, Lin YQ, Karunanithi S, Ramaswami M (2009) Fos and Jun potentiate individual release sites and mobilize the reserve synaptic vesicle pool at the Drosophila larval motor synapse. Proc Natl Acad Sci U S A 106:4000-4005.

King GF (2007) Modulation of insect Ca(v) channels by peptidic spider toxins. Toxicon 49:513-530.

Kirischuk S, Grantyn R (2003) Intraterminal Ca2+ concentration and asynchronous transmitter release at single GABAergic boutons in rat collicular cultures. J Physiol 548:753-764.

Kittel RJ, Wichmann C, Rasse TM, Fouquet W, Schmidt M, Schmid A, Wagh DA, Pawlu C, Kellner RR, Willig KI, Hell SW, Buchner E, Heckmann M, Sigrist SJ (2006) Bruchpilot promotes active zone assembly, Ca2+ channel clustering, and vesicle release. Science 312:1051-1054.

Kiyonaka S, Nakajima H, Takada Y, Hida Y, Yoshioka T, Hagiwara A, Kitajima I, Mori Y, Ohtsuka T (2012) Physical and functional interaction of the active zone protein CAST/ERC2 and the beta-subunit of the voltage-dependent Ca(2+) channel. J Biochem 152:149-159.

Klugmann M, Symes CW, Leichtlein CB, Klaussner BK, Dunning J, Fong D, Young D, During MJ (2005) AAV-mediated hippocampal expression of short and long Homer 1 proteins differentially affect cognition and seizure activity in adult rats. Mol Cell Neurosci 28:347-360.

Konishi H, Shinomura T, Kuroda S, Ono Y, Kikkawa U (1994) Molecular cloning of rat RAC protein kinase alpha and beta and their association with protein kinase C zeta. Biochem Biophys Res Commun 205:817-825.

Kumar CC, Madison V (2005) AKT crystal structure and AKT-specific inhibitors. Oncogene 24:7493-7501.

Kurdyak P, Atwood HL, Stewart BA, Wu CF (1994) Differential physiology and morphology of motor axons to ventral longitudinal muscles in larval Drosophila. J Comp Neurol 350:463-472.

Kwon JS, O'Donnell BF, Wallenstein GV, Greene RW, Hirayasu Y, Nestor PG, Hasselmo ME, Potts GF, Shenton ME, McCarley RW (1999) Gamma frequency-range abnormalities to auditory stimulation in schizophrenia. Arch Gen Psychiatry 56:1001-1005.

Kwon SE, Chapman ER (2011) Synaptophysin regulates the kinetics of synaptic vesicle endocytosis in central neurons. Neuron 70:847-854.

Lambe EK, Picciotto MR, Aghajanian GK (2003) Nicotine induces glutamate release from thalamocortical terminals in prefrontal cortex. Neuropsychopharmacology 28:216-225.

Lee CC, Huang CC, Hsu KS (2011a) Insulin promotes dendritic spine and synapse formation by the PI3K/Akt/mTOR and Rac1 signaling pathways. Neuropharmacology 61:867-879.

Lee HG, Zhao N, Campion BK, Nguyen MM, Selleck SB (2013a) Akt regulates glutamate receptor trafficking and postsynaptic membrane elaboration at the Drosophila neuromuscular junction. Developmental neurobiology.

Lee J, Guan Z, Akbergenova Y, Littleton JT (2013b) Genetic analysis of synaptotagmin C2 domain specificity in regulating spontaneous and evoked neurotransmitter release. J Neurosci 33:187-200.

Lee KH, Williams LM, Haig A, Goldberg E, Gordon E (2001) An integration of 40 Hz Gamma and phasic arousal: novelty and routinization processing in schizophrenia. Clin Neurophysiol 112:1499-1507.

Lee MW, Kim DS, Lee JH, Lee BS, Lee SH, Jung HL, Sung KW, Kim HT, Yoo KH, Koo HH (2011b) Roles of AKT1 and AKT2 in non-small cell lung cancer cell survival, growth, and migration. Cancer Sci 102:1822-1828.

Lee RS, House CM, Cristiano BE, Hannan RD, Pearson RB, Hannan KM (2011c) Relative Expression Levels Rather Than Specific Activity Plays the Major Role in Determining In Vivo AKT Isoform Substrate Specificity. Enzyme Res 2011:720985.

Lena C, Changeux JP, Mulle C (1993) Evidence for "preterminal" nicotinic receptors on GABAergic axons in the rat interpeduncular nucleus. J Neurosci 13:2680-2688.

Leung HT, Byerly L (1991) Characterization of single calcium channels in Drosophila embryonic nerve and muscle cells. J Neurosci 11:3047-3059.

Lewis DA, Hashimoto T, Volk DW (2005) Cortical inhibitory neurons and schizophrenia. Nat Rev Neurosci 6:312-324.

Li C, Ullrich B, Zhang JZ, Anderson RG, Brose N, Sudhof TC (1995) Ca(2+)-dependent and -independent activities of neural and non-neural synaptotagmins. Nature 375:594-599.

Lin CC, Summerville JB, Howlett E, Stern M (2011) The Metabotropic Glutamate Receptor Activates the Lipid Kinase PI3K in Drosophila Motor Neurons through the Calcium/Calmodulin-dependent Protein Kinase II (CaMKII) and the Non-receptor Tyrosine Protein Kinase DFak. Genetics.

Linassier C, MacDougall LK, Domin J, Waterfield MD (1997) Molecular cloning and biochemical characterization of a Drosophila phosphatidylinositol-specific phosphoinositide 3-kinase. Biochem J 321 (Pt 3):849-856.

Lisman JE (1997) Bursts as a unit of neural information: making unreliable synapses reliable. Trends Neurosci 20:38-43.

Littleton JT, Ganetzky B (2000) Ion channels and synaptic organization: analysis of the Drosophila genome. Neuron 26:35-43.

Littleton JT, Stern M, Perin M, Bellen HJ (1994) Calcium dependence of neurotransmitter release and rate of spontaneous vesicle fusions are altered in Drosophila synaptotagmin mutants. Proc Natl Acad Sci U S A 91:10888-10892.

Littleton JT, Stern M, Schulze K, Perin M, Bellen HJ (1993) Mutational analysis of Drosophila synaptotagmin demonstrates its essential role in Ca(2+)-activated neurotransmitter release. Cell 74:1125-1134.

Littleton JT, Bai J, Vyas B, Desai R, Baltus AE, Garment MB, Carlson SD, Ganetzky B, Chapman ER (2001) synaptotagmin mutants reveal essential functions for the C2B domain in Ca2+-triggered fusion and recycling of synaptic vesicles in vivo. J Neurosci 21:1421-1433.

Liu H, Dean C, Arthur CP, Dong M, Chapman ER (2009) Autapses and networks of hippocampal neurons exhibit distinct synaptic transmission phenotypes in the absence of synaptotagmin I. J Neurosci 29:7395-7403.

Llano I, Gonzalez J, Caputo C, Lai FA, Blayney LM, Tan YP, Marty A (2000) Presynaptic calcium stores underlie large-amplitude miniature IPSCs and spontaneous calcium transients. Nat Neurosci 3:1256-1265.

Llinas R, Yarom Y (1981) Electrophysiology of mammalian inferior olivary neurones in vitro. Different types of voltage-dependent ionic conductances. J Physiol 315:549-567.

Llinas R, Sugimori M, Silver RB (1992) Microdomains of high calcium concentration in a presynaptic terminal. Science 256:677-679.

Llinas R, Sugimori M, Silver RB (1995) The concept of calcium concentration microdomains in synaptic transmission. Neuropharmacology 34:1443-1451.

Llinas RR, Sugimori M, Cherksey B (1989) Voltage-dependent calcium conductances in mammalian neurons. The P channel. Ann N Y Acad Sci 560:103-111.

Lloyd TE, Verstreken P, Ostrin EJ, Phillippi A, Lichtarge O, Bellen HJ (2000) A genome-wide search for synaptic vesicle cycle proteins in Drosophila. Neuron 26:45-50.

Lnenicka GA, Keshishian H (2000) Identified motor terminals in Drosophila larvae show distinct differences in morphology and physiology. J Neurobiol 43:186-197.

Lnenicka GA, Grizzaffi J, Lee B, Rumpal N (2006) Ca2+ dynamics along identified synaptic terminals in Drosophila larvae. J Neurosci 26:12283-12293.

Lou X, Scheuss V, Schneggenburger R (2005) Allosteric modulation of the presynaptic Ca2+ sensor for vesicle fusion. Nature 435:497-501.

Lu T, Trussell LO (2000) Inhibitory transmission mediated by asynchronous transmitter release. Neuron 26:683-694.

M. M. Knodel RG, L. Ge, D. Bucher, A. Grillo, G. Wittum, C. M. Schuster & G. Queisser. (2014) Synaptic Bouton Properties Are Tuned to Best Fit the Prevailing Firing Pattern. . Frontiers in computational neuroscience, in press.

Ma C, Su L, Seven AB, Xu Y, Rizo J (2012) Reconstitution of the vital functions of Munc18 and Munc13 in neurotransmitter release. Science 339:421-425.

Mackler JM, Drummond JA, Loewen CA, Robinson IM, Reist NE (2002) The C(2)B Ca(2+)-binding motif of synaptotagmin is required for synaptic transmission in vivo. Nature 418:340-344.

Macleod GT, Marin L, Charlton MP, Atwood HL (2004) Synaptic vesicles: test for a role in presynaptic calcium regulation. J Neurosci 24:2496-2505.

Maehama T, Dixon JE (1998) The tumor suppressor, PTEN/MMAC1, dephosphorylates the lipid second messenger, phosphatidylinositol 3,4,5-trisphosphate. J Biol Chem 273:13375-13378.

Majumdar D, Nebhan CA, Hu L, Anderson B, Webb DJ (2011) An APPL1/Akt signaling complex regulates dendritic spine and synapse formation in hippocampal neurons. Mol Cell Neurosci 46:633-644.

Malsam J, Kreye S, Sollner TH (2008) Membrane fusion: SNAREs and regulation. Cell Mol Life Sci 65:2814-2832.

Manning BD, Cantley LC (2007) AKT/PKB signaling: navigating downstream. Cell 129:1261-1274.

Maravelli AJ, Skiendzielewski JJ, Snover W (2000) Pneumomediastinum acquired by glass blowing. J Emerg Med 19:145-147.

Markus A, Zhong J, Snider WD (2002) Raf and akt mediate distinct aspects of sensory axon growth. Neuron 35:65-76.

Marte BM, Downward J (1997) PKB/Akt: connecting phosphoinositide 3-kinase to cell survival and beyond. Trends in biochemical sciences 22:355-358.

Martin-Pena A, Acebes A, Rodriguez JR, Sorribes A, de Polavieja GG, Fernandez-Funez P, Ferrus A (2006) Age-independent synaptogenesis by phosphoinositide 3 kinase. The Journal of neuroscience : the official journal of the Society for Neuroscience 26:10199-10208.

Martin JA, Hu Z, Fenz KM, Fernandez J, Dittman JS (2011) Complexin has opposite effects on two modes of synaptic vesicle fusion. Curr Biol 21:97-105.

Mathur A, Law MH, Megson IL, Shaw DJ, Wei J (2010) Genetic association of the AKT1 gene with schizophrenia in a British population. Psychiatr Genet 20:118-122.

Matthew WD, Tsavaler L, Reichardt LF (1981) Identification of a synaptic vesicle-specific membrane protein with a wide distribution in neuronal and neurosecretory tissue. J Cell Biol 91:257-269.

Mauceri D, Freitag HE, Oliveira AM, Bengtson CP, Bading H (2011) Nuclear calcium-VEGFD signaling controls maintenance of dendrite arborization necessary for memory formation. Neuron 71:117-130.

Maximov A, Sudhof TC (2005) Autonomous function of synaptotagmin 1 in triggering synchronous release independent of asynchronous release. Neuron 48:547-554.

Maximov A, Tang J, Yang X, Pang ZP, Sudhof TC (2009) Complexin controls the force transfer from SNARE complexes to membranes in fusion. Science 323:516-521.

McKinney RA, Capogna M, Durr R, Gahwiler BH, Thompson SM (1999) Miniature synaptic events maintain dendritic spines via AMPA receptor activation. Nat Neurosci 2:44-49.

McLachlan EM, Martin AR (1981) Non-linear summation of end-plate potentials in the frog and mouse. J Physiol 311:307-324.

McMahon HT, Missler M, Li C, Sudhof TC (1995) Complexins: cytosolic proteins that regulate SNAP receptor function. Cell 83:111-119.

Meinrenken CJ, Borst JG, Sakmann B (2002) Calcium secretion coupling at calyx of Held governed by nonuniform channel-vesicle topography. J Neurosci 22:1648-1667.

Meinrenken CJ, Borst JG, Sakmann B (2003) Local routes revisited: the space and time dependence of the Ca2+ signal for phasic transmitter release at the rat calyx of Held. J Physiol 547:665-689.

Melom JE, Akbergenova Y, Gavornik JP, Littleton JT (2013) Spontaneous and evoked release are independently regulated at individual active zones. The Journal of neuroscience : the official journal of the Society for Neuroscience 33:17253-17263.

Miesenbock G, De Angelis DA, Rothman JE (1998) Visualizing secretion and synaptic transmission with pH-sensitive green fluorescent proteins. Nature 394:192-195.

Mintz IM, Adams ME, Bean BP (1992) P-type calcium channels in rat central and peripheral neurons. Neuron 9:85-95.

Missler M, Zhang W, Rohlmann A, Kattenstroth G, Hammer RE, Gottmann K, Sudhof TC (2003) Alpha-neurexins couple Ca2+ channels to synaptic vesicle exocytosis. Nature 423:939-948.

Misura KM, Scheller RH, Weis WI (2000) Three-dimensional structure of the neuronal-Sec1-syntaxin 1a complex. Nature 404:355-362.

Miyagishi M, Taira K (2002) U6 promoter-driven siRNAs with four uridine 3' overhangs efficiently suppress targeted gene expression in mammalian cells. Nat Biotechnol 20:497-500.

Mochida S, Sheng ZH, Baker C, Kobayashi H, Catterall WA (1996) Inhibition of neurotransmission by peptides containing the synaptic protein interaction site of N-type Ca2+ channels. Neuron 17:781-788.

Momiyama A, Takahashi T (1994) Calcium channels responsible for potassium-induced transmitter release at rat cerebellar synapses. J Physiol 476:197-202.

Mozhayeva MG, Sara Y, Liu X, Kavalali ET (2002) Development of vesicle pools during maturation of hippocampal synapses. J Neurosci 22:654-665.

Muller M, Felmy F, Schwaller B, Schneggenburger R (2007) Parvalbumin is a mobile presynaptic Ca2+ buffer in the calyx of held that accelerates the decay of Ca2+ and short-term facilitation. J Neurosci 27:2261-2271.

Murthy VN, Stevens CF (1999) Reversal of synaptic vesicle docking at central synapses. Nat Neurosci 2:503-507.

Murthy VN, De Camilli P (2003) Cell biology of the presynaptic terminal. Annu Rev Neurosci 26:701-728.

Nadkarni S, Bartol TM, Stevens CF, Sejnowski TJ, Levine H (2012) Short-term plasticity constrains spatial organization of a hippocampal presynaptic terminal. Proc Natl Acad Sci U S A 109:14657-14662.

Nakai J, Ohkura M, Imoto K (2001) A high signal-to-noise Ca(2+) probe composed of a single green fluorescent protein. Nat Biotechnol 19:137-141.

Naraghi M, Neher E (1997) Linearized buffered Ca2+ diffusion in microdomains and its implications for calculation of [Ca2+] at the mouth of a calcium channel. J Neurosci 17:6961-6973.

Nave BT, Ouwens M, Withers DJ, Alessi DR, Shepherd PR (1999) Mammalian target of rapamycin is a direct target for protein kinase B: identification of a convergence point for opposing effects of insulin and amino-acid deficiency on protein translation. Biochem J 344 Pt 2:427-431.

Neher E (1995) The use of fura-2 for estimating Ca buffers and Ca fluxes. Neuropharmacology 34:1423-1442.

Neher E (1998) Vesicle pools and Ca2+ microdomains: new tools for understanding their roles in neurotransmitter release. Neuron 20:389-399.

Nelson N (1992) The vacuolar H(+)-ATPase--one of the most fundamental ion pumps in nature. J Exp Biol 172:19-27.

Nernst WH (1888) Zur Kinetik der Lösung befindlichen Körper: Theorie der Diffusion. Zeitschrift für Physikalische Chemie 3:613-637.

Newcomb R, Szoke B, Palma A, Wang G, Chen X, Hopkins W, Cong R, Miller J, Urge L, Tarczy-Hornoch K, Loo JA, Dooley DJ, Nadasdi L, Tsien RW, Lemos J, Miljanich G (1998) Selective peptide antagonist of the class E calcium channel from the venom of the tarantula Hysterocrates gigas. Biochemistry 37:15353-15362.

Nicholson-Tomishima K, Ryan TA (2004) Kinetic efficiency of endocytosis at mammalian CNS synapses requires synaptotagmin I. Proc Natl Acad Sci U S A 101:16648-16652.

Nicholson KM, Anderson NG (2002) The protein kinase B/Akt signalling pathway in human malignancy. Cell Signal 14:381-395.

Nishikawa K, Kidokoro Y (1995) Junctional and extrajunctional glutamate receptor channels in Drosophila embryos and larvae. J Neurosci 15:7905-7915.

Nishiki T, Augustine GJ (2004a) Dual roles of the C2B domain of synaptotagmin I in synchronizing Ca2+-dependent neurotransmitter release. J Neurosci 24:8542-8550.

Nishiki T, Augustine GJ (2004b) Synaptotagmin I synchronizes transmitter release in mouse hippocampal neurons. J Neurosci 24:6127-6132.

Nosyreva E, Szabla K, Autry AE, Ryazanov AG, Monteggia LM, Kavalali ET (2013) Acute suppression of spontaneous neurotransmission drives synaptic potentiation. J Neurosci 33:6990-7002.

Nowycky MC, Fox AP, Tsien RW (1985) Three types of neuronal calcium channel with different calcium agonist sensitivity. Nature 316:440-443.

Obata T, Yaffe MB, Leparc GG, Piro ET, Maegawa H, Kashiwagi A, Kikkawa R, Cantley LC (2000) Peptide and protein library screening defines optimal substrate motifs for AKT/PKB. J Biol Chem 275:36108-36115.

Oheim M, Kirchhoff F, Stuhmer W (2006) Calcium microdomains in regulated exocytosis. Cell Calcium 40:423-439.

Olney JW, Labruyere J, Wang G, Wozniak DF, Price MT, Sesma MA (1991) NMDA antagonist neurotoxicity: mechanism and prevention. Science 254:1515-1518.

Otmakhov N, Shirke AM, Malinow R (1993) Measuring the impact of probabilistic transmission on neuronal output. Neuron 10:1101-1111.

Otsu Y, Murphy TH (2003) Miniature transmitter release: accident of nature or careful design? Sci STKE 2003:pe54.

Otsu Y, Murphy TH (2004) Optical postsynaptic measurement of vesicle release rates for hippocampal synapses undergoing asynchronous release during train stimulation. J Neurosci 24:9076-9086.

Packard M, Koo ES, Gorczyca M, Sharpe J, Cumberledge S, Budnik V (2002) The Drosophila Wnt, wingless, provides an essential signal for pre- and postsynaptic differentiation. Cell 111:319-330.

Pang ZP, Sun J, Rizo J, Maximov A, Sudhof TC (2006) Genetic analysis of synaptotagmin 2 in spontaneous and Ca2+-triggered neurotransmitter release. EMBO J 25:2039-2050.

Paulsen O, Sejnowski TJ (2000) Natural patterns of activity and long-term synaptic plasticity. Curr Opin Neurobiol 10:172-179.

Peled ES, Newman ZL, Isacoff EY (2014) Evoked and spontaneous transmission favored by distinct sets of synapses. Current biology : CB 24:484-493.

Peng XD, Xu PZ, Chen ML, Hahn-Windgassen A, Skeen J, Jacobs J, Sundararajan D, Chen WS, Crawford SE, Coleman KG, Hay N (2003) Dwarfism, impaired skin development, skeletal muscle atrophy, delayed bone development, and impeded adipogenesis in mice lacking Akt1 and Akt2. Genes Dev 17:1352-1365.

Perin MS, Brose N, Jahn R, Sudhof TC (1991a) Domain structure of synaptotagmin (p65). J Biol Chem 266:623-629.

Perin MS, Fried VA, Mignery GA, Jahn R, Sudhof TC (1990) Phospholipid binding by a synaptic vesicle protein homologous to the regulatory region of protein kinase C. Nature 345:260-263.

Perin MS, Johnston PA, Ozcelik T, Jahn R, Francke U, Sudhof TC (1991b) Structural and functional conservation of synaptotagmin (p65) in Drosophila and humans. J Biol Chem 266:615-622.

Pozo K, Goda Y (2010) Unraveling mechanisms of homeostatic synaptic plasticity. Neuron 66:337-351.

Prestwich SA, Forda SR, Dolphin AC (1987) Adenosine antagonists increase spontaneous and evoked transmitter release from neuronal cells in culture. Brain research 405:130-139.

Radcliffe KA, Fisher JL, Gray R, Dani JA (1999) Nicotinic modulation of glutamate and GABA synaptic transmission of hippocampal neurons. Ann N Y Acad Sci 868:591-610.

Ramirez DM, Kavalali ET (2011) Differential regulation of spontaneous and evoked neurotransmitter release at central synapses. Curr Opin Neurobiol 21:275-282.

Randall A, Tsien RW (1995) Pharmacological dissection of multiple types of Ca2+ channel currents in rat cerebellar granule neurons. J Neurosci 15:2995-3012.

Reid CA, Bekkers JM, Clements JD (1998) N- and P/Q-type Ca2+ channels mediate transmitter release with a similar cooperativity at rat hippocampal autapses. J Neurosci 18:2849-2855.

Reim K, Mansour M, Varoqueaux F, McMahon HT, Sudhof TC, Brose N, Rosenmund C (2001) Complexins regulate a late step in Ca2+-dependent neurotransmitter release. Cell 104:71-81.

Ren D, Xu H, Eberl DF, Chopra M, Hall LM (1998) A mutation affecting dihydropyridine-sensitive current levels and activation kinetics in Drosophila muscle and mammalian heart calcium channels. J Neurosci 18:2335-2341.

Richmond JE, Weimer RM, Jorgensen EM (2001) An open form of syntaxin bypasses the requirement for UNC-13 in vesicle priming. Nature 412:338-341.

Ripke S et al. (2014) Biological insights from 108 schizophrenia-associated genetic loci. Nature 511:421-427.

Rippon G, Brock J, Brown C, Boucher J (2007) Disordered connectivity in the autistic brain: challenges for the "new psychophysiology". Int J Psychophysiol 63:164-172.

Rizo J, Rosenmund C (2008) Synaptic vesicle fusion. Nat Struct Mol Biol 15:665-674.

Roos A, Boron WF (1981) Intracellular pH. Physiol Rev 61:296-434.

Rozov A, Burnashev N, Sakmann B, Neher E (2001) Transmitter release modulation by intracellular Ca2+ buffers in facilitating and depressing nerve terminals of pyramidal cells in layer 2/3 of the rat neocortex indicates a target cell-specific difference in presynaptic calcium dynamics. J Physiol 531:807-826.

Sabatini BL, Regehr WG (1996) Timing of neurotransmission at fast synapses in the mammalian brain. Nature 384:170-172.

Saji M, Narahara K, McCarty SK, Vasko VV, La Perle KM, Porter K, Jarjoura D, Lu C, Cheng SY, Ringel MD (2011) Akt1 deficiency delays tumor progression, vascular invasion, and distant metastasis in a murine model of thyroid cancer. Oncogene 30:4307-4315.

Sankaranarayanan S, De Angelis D, Rothman JE, Ryan TA (2000) The use of pHluorins for optical measurements of presynaptic activity. Biophys J 79:2199-2208.

Santi SA, Lee H (2009) The Akt isoforms are present at distinct subcellular locations. Am J Physiol Cell Physiol 298:C580-591.

Sanyal S, Consoulas C, Kuromi H, Basole A, Mukai L, Kidokoro Y, Krishnan KS, Ramaswami M (2005) Analysis of conditional paralytic mutants in Drosophila sarco-endoplasmic reticulum calcium ATPase reveals novel mechanisms for regulating membrane excitability. Genetics 169:737-750.

Sara Y, Virmani T, Deak F, Liu X, Kavalali ET (2005) An isolated pool of vesicles recycles at rest and drives spontaneous neurotransmission. Neuron 45:563-573.

Sarbassov DD, Guertin DA, Ali SM, Sabatini DM (2005) Phosphorylation and regulation of Akt/PKB by the rictor-mTOR complex. Science 307:1098-1101.

Scanga SE, Ruel L, Binari RC, Snow B, Stambolic V, Bouchard D, Peters M, Calvieri B, Mak TW, Woodgett JR, Manoukian AS (2000) The conserved PI3'K/PTEN/Akt signaling pathway regulates both cell size and survival in Drosophila. Oncogene 19:3971-3977.

Schaefer JE, Worrell JW, Levine RB (2010) Role of intrinsic properties in Drosophila motoneuron recruitment during fictive crawling. J Neurophysiol 104:1257-1266.

Schmidt H, Brachtendorf S, Arendt O, Hallermann S, Ishiyama S, Bornschein G, Gall D, Schiffmann SN, Heckmann M, Eilers J (2013) Nanodomain coupling at an excitatory cortical synapse. Curr Biol 23:244-249.

Scimemi A, Diamond JS (2012) The number and organization of Ca2+ channels in the active zone shapes neurotransmitter release from Schaffer collateral synapses. J Neurosci 32:18157-18176.

Serantes R, Arnalich F, Figueroa M, Salinas M, Andres-Mateos E, Codoceo R, Renart J, Matute C, Cavada C, Cuadrado A, Montiel C (2006) Interleukin-1beta enhances GABAA receptor cell-surface expression by a phosphatidylinositol 3-kinase/Akt pathway: relevance to sepsis-associated encephalopathy. J Biol Chem 281:14632-14643.

Shahrezaei V, Cao A, Delaney KR (2006) Ca2+ from one or two channels controls fusion of a single vesicle at the frog neuromuscular junction. J Neurosci 26:13240-13249.

Sharma G, Vijayaraghavan S (2003) Modulation of presynaptic store calcium induces release of glutamate and postsynaptic firing. Neuron 38:929-939.

Sheng ZH, Rettig J, Takahashi M, Catterall WA (1994) Identification of a syntaxin-binding site on N-type calcium channels. Neuron 13:1303-1313.

Shin OH, Xu J, Rizo J, Sudhof TC (2009) Differential but convergent functions of Ca2+ binding to synaptotagmin-1 C2 domains mediate neurotransmitter release. Proc Natl Acad Sci U S A 106:16469-16474.

Sigrist SJ, Reiff DF, Thiel PR, Steinert JR, Schuster CM (2003) Experience-dependent strengthening of Drosophila neuromuscular junctions. J Neurosci 23:6546-6556.

Simkus CR, Stricker C (2002) The contribution of intracellular calcium stores to mEPSCs recorded in layer II neurones of rat barrel cortex. J Physiol 545:521-535.

Singer W (1993) Synchronization of cortical activity and its putative role in information processing and learning. Annu Rev Physiol 55:349-374.

Smillie KJ, Cousin MA (2012) Akt/PKB controls the activity-dependent bulk endocytosis of synaptic vesicles. Traffic 13:1004-1011.

Sollner T, Bennett MK, Whiteheart SW, Scheller RH, Rothman JE (1993a) A protein assembly-disassembly pathway in vitro that may correspond to sequential steps of synaptic vesicle docking, activation, and fusion. Cell 75:409-418.

Sollner T, Whiteheart SW, Brunner M, Erdjument-Bromage H, Geromanos S, Tempst P, Rothman JE (1993b) SNAP receptors implicated in vesicle targeting and fusion. Nature 362:318-324.

Sorensen JB, Fernandez-Chacon R, Sudhof TC, Neher E (2003) Examining synaptotagmin 1 function in dense core vesicle exocytosis under direct control of Ca2+. J Gen Physiol 122:265-276.

Spencer KM, Niznikiewicz MA, Shenton ME, McCarley RW (2008) Sensory-evoked gamma oscillations in chronic schizophrenia. Biol Psychiatry 63:744-747.

Stahl JM, Sharma A, Cheung M, Zimmerman M, Cheng JQ, Bosenberg MW, Kester M, Sandirasegarane L, Robertson GP (2004) Deregulated Akt3 activity promotes development of malignant melanoma. Cancer Res 64:7002-7010.

Stambolic V, Suzuki A, de la Pompa JL, Brothers GM, Mirtsos C, Sasaki T, Ruland J, Penninger JM, Siderovski DP, Mak TW (1998) Negative regulation of PKB/Akt-dependent cell survival by the tumor suppressor PTEN. Cell 95:29-39.

Stanley EF (1993) Single calcium channels and acetylcholine release at a presynaptic nerve terminal. Neuron 11:1007-1011.

Staveley BE, Ruel L, Jin J, Stambolic V, Mastronardi FG, Heitzler P, Woodgett JR, Manoukian AS (1998) Genetic analysis of protein kinase B (AKT) in Drosophila. Curr Biol 8:599-602.

Steinert JR, Kuromi H, Hellwig A, Knirr M, Wyatt AW, Kidokoro Y, Schuster CM (2006) Experience-dependent formation and recruitment of large vesicles from reserve pool. Neuron 50:723-733.

Stevens CF, Sullivan JM (2003) The synaptotagmin C2A domain is part of the calcium sensor controlling fast synaptic transmission. Neuron 39:299-308.

Stewart BA, Schuster CM, Goodman CS, Atwood HL (1996) Homeostasis of synaptic transmission in Drosophila with genetically altered nerve terminal morphology. J Neurosci 16:3877-3886.

Stewart BA, Atwood HL, Renger JJ, Wang J, Wu CF (1994) Improved stability of Drosophila larval neuromuscular preparations in haemolymph-like physiological solutions. J Comp Physiol [A] 175:179-191.

Sudhof TC (2002) Synaptotagmins: why so many? J Biol Chem 277:7629-7632.

Sudhof TC (2012) Calcium control of neurotransmitter release. Cold Spring Harb Perspect Biol 4:a011353.

Sudhof TC (2013) Neurotransmitter release: the last millisecond in the life of a synaptic vesicle. Neuron 80:675-690.

Sudhof TC, Rothman JE (2009) Membrane fusion: grappling with SNARE and SM proteins. Science 323:474-477.

Sun J, Pang ZP, Qin D, Fahim AT, Adachi R, Sudhof TC (2007) A dual-Ca2+-sensor model for neurotransmitter release in a central synapse. Nature 450:676-682.

Suresh K, Chandrashekara S (2012) Sample size estimation and power analysis for clinical research studies. J Hum Reprod Sci 5:7-13.

Sutton MA, Schuman EM (2006) Dendritic protein synthesis, synaptic plasticity, and memory. Cell 127:49-58.

Sutton MA, Schuman EM (2009) Partitioning the synaptic landscape: distinct microdomains for spontaneous and spike-triggered neurotransmission. Sci Signal 2:pe19.

Sutton MA, Wall NR, Aakalu GN, Schuman EM (2004) Regulation of dendritic protein synthesis by miniature synaptic events. Science 304:1979-1983.

Sutton MA, Taylor AM, Ito HT, Pham A, Schuman EM (2007) Postsynaptic decoding of neural activity: eEF2 as a biochemical sensor coupling miniature synaptic transmission to local protein synthesis. Neuron 55:648-661.

Sutton MA, Ito HT, Cressy P, Kempf C, Woo JC, Schuman EM (2006) Miniature neurotransmission stabilizes synaptic function via tonic suppression of local dendritic protein synthesis. Cell 125:785-799.

Sutton RB, Davletov BA, Berghuis AM, Sudhof TC, Sprang SR (1995) Structure of the first C2 domain of synaptotagmin I: a novel Ca2+/phospholipid-binding fold. Cell 80:929-938.

Takahashi M, Seagar MJ, Jones JF, Reber BF, Catterall WA (1987) Subunit structure of dihydropyridine-sensitive calcium channels from skeletal muscle. P Natl Acad Sci USA 84:5478-5482.

Takamori S et al. (2006) Molecular anatomy of a trafficking organelle. Cell 127:831-846.

Tang J, Maximov A, Shin OH, Dai H, Rizo J, Sudhof TC (2006) A complexin/synaptotagmin 1 switch controls fast synaptic vesicle exocytosis. Cell 126:1175-1187.

Thiselton DL, Vladimirov VI, Kuo PH, McClay J, Wormley B, Fanous A, O'Neill FA, Walsh D, Van den Oord EJ, Kendler KS, Riley BP (2008) AKT1 is associated with schizophrenia across multiple symptom dimensions in the Irish study of high density schizophrenia families. Biol Psychiatry 63:449-457.

Toker A, Newton AC (2000) Akt/protein kinase B is regulated by autophosphorylation at the hypothetical PDK-2 site. J Biol Chem 275:8271-8274.

Tokumaru H, Umayahara K, Pellegrini LL, Ishizuka T, Saisu H, Betz H, Augustine GJ, Abe T (2001) SNARE complex oligomerization by synaphin/complexin is essential for synaptic vesicle exocytosis. Cell 104:421-432.

Tottene A, Moretti A, Pietrobon D (1996) Functional diversity of P-type and R-type calcium channels in rat cerebellar neurons. J Neurosci 16:6353-6363.

Toyota T, Yamada K, Detera-Wadleigh SD, Yoshikawa T (2003) Analysis of a cluster of polymorphisms in AKT1 gene in bipolar pedigrees: a family-based association study. Neurosci Lett 339:5-8.

Tseng Q (2015) Template Matching and Slice Alignment - ImageJ Plugins. In.

Tsien RW, Lipscombe D, Madison DV, Bley KR, Fox AP (1988) Multiple types of neuronal calcium channels and their selective modulation. Trends Neurosci 11:431-438.

Ubach J, Zhang X, Shao X, Sudhof TC, Rizo J (1998) Ca2+ binding to synaptotagmin: how many Ca2+ ions bind to the tip of a C2-domain? EMBO J 17:3921-3930.

Ueda Y, Hayashi Y (2013) PIP(3) regulates spinule formation in dendritic spines during structural long-term potentiation. J Neurosci 33:11040-11047.

Uhlhaas PJ, Singer W (2007) What do disturbances in neural synchrony tell us about autism? Biol Psychiatry 62:190-191.

Vactor DV, Sink H, Fambrough D, Tsoo R, Goodman CS (1993) Genes that control neuromuscular specificity in Drosophila. Cell 73:1137-1153.

van Spronsen M, Hoogenraad CC (2010) Synapse pathology in psychiatric and neurologic disease. Curr Neurol Neurosci Rep 10:207-214.

Verdu J, Buratovich MA, Wilder EL, Birnbaum MJ (1999) Cell-autonomous regulation of cell and organ growth in Drosophila by Akt/PKB. Nature cell biology 1:500-506.

Vrljic M, Strop P, Hill RC, Hansen KC, Chu S, Brunger AT (2011) Post-translational modifications and lipid binding profile of insect cell-expressed full-length mammalian synaptotagmin 1. Biochemistry 50:9998-10012.

Vyleta NP, Jonas P (2014) Loose coupling between Ca2+ channels and release sensors at a plastic hippocampal synapse. Science 343:665-670.

Walker AG, Miller BR, Fritsch JN, Barton SJ, Rebec GV (2008) Altered information processing in the prefrontal cortex of Huntington's disease mouse models. J Neurosci 28:8973-8982.

Wang X, Hu B, Zieba A, Neumann NG, Kasper-Sonnenberg M, Honsbein A, Hultqvist G, Conze T, Witt W, Limbach C, Geitmann M, Danielson H, Kolarow R, Niemann G, Lessmann V, Kilimann MW (2009) A protein interaction node at the neurotransmitter release site: domains of Aczonin/Piccolo, Bassoon, CAST, and rim converge on the N-terminal domain of Munc13-1. J Neurosci 29:12584-12596.

Wang Y, Sugita S, Sudhof TC (2000) The RIM/NIM family of neuronal C2 domain proteins. Interactions with Rab3 and a new class of Src homology 3 domain proteins. J Biol Chem 275:20033-20044.

Wang Y, Okamoto M, Schmitz F, Hofmann K, Sudhof TC (1997) Rim is a putative Rab3 effector in regulating synaptic-vesicle fusion. Nature 388:593-598.

Weingarten J, Lassek M, Mueller BF, Rohmer M, Lunger I, Baeumlisberger D, Dudek S, Gogesch P, Karas M, Volknandt W (2014) The proteome of the presynaptic active zone from mouse brain. Mol Cell Neurosci 59:106-118.

Welling A (2009) Voltage-Dependent Calcium Channels. In: BIOTREND Reviews, pp 1-11.

Welsh JP, Ahn ES, Placantonakis DG (2005) Is autism due to brain desynchronization? Int J Dev Neurosci 23:253-263.

Wenner P (2013) The effects of endocannabinoid signaling on network activity in developing and motor circuits. Ann N Y Acad Sci 1279:135-142.

Wheeler DB, Randall A, Tsien RW (1994) Roles of N-type and Q-type Ca2+ channels in supporting hippocampal synaptic transmission. Science 264:107-111.

Wheeler DG, Barrett CF, Groth RD, Safa P, Tsien RW (2008) CaMKII locally encodes L-type channel activity to signal to nuclear CREB in excitation-transcription coupling. J Cell Biol 183:849-863.

Wierda KD, Sorensen JB (2014) Innervation by a GABAergic neuron depresses spontaneous release in glutamatergic neurons and unveils the clamping phenotype of synaptotagmin-1. J Neurosci 34:2100-2110.

Wilhelm BG, Mandad S, Truckenbrodt S, Krohnert K, Schafer C, Rammner B, Koo SJ, Classen GA, Krauss M, Haucke V, Urlaub H, Rizzoli SO (2014) Composition of isolated synaptic boutons reveals the amounts of vesicle trafficking proteins. Science 344:1023-1028.

Williams C, Chen W, Lee CH, Yaeger D, Vyleta NP, Smith SM (2012) Coactivation of multiple tightly coupled calcium channels triggers spontaneous release of GABA. Nat Neurosci 15:1195-1197.

Worrell JW, Levine RB (2008) Characterization of voltage-dependent Ca2+ currents in identified Drosophila motoneurons in situ. J Neurophysiol 100:868-878.

Xing B, Ashleigh Long A, Harrison DA, Cooper RL (2005) Developmental consequences of neuromuscular junctions with reduced presynaptic calcium channel function. Synapse 57:132-147.

Xu J, Mashimo T, Sudhof TC (2007) Synaptotagmin-1, -2, and -9: Ca(2+) sensors for fast release that specify distinct presynaptic properties in subsets of neurons. Neuron 54:567-581.

Xu J, Pang ZP, Shin OH, Sudhof TC (2009) Synaptotagmin-1 functions as a Ca2+ sensor for spontaneous release. Nat Neurosci 12:759-766.

Xu J, Brewer KD, Perez-Castillejos R, Rizo J (2013) Subtle Interplay between synaptotagmin and complexin binding to the SNARE complex. Journal of molecular biology 425:3461-3475.

Xu R, Janson CG, Mastakov M, Lawlor P, Young D, Mouravlev A, Fitzsimons H, Choi KL, Ma H, Dragunow M, Leone P, Chen Q, Dicker B, During MJ (2001) Quantitative comparison of expression with adeno-associated virus (AAV-2) brain-specific gene cassettes. Gene Ther 8:1323-1332.

Xue M, Lin YQ, Pan H, Reim K, Deng H, Bellen HJ, Rosenmund C (2009) Tilting the balance between facilitatory and inhibitory functions of mammalian and Drosophila Complexins orchestrates synaptic vesicle exocytosis. Neuron 64:367-380.

Xue M, Reim K, Chen X, Chao HT, Deng H, Rizo J, Brose N, Rosenmund C (2007) Distinct domains of complexin I differentially regulate neurotransmitter release. Nat Struct Mol Biol 14:949-958.

Yaffe MB, Leparc GG, Lai J, Obata T, Volinia S, Cantley LC (2001) A motif-based profile scanning approach for genome-wide prediction of signaling pathways. Nat Biotechnol 19:348-353.

Yang X, Kaeser-Woo YJ, Pang ZP, Xu W, Sudhof TC (2010) Complexin clamps asynchronous release by blocking a secondary Ca(2+) sensor via its accessory alpha helix. Neuron 68:907-920.

Yang ZZ, Tschopp O, Baudry A, Dummler B, Hynx D, Hemmings BA (2004) Physiological functions of protein kinase B/Akt. Biochem Soc Trans 32:350-354.

Yang ZZ, Tschopp O, Di-Poi N, Bruder E, Baudry A, Dummler B, Wahli W, Hemmings BA (2005) Dosage-dependent effects of Akt1/protein kinase Balpha (PKBalpha) and Akt3/PKBgamma on thymus, skin, and cardiovascular and nervous system development in mice. Mol Cell Biol 25:10407-10418.

Yano S, Tokumitsu H, Soderling TR (1998) Calcium promotes cell survival through CaM-K kinase activation of the protein-kinase-B pathway. Nature 396:584-587.

Yoshihara M, Guan Z, Littleton JT (2010) Differential regulation of synchronous versus asynchronous neurotransmitter release by the C2 domains of synaptotagmin 1. Proc Natl Acad Sci U S A 107:14869-14874.

Zhang B, Stewart B (2010) Electrophysiological recording from Drosophila larval body-wall muscles. Cold Spring Harb Protoc 2010:pdb prot5487.

Zhang B, Gu F, She C, Guo H, Li W, Niu R, Fu L, Zhang N, Ma Y (2009) Reduction of Akt2 inhibits migration and invasion of glioma cells. Int J Cancer 125:585-595.

Zhang X, Zhang S, Yamane H, Wahl R, Ali A, Lofgren JA, Kendall RL (2006) Kinetic mechanism of AKT/PKB enzyme family. J Biol Chem 281:13949-13956.

Zheng W, Feng G, Ren D, Eberl DF, Hannan F, Dubald M, Hall LM (1995) Cloning and characterization of a calcium channel alpha 1 subunit from Drosophila melanogaster with similarity to the rat brain type D isoform. J Neurosci 15:1132-1143.

Zheng W, Wang H, Zeng Z, Lin J, Little PJ, Srivastava LK, Quirion R (2012) The possible role of the Akt signaling pathway in schizophrenia. Brain research 1470:145-158.

Zhou P, Pang ZP, Yang X, Zhang Y, Rosenmund C, Bacaj T, Sudhof TC (2012) Syntaxin-1 N-peptide and Habc-domain perform distinct essential functions in synaptic vesicle fusion. EMBO J 32:159-171.

Zhu Y, Xu J, Heinemann SF (2009) Two pathways of synaptic vesicle retrieval revealed by single-vesicle imaging. Neuron 61:397-411.

Zimmermann S, Moelling K (1999) Phosphorylation and regulation of Raf by Akt (protein kinase B). Science 286:1741-1744.

Zinda MJ, Johnson MA, Paul JD, Horn C, Konicek BW, Lu ZH, Sandusky G, Thomas JE, Neubauer BL, Lai MT, Graff JR (2001) AKT-1, -2, and -3 are expressed in both normal and tumor tissues of the lung, breast, prostate, and colon. Clin Cancer Res 7:2475-2479.

Zucker RS (1989) Short-term synaptic plasticity. Annu Rev Neurosci 12:13-31.

Zucker RS (2005) Minis: whence and wherefore? Neuron 45:482-484.

8. ACKNOWLEDGEMENTS

First and foremost, my deepest gratitude goes to my supervisor, Prof. Dr. Christoph M. Schuster, for his kindness, guidance and encouragement. I am extremely thankful for his valuable support and encouragement during different hard times. I enjoy his positive vibe, kindness and understanding, which motivated me through ups and downs during my study. His patience in teaching and stimulating discussions have made the findings of this project possible.

I also wish to express my sincere thanks to my second supervisor, Prof. Dr. Hilmar Bading, for the helpful discussions and support during my study. His valuable advice in virus production and the support from his laboratory is essential to the success of this project.

Furthermore, I would like to express my wholehearted thanks to the members of the groups of Prof. Schuster and Prof. Bading, for the enjoyable atmosphere, helpfulness and many inspirations. My special thanks goes to Lihao Ge, for his countless guidance, help and support throughout my PhD work and also life in Germany. I wish to present my warm thanks to Romina Geiger for her many kind help, support, sharing and encouragements, Sara Khouaja for her cheerful kindness, as well as Jan Hörtzsch and Emilia Sancho Vargas for their help and support. I deeply thank Yanwei Tan, for her generous help and advice in the virus production. I am also extremely grateful to David Lau, for his knowledgeable advice, insightful discussions and generous help in many molecular works. I must thank Peter Bengtson for his very generous and knowledgeable advices in electrophysiology. Many thanks goes to Eckehard Freitag for his generous help and advice in cell culture issues, Ana Oliveira and Benjamin Zeuch for their kind teaching of virus production, Anna Hagenston for her brilliant advice and teachings, Carlos Bas Orth, Jing and Thomas Lissek for the very helpful advice and discussions. I also am very grateful to Yan Yu, Priit Pruunsild, and Oscar for their very kind help and useful discussions.

Moreoever, I would like to present my great thanks to Martin Stepniewski, for his help and insightful discussion during the collaborative work, Marlena Lübke for her

contribution in the western blot experiment as well as Daniel Parisotto for the enlightening discussion and contribution in the co-immunoprecipitation experiment that is not presented in this thesis. I am very grateful to Prof. Thomas Söllner for his inspiring discussions and generous gift of M48 anti-bodies. Also I want to express my gratitude to Prof. Thomas Kuner and Michaela Kaiser for their generous gift of SypHluorin virus.

Furthermore, I also want to thank Otto Bräunling and Irmela Meng for their support in fulfilling essential formalities, Allan Summerfield for this kind support in IT matters and Andrea Hellwig for her kind help and support.

Last but not least, I want to thank my beloved family and friends for their endless support and understanding. A special thanks goes to Denis Ludwig for his great encouragement and support.